

Wireless Power Transfer: My Research and Future Outlook

Tianlu Ma

Email: tianlu.ma@my.cityu.edu.hk

14 March 2025

01

Background and Motivation

02

Modeling and Control for Stationary WPT

03

Modeling and Control for Dynamic WPT

04

MHz WPT in Biomedical Application

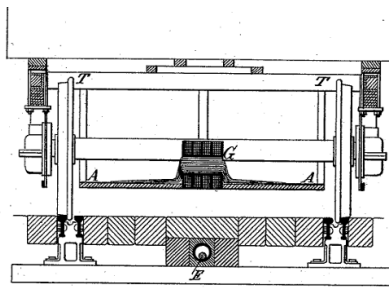
05

Conclusion and Future Outlook

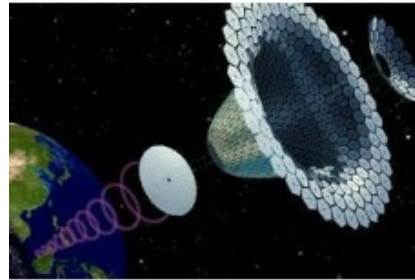
Development Overview of WPT Technology



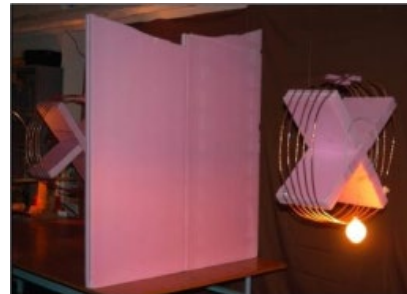
Faraday's law



The first patent of WPT for railcars



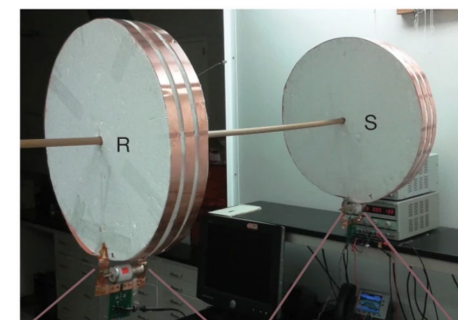
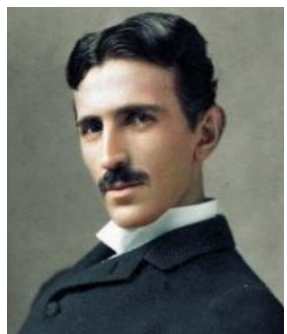
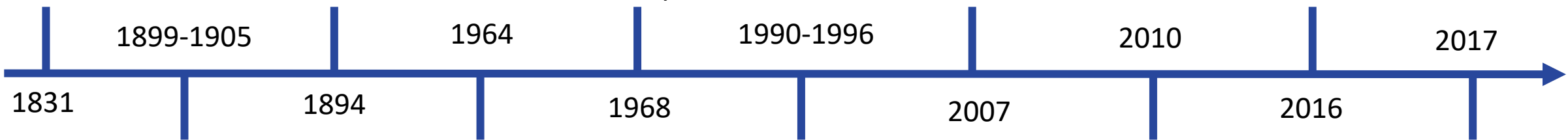
P.E. Glass proposed a solar satellite system



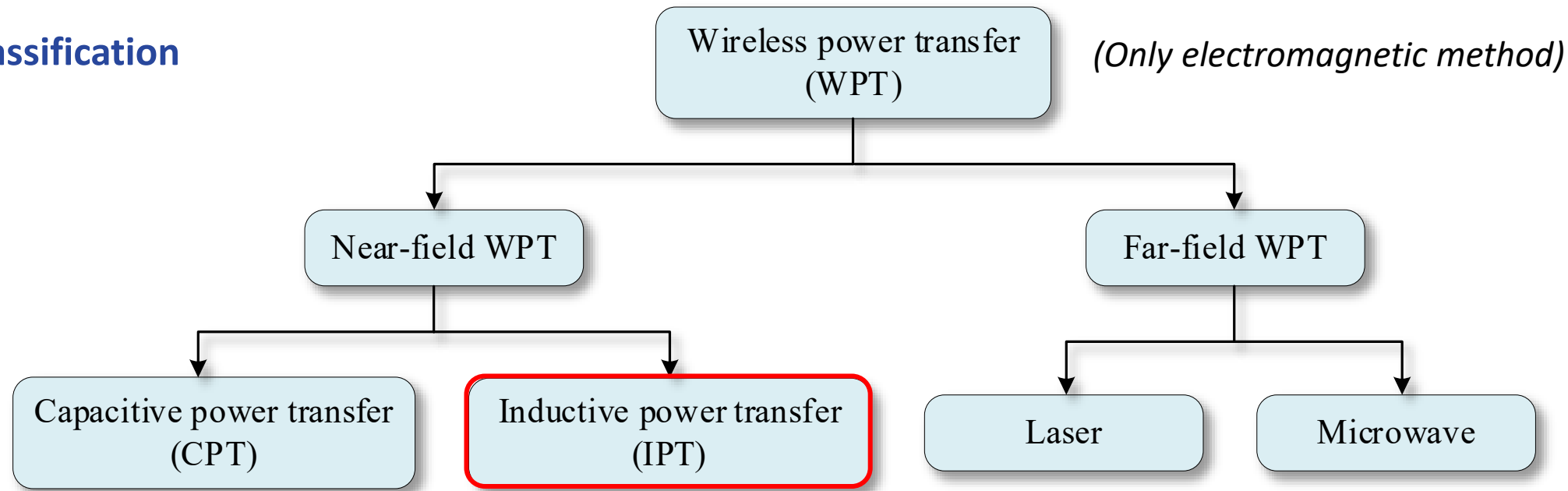
MIT lights up a 60W bulb 2m away



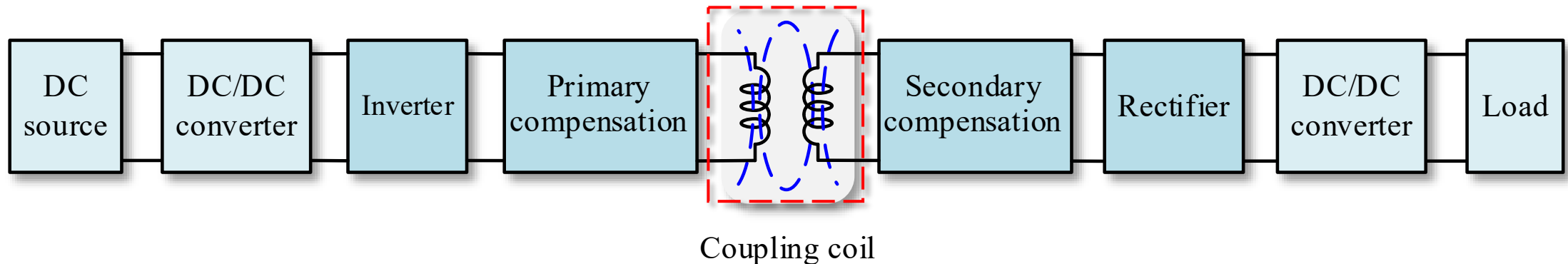
J2954, WPT standard for EVs by IEEE



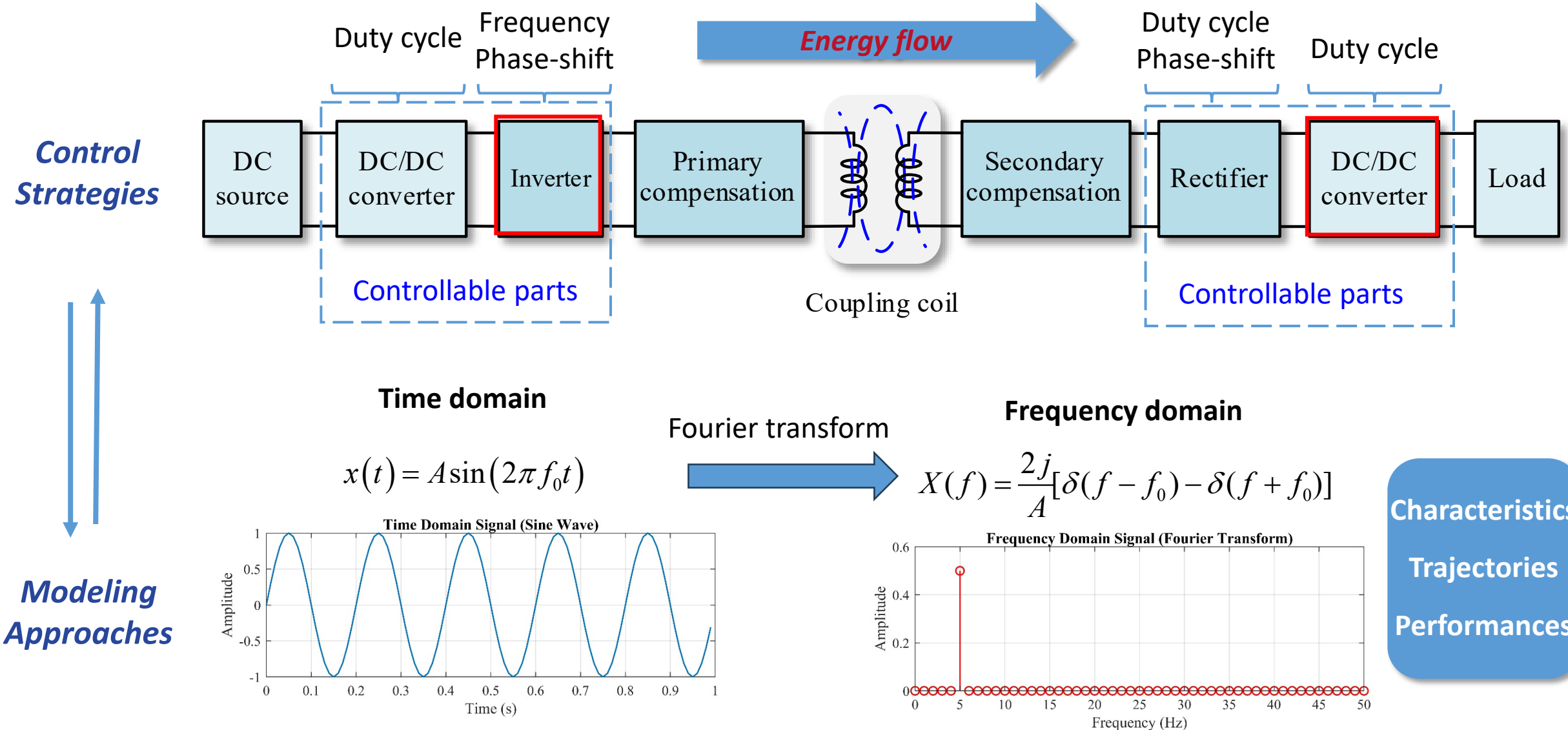
➤ Classification



➤ Overall structure block diagram of the IPT system



Research Motivation



01

Background and Motivation

02

Modeling and Control for Stationary WPT

03

Modeling and Control for Dynamic WPT

04

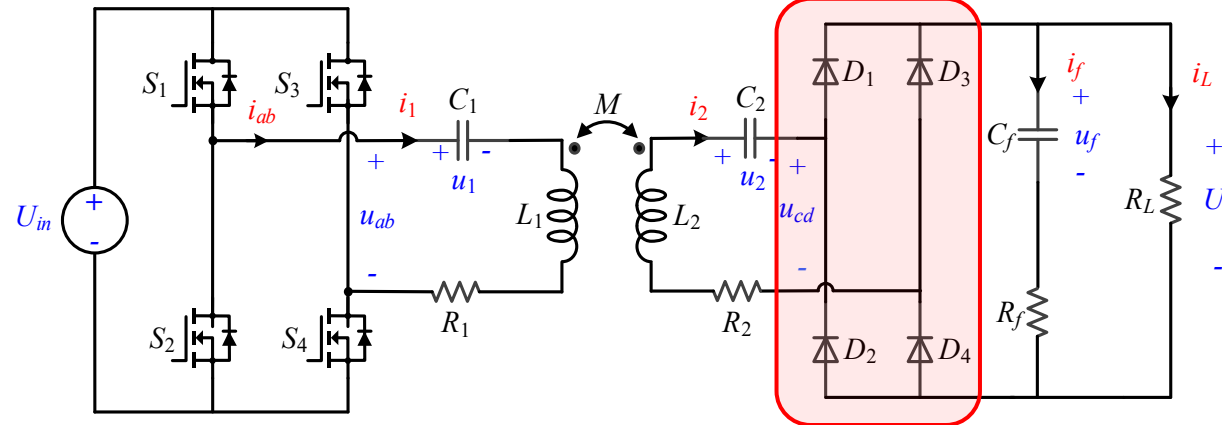
MHz WPT in Biomedical Application

05

Conclusion and Future Outlook

Unified Full-load Discrete-time Model

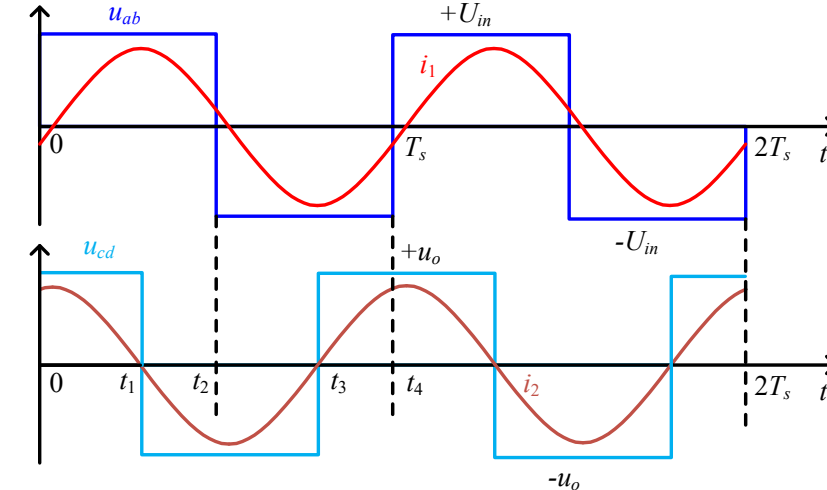
Equivalent circuit of the S-S compensated WPT system



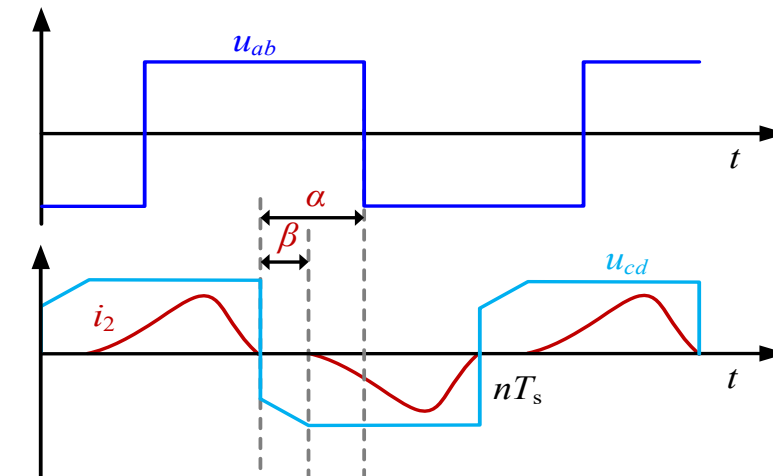
- At the **heavy load**, the rectifier works at the continuous conduction mode (**CCM**), and the fundamental harmonic is predominant in the system.
- At the **light load**, the rectifier works at the discontinuous conduction mode (**DCM**), and the IPT system contains rich harmonics. The high-order harmonics should be considered in the model to get high accuracy.

[1] T. Ma, C. Jiang, J. Xiang, X. Wang, K. T. Chau, and T. Long, "Modeling and Analysis of Wireless Power Transfer System Via Unified Full-Load Discrete-Time Model," in *IEEE Transactions on Industrial Electronics*, vol. 70, no. 6, pp. 5626-5636, June 2023.

Main waveforms at **heavy load**

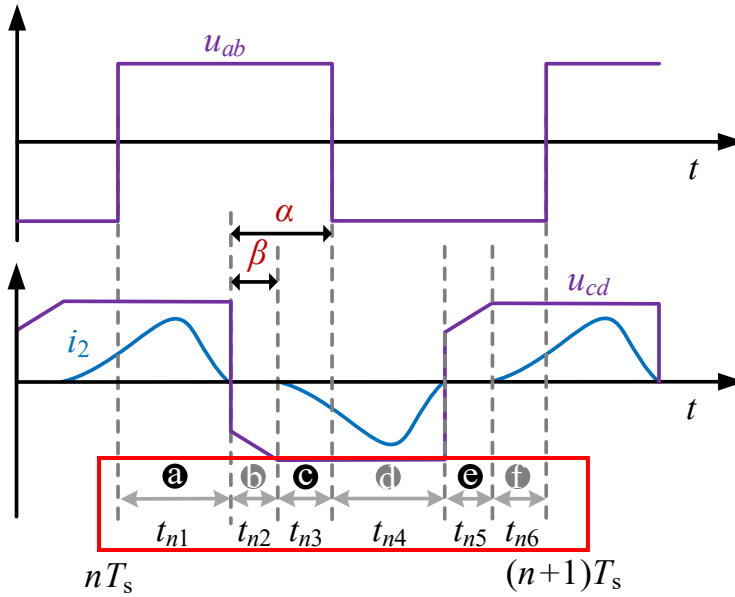


Main waveforms at **light load**



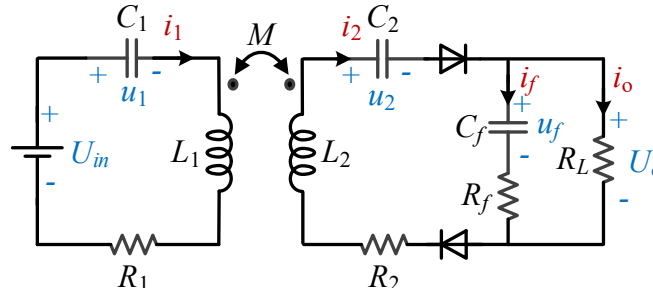
Unified Full-load Discrete-time Model

Main waveforms at **light load**

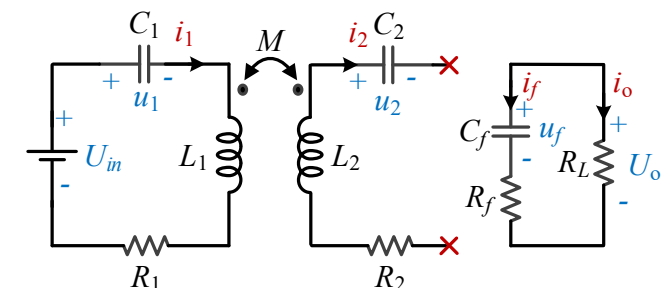


- Each switching cycle consists of **six state intervals** for DCM, i.e., state interval a-f, and the time duration of each state interval is $t_{n1}-t_{n6}$. As for the CCM, two state intervals will disappear because their time durations are 0.

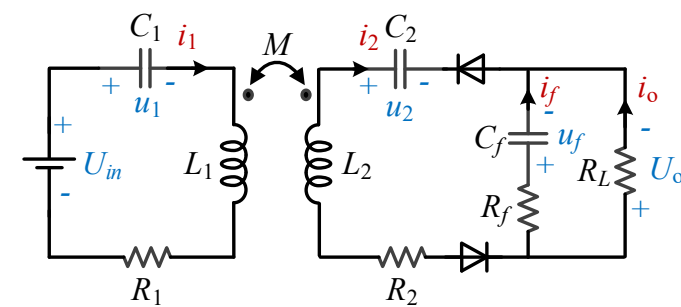
State interval a: $u_{ab} > 0, i_2 > 0$.



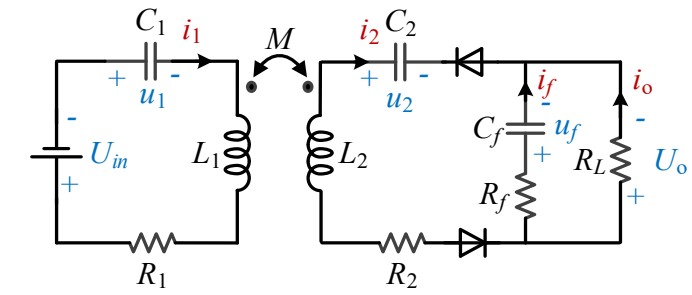
State interval b: $u_{ab} > 0, i_2 = 0$.



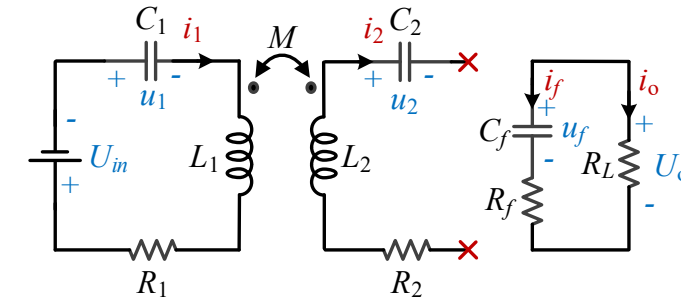
State interval c: $u_{ab} > 0, i_2 < 0$.



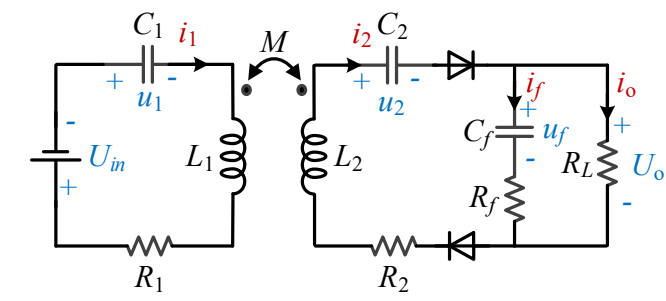
State interval d: $u_{ab} < 0, i_2 < 0$.



State interval e: $u_{ab} < 0, i_2 = 0$.



State interval f: $u_{ab} < 0, i_2 > 0$.



Unified Full-load Discrete-time Model

- The state equation of **each state interval** can be easily obtained, i.e.,

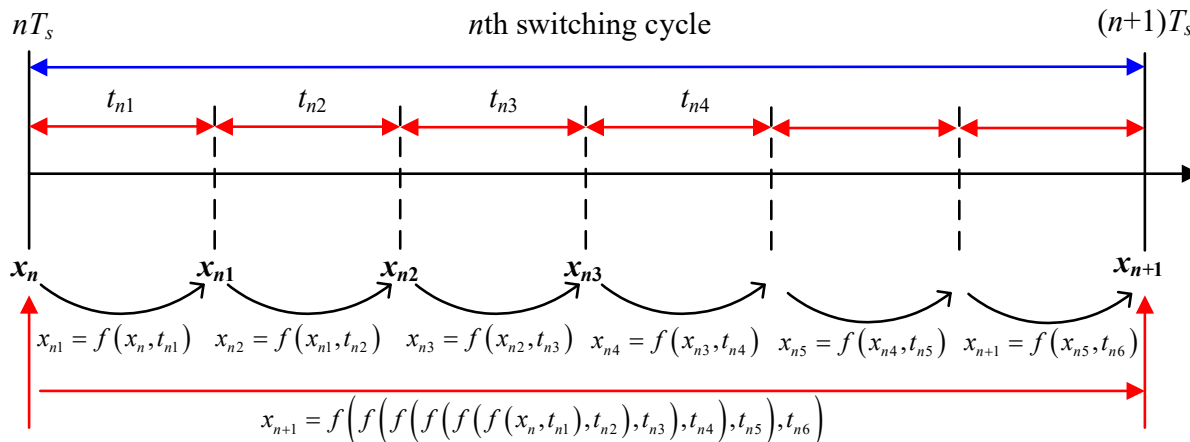
$$\frac{dx(t)}{dt} = A_i x(t) + B_i U_{in}$$

where the state vector is defined as $x = [i_1, i_2, u_1, u_2, u_f]^T$, and the number i corresponds to different state intervals.

- The state equation yields the following solution, i.e.,

$$x(t) = e^{A_i(t-t_0)} x(t_0) + \int_{t_0}^t e^{A_i(t-\tau)} B_i U_{in} d\tau$$

$$x(t) = e^{A_i(t-t_0)} x(t_0) + A_i^{-1} (e^{A_i(t-t_0)} - I) B_i U_{in} \quad (\text{System matrix is invertible})$$



- The state equation of **each switching cycle** can be derived by iterating state equations of six state intervals, i.e.,

$$x_{n+1} = F_{UF} x_n + G_{UF} U_{in}$$

The steady-state model:

$$X_{ss} = (I - F_{UF})^{-1} G_{UF} U_{in}$$

where

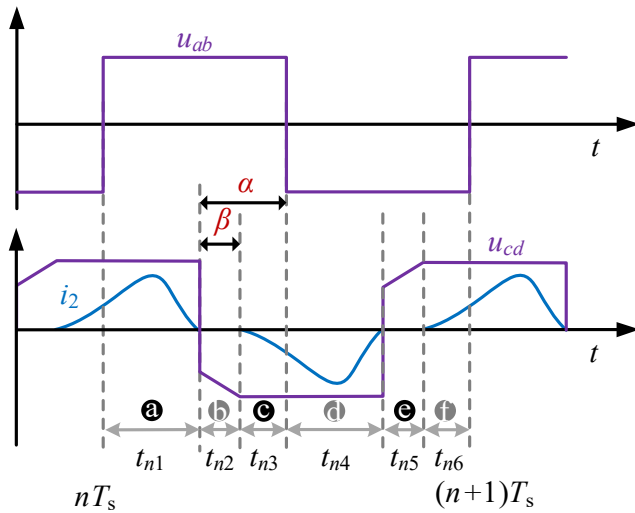
$$\begin{aligned} F_{UF} &= e^{A_6 t_{n6}} e^{A_5 t_{n5}} e^{A_4 t_{n4}} e^{A_3 t_{n3}} e^{A_2 t_{n2}} e^{A_1 t_{n1}} \\ G_{UF} &= e^{A_6 t_{n6}} e^{A_5 t_{n5}} e^{A_4 t_{n4}} e^{A_3 t_{n3}} e^{A_2 t_{n2}} A_1^{-1} (e^{A_1 t_{n1}} - I) B_1 \\ &\quad + e^{A_6 t_{n6}} e^{A_5 t_{n5}} e^{A_4 t_{n4}} e^{A_3 t_{n3}} \int_0^{t_{n2}} e^{A_2(t_{n2}-\tau)} B_2 d\tau \\ &\quad + e^{A_6 t_{n6}} e^{A_5 t_{n5}} e^{A_4 t_{n4}} A_3^{-1} (e^{A_3 t_{n3}} - I) B_3 \\ &\quad + e^{A_6 t_{n6}} e^{A_5 t_{n5}} A_4^{-1} (e^{A_4 t_{n4}} - I) B_4 \\ &\quad + e^{A_6 t_{n6}} \int_0^{t_{n5}} e^{A_5(t_{n5}-\tau)} B_5 d\tau \\ &\quad + A_6^{-1} (e^{A_6 t_{n6}} - I) B_6 \end{aligned}$$

Output voltage: $U_o = \frac{R_L R_f}{R_L + R_f} i_2 + \frac{R_L}{R_L + R_f} u_f$

Unified Full-load Discrete-time Model

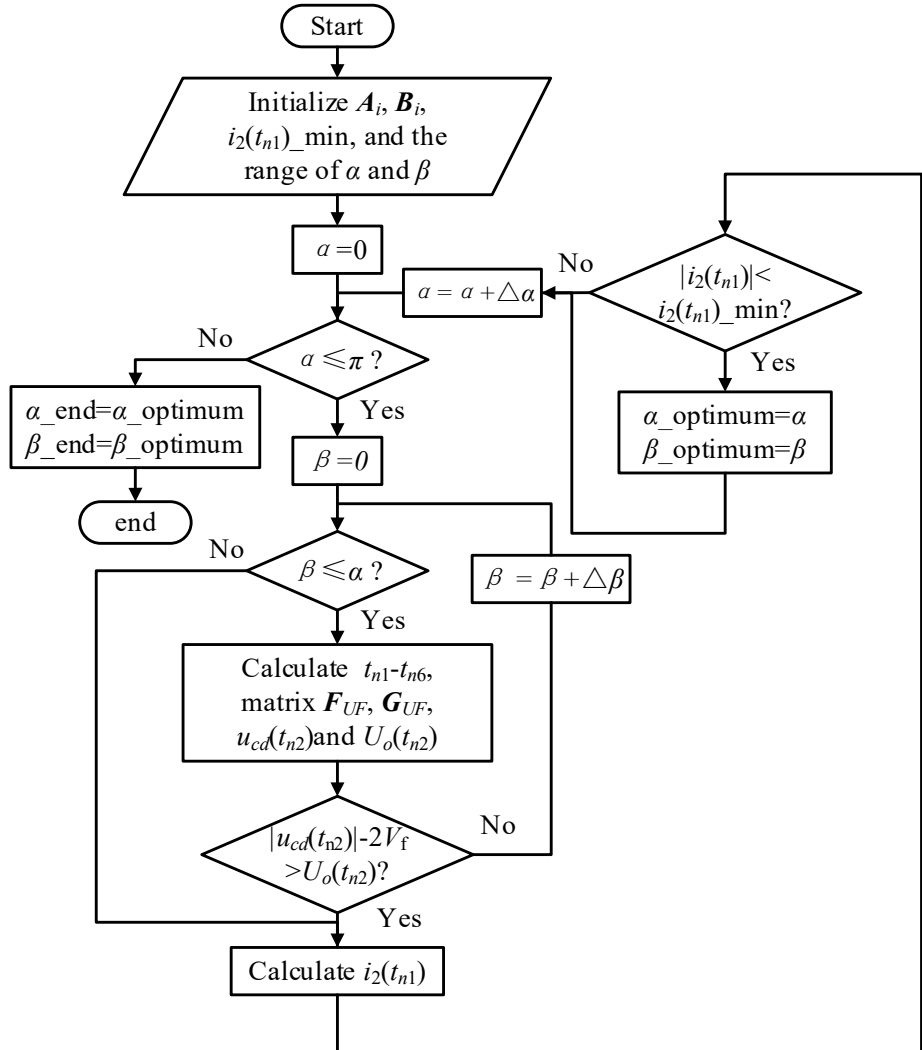
➤ Solutions of State Interval Durations

| Categories | t_{n1} and t_{n4} | t_{n2} and t_{n5} | t_{n3} and t_{n6} |
|------------|--------------------------------|-----------------------------|--------------------------------------|
| Case 1 | $(\pi - \alpha) / (2\pi)T_s$ | $\beta / (2\pi)T_s$ | $(\alpha - \beta) / (2\pi)T_s$ |
| Case 2 | $(\beta - \alpha) / (2\pi)T_s$ | $(\pi - \beta) / (2\pi)T_s$ | $\alpha / (2\pi)T_s$ |
| Case 3 | $-\alpha / (2\pi)T_s$ | $\beta / (2\pi)T_s$ | $(\pi + \alpha - \beta) / (2\pi)T_s$ |
| Case 4 | $(\pi + \alpha) / (2\pi)T_s$ | $(\pi - \beta) / (2\pi)T_s$ | $(\beta - \alpha - \pi) / (2\pi)T_s$ |



- The outer loop is α , and the inner loop is β . Two important loop judgment indicators are:
 - $|u_{cd}(t_{n2})| - 2V_f > U_o(t_{n2})$;
 - $|i_2(t_{n1})| = |\min(i_2(t_{n1}))|$.

Algorithm execution to solve α and β in Case 1.

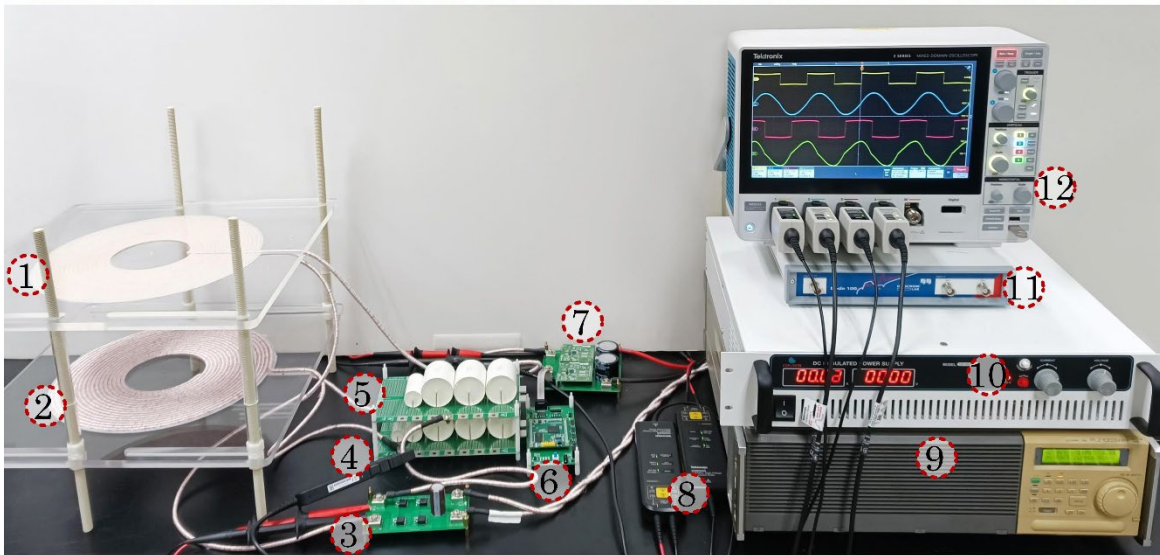


Unified Full-load Discrete-time Model

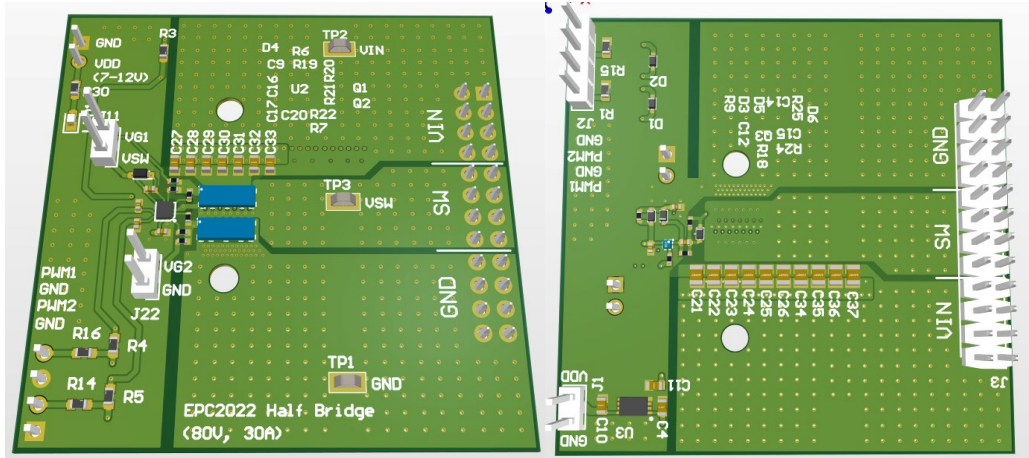
➤ Model Validation

Experimental setup of the WPT system

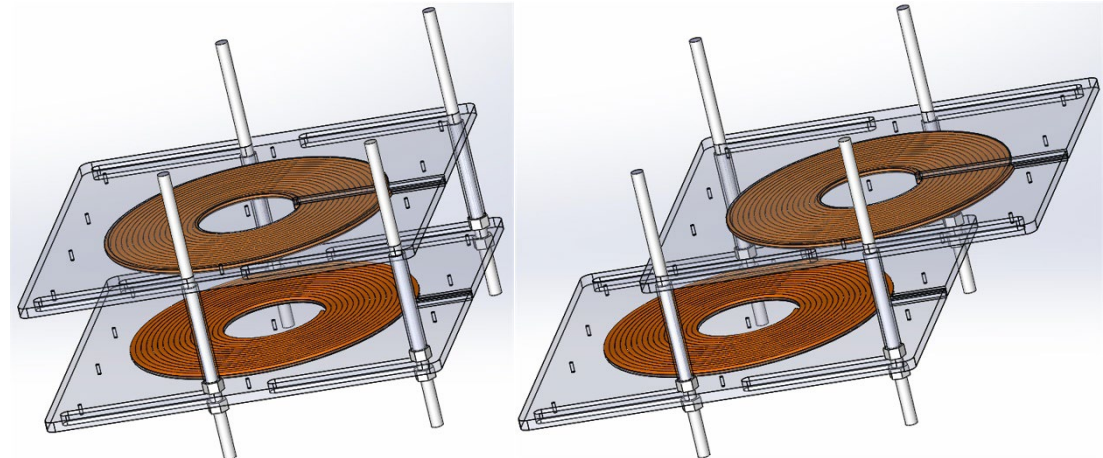
- 1. Transmitter pad
- 2. Receiver pad
- 3. Passive rectifier
- 4. Current probes
- 5. Compensated capacitors
- 6. DSP controller
- 7. H-bridge inverter
- 8. Voltage probes
- 9. DC electronic load
- 10. DC power supply
- 11. Network analyzer
- 12. Oscilloscope



A universal half-bridge inverter (4-layer PCB)

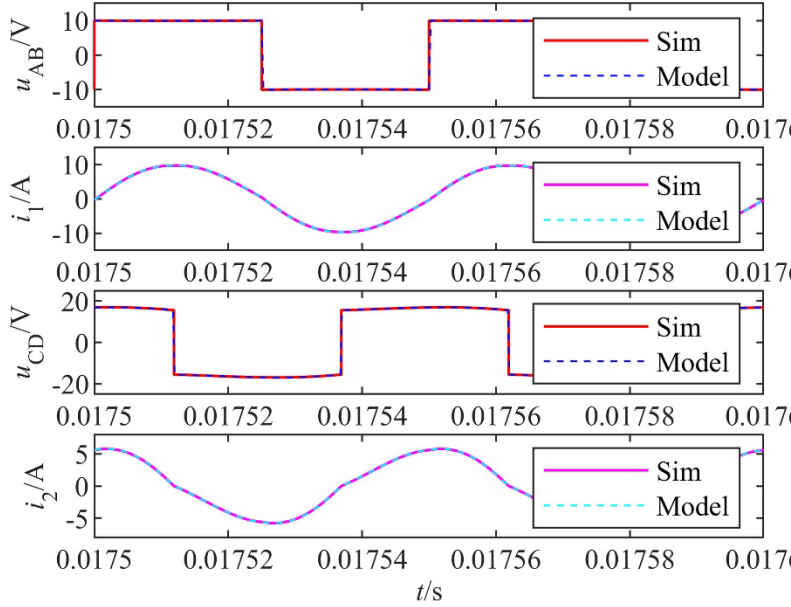
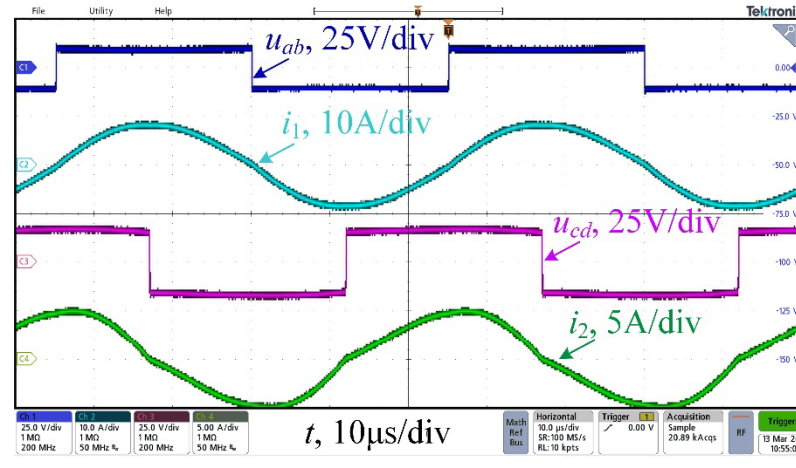


3D drawing of coupling coil

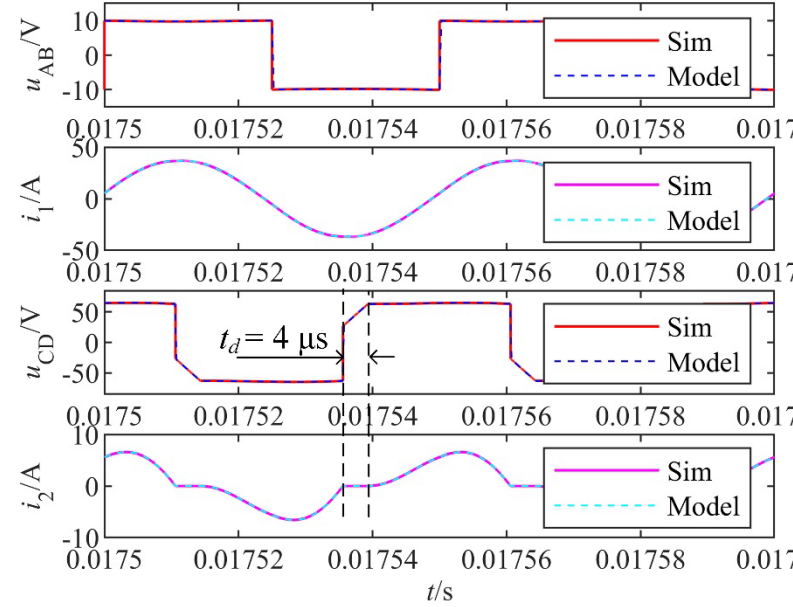
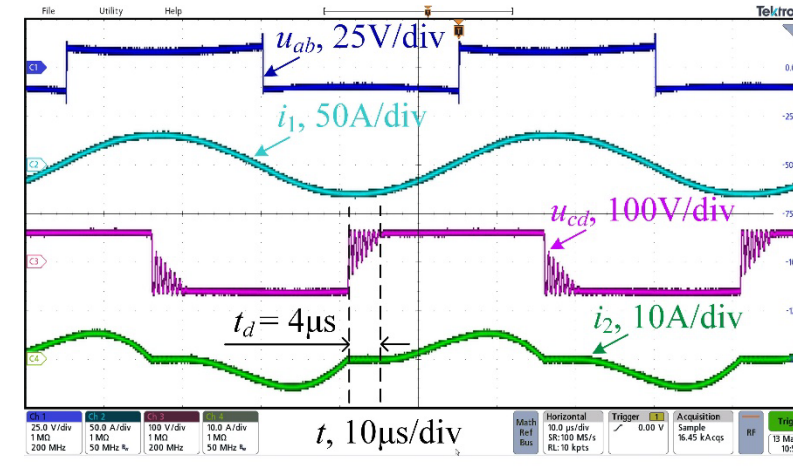


Unified Full-load Discrete-time Model

CCM, $R_L = 4 \Omega$



DCM, $R_L = 20 \Omega$

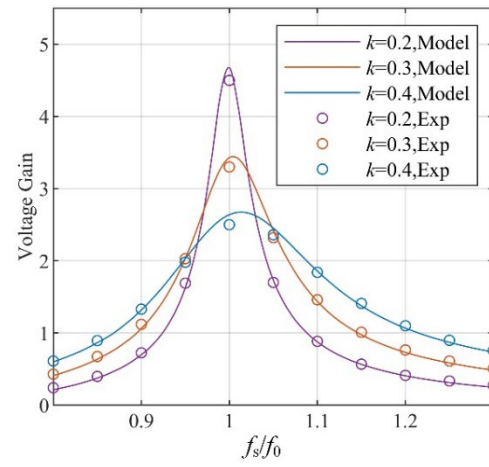
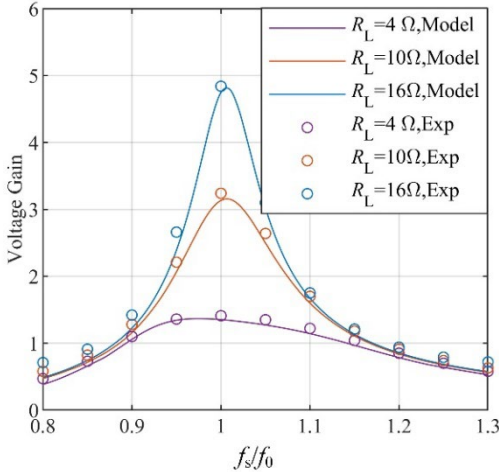


- The UFDT model's results are also consistent with the experiments and simulations, including the amplitude of the voltage and current.

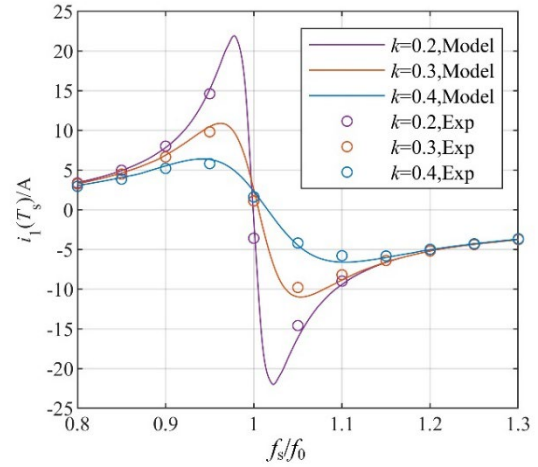
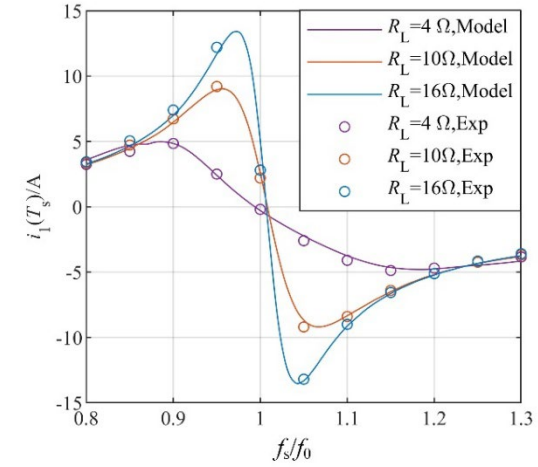
- The discontinuous conduction time in the UFDT model is also 4 μs.

Unified Full-load Discrete-time Model

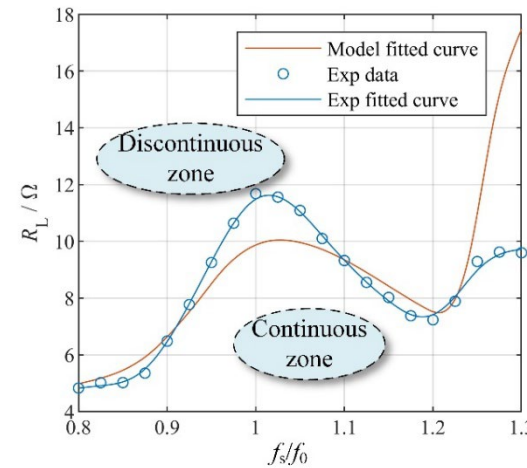
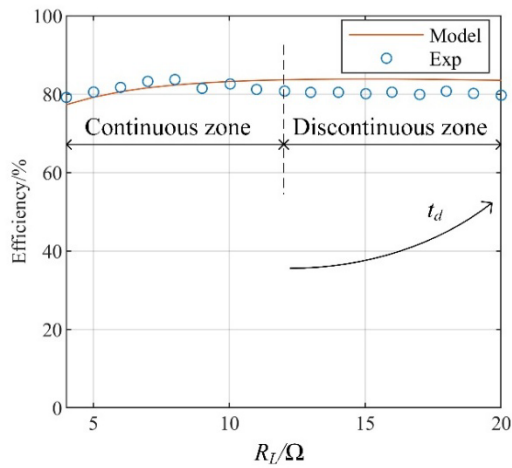
Voltage gains versus the switching frequency.



Inverter output current i_1 at $t = nT_s$. (ZVS range)



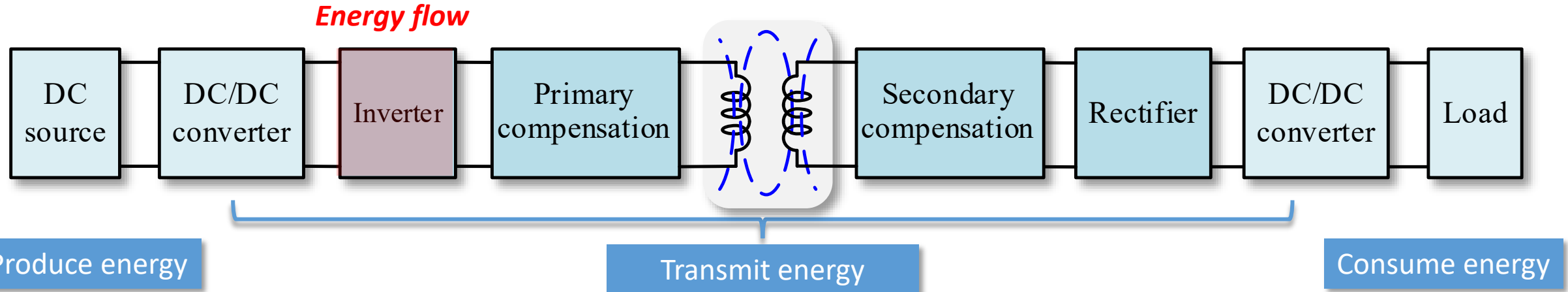
Comparative features of CCM and DCM.



- The results prove that the established model is accurate.
- The efficiency curve changes continuously between CCM and DCM, and the discontinuous conduction time will be enlarged as the load resistor increases.
- The influence of load resistance and switching frequency on the CCM and DCM boundaries obtained by the model can also be reflected in the experimental measurement results.

[1] T. Ma, C. Jiang, J. Xiang, X. Wang, K. T. Chau, and T. Long, "Modeling and Analysis of Wireless Power Transfer System Via Unified Full-Load Discrete-Time Model," in *IEEE Transactions on Industrial Electronics*, vol. 70, no. 6, pp. 5626-5636, June 2023.

Periodic Energy Control for SWPT Systems



❖ How to achieve energy control?

➤ **Direct method:** Integration calculation

$$E_{AB}(t) = \int_0^t u_{AB}(\xi) i_{AB}(\xi) d\xi$$

- Huge computational burden
- Low system robustness

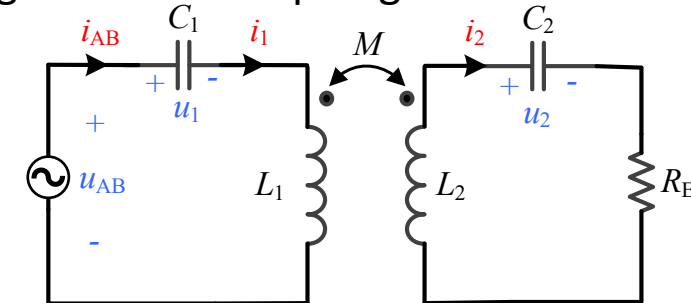


➤ **Simplified method:** Calculation energy using features of topologies.

$$E_{AB}(T) = \int_0^T u_{AB}(\xi) i_{AB}(\xi) d\xi = 2U_{in} \int_0^{\frac{1}{2}T} i_{AB}(\xi) d\xi$$

$$i_{AB} = i_1 = C_1 \frac{du_1}{dt}$$

$$E_{AB}(T) = 2U_{in} C_1 (U_{1_PN} - U_{1_NP})$$

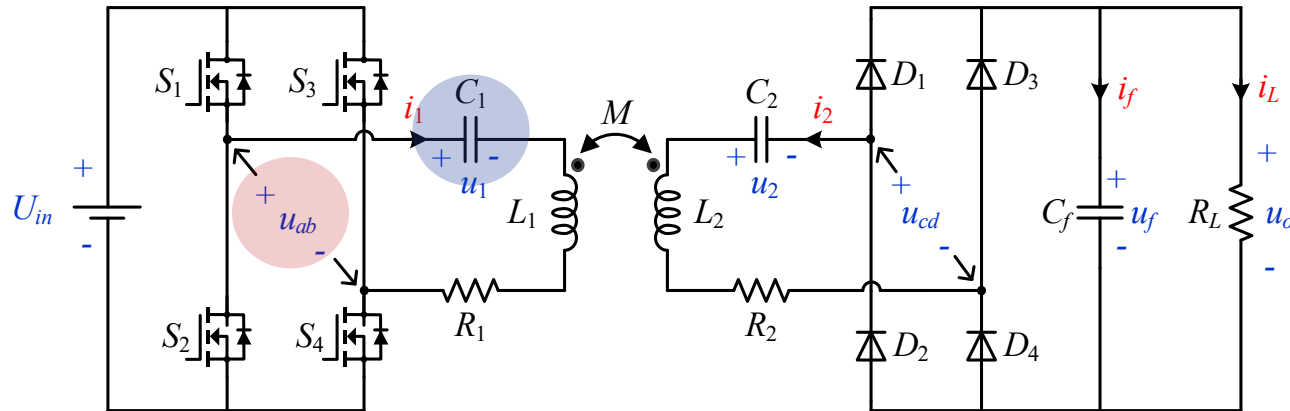


Equivalent circuit of SS-compensated WPT system

[2] T. Ma, Y. Wang, X. Hu, D. Zhao, Y. Jiang, and C. Jiang, "Periodic Energy Control for Wireless Power Transfer System," in *IEEE Transactions on Power Electronics*, vol. 37, no. 4, pp. 3775-3780, April 2022.

Periodic Energy Control for SWPT Systems

- The implementation of PEC in the SS-compensated WPT system.

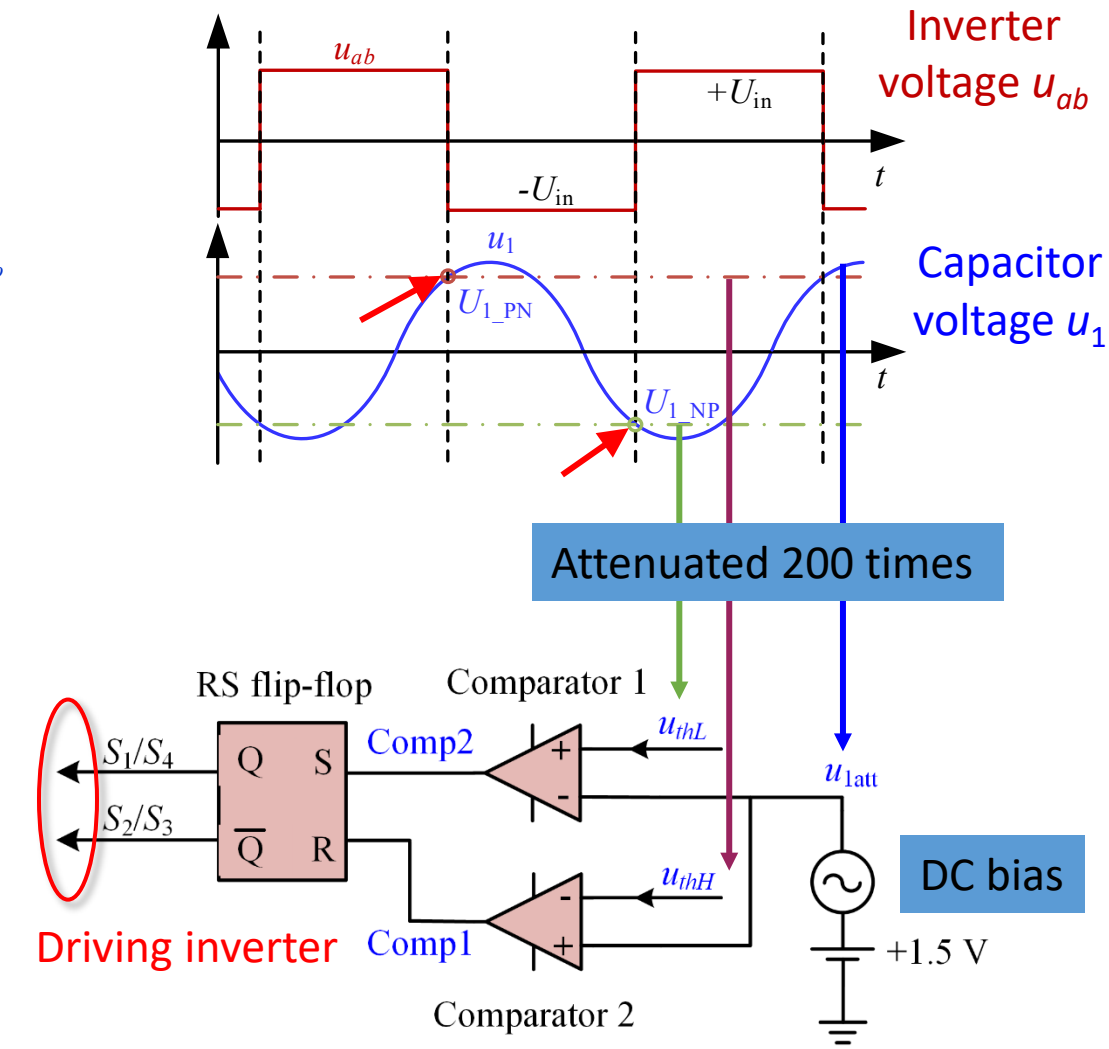


➤ The energy through the inverter in each cycle:

$$E_{AB}(T) = 2U_{in}C_1(U_{1_PN} - U_{1_NP})$$

- U_{1_PN} : The value of the capacitor voltage u_1 at the moment when the inverter voltage u_{ab} switches from positive to negative.
- U_{1_NP} : The value of the capacitor voltage u_1 at the moment when the inverter voltage u_{ab} switches from negative to positive.

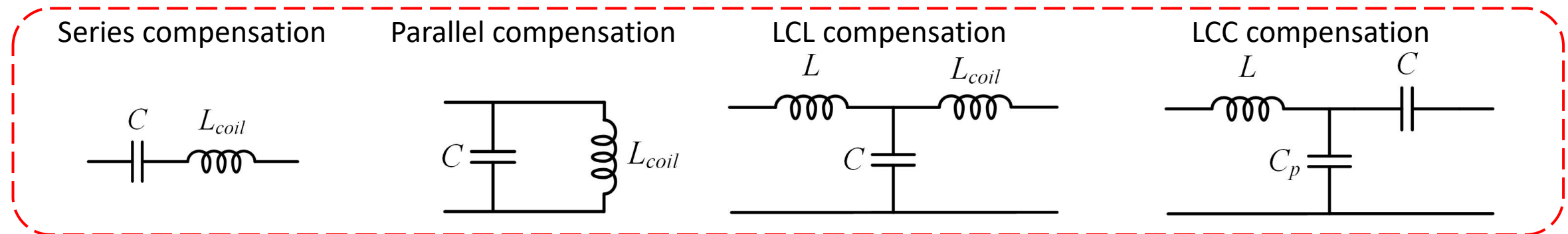
- Two threshold voltages are given by DSP based on the target port energy, and the driving signals of the inverter will be generated through two comparators and one RS flip-flop.



Periodic Energy Control for SWPT Systems

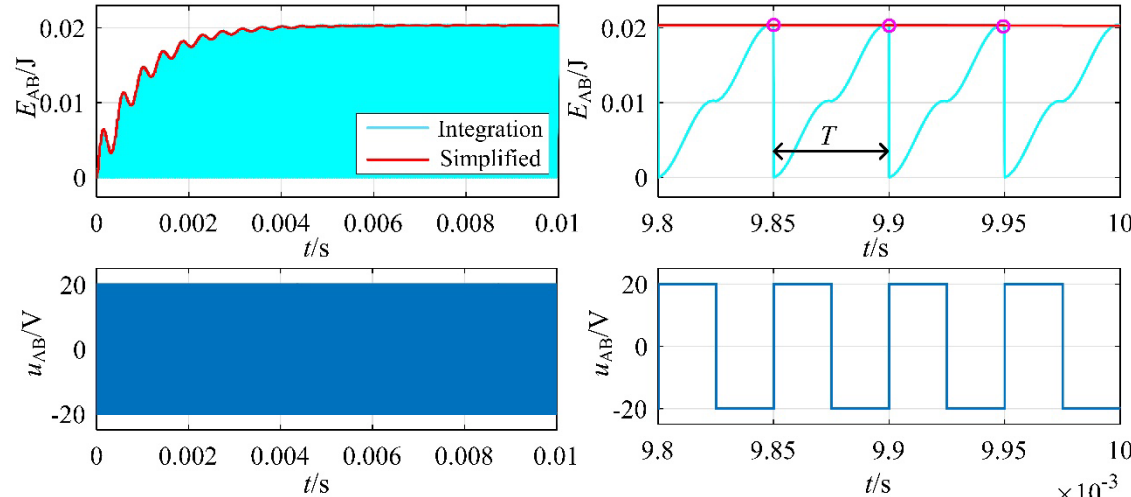
- The calculation of energy out of the inverter for **different compensation networks** of WPT systems.

| DC source type | Primary compensation topology | Secondary compensation topology | Energy out of the inverter |
|----------------|-------------------------------|---------------------------------|--|
| Voltage source | Series | Any topologies | $2U_{\text{in}} C_1 (U_{1_PN} - U_{1_NP})$ |
| | | Any topologies | $2U_{\text{in}} [C_1 (U_{1_PN} - U_{1_NP}) + C_p (U_{p_PN} - U_{p_NP})]$ |
| | LCL | Series | $2U_{\text{in}} [(C_1 - 1/\omega_s^2 L_1)(U_{p_PN} - U_{p_NP}) + MC_2/L_1 \cdot (U_{2_PN} - U_{2_NP})]$ |
| | | Parallel | $2U_{\text{in}} \left[\left(C_p - \frac{L_2}{\omega_s^2 (L_1 L_2 - M^2)} \right) (U_{p_PN} - U_{p_NP}) + \frac{M}{\omega_s^2 (L_1 L_2 - M^2)} (U_{s_PN} - U_{s_NP}) \right]$ |
| | | LCL | |
| Current source | Parallel | Any topologies | $2I_{\text{in}} [L_1 (I_{1_PN} - I_{1_NP}) - M (I_{2_PN} - I_{2_NP})]$ |

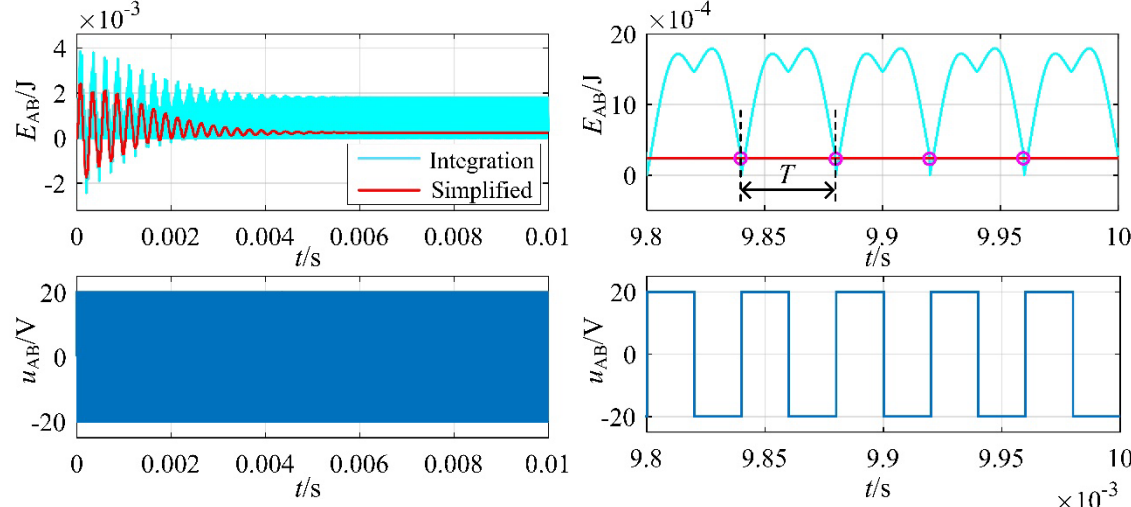


Periodic Energy Control for SWPT Systems

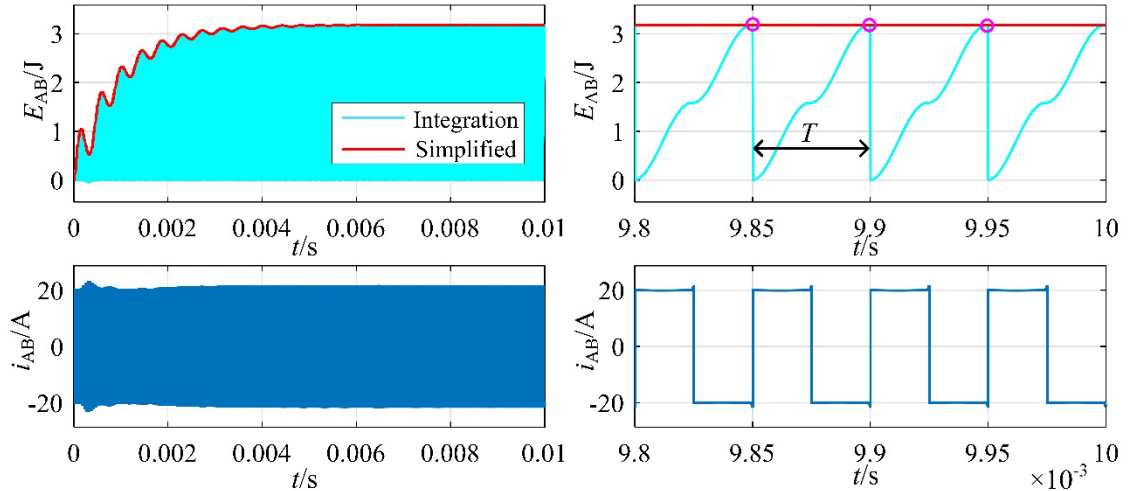
- SS compensation, $f_s = f_0$; DC source: Voltage source



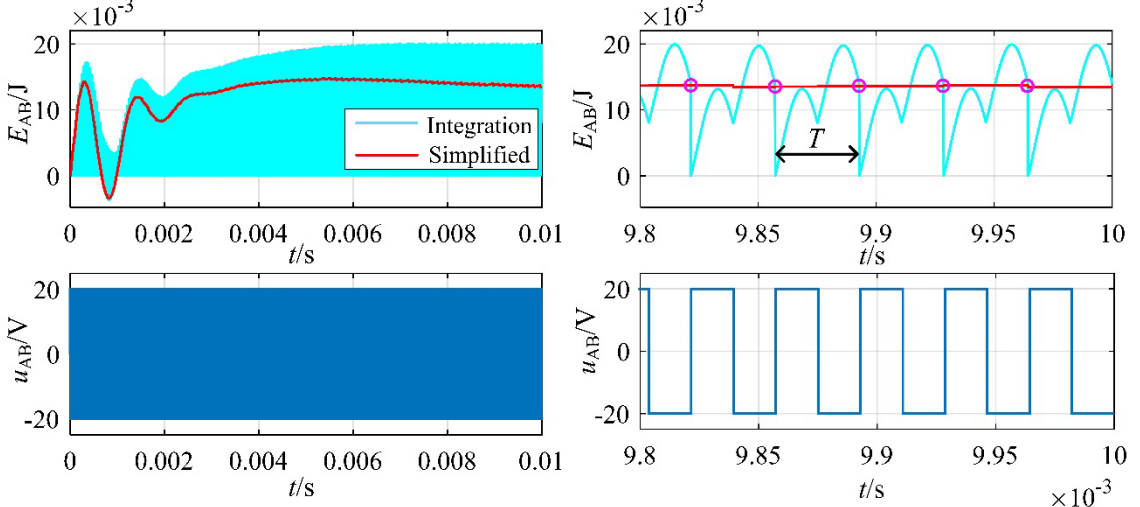
- LCL-S compensation, $f_s = f_0$; DC source: Voltage source



- PS compensation, $f_s = f_0$; DC source: Current source



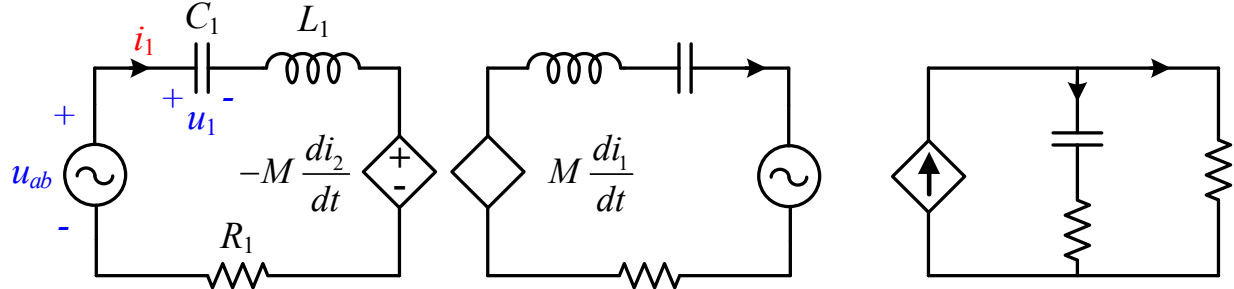
- LCL-S compensation, $f_s = 1.12f_0$; DC source: Voltage source



Characteristics of PEC -- Mathematical Model

- The extended describing function (EDF) model of PEC is built first in the SS-compensated WPT system.

- The equivalent circuit of the SS-compensated WPT system

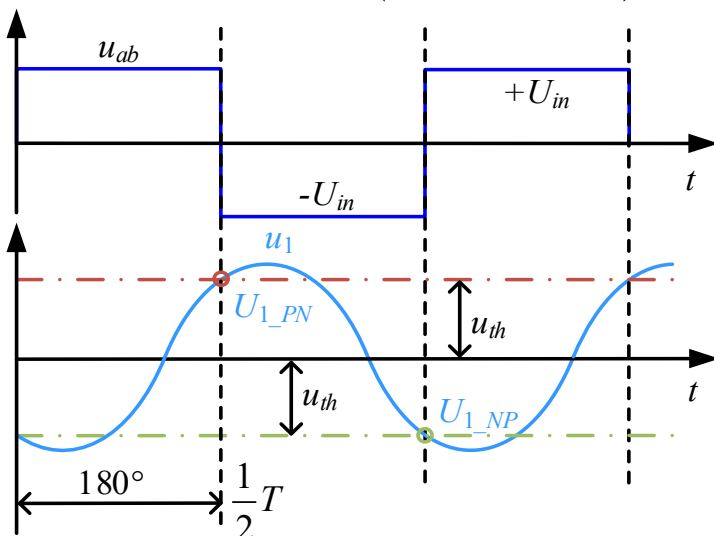


- EDF method: sine item + cosine item

$$\begin{aligned}x(t) &= A(t) \sin(\omega_s t + \theta) \\x(t) &= x_s(t) \sin(\omega_s t) + x_c(t) \cos(\omega_s t) \\u_1(t) &= u_{1s} \sin(\omega_s t) + u_{1c} \cos(\omega_s t)\end{aligned}$$

The energy input to the resonant network:

$$E_m(T) = 2U_{in}C_1(U_{1_PN} - U_{1_NP})$$



$$\begin{cases} U_{1_PN} = u_1(t) \Big|_{t=\frac{T}{2}} = u_{1s} \sin\left(\frac{2\pi}{T} \cdot \frac{T}{2}\right) + u_{1c} \cos\left(\frac{2\pi}{T} \cdot \frac{T}{2}\right) = -u_{1c} \\ U_{1_NP} = u_1(t) \Big|_{t=T} = u_{1s} \sin\left(\frac{2\pi}{T} \cdot T\right) + u_{1c} \cos\left(\frac{2\pi}{T} \cdot T\right) = u_{1c} \end{cases}$$

Small-signal model: $u_{th} = C_u x$ $C_u = [0, 0, 0, 0, 0, -1, 0, 0, 0]$

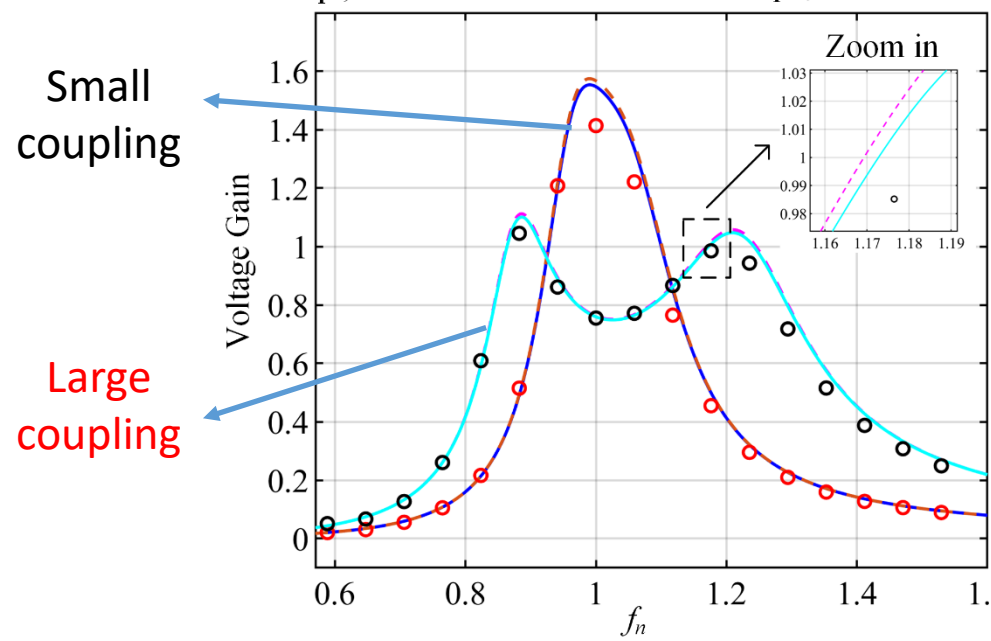
$$G_u(s) = \frac{\hat{u}_{th}}{\hat{\omega}_s} = C_u(sI - A)^{-1} B(:,1) \quad G_p(s) = \frac{\hat{u}_o}{\hat{u}_{th}} = \frac{G_f(s)}{G_u(s)} = \frac{C(sI - A)^{-1} B(:,1)}{C_u(sI - A)^{-1} B(:,1)}$$

[3] T. Ma, C. Jiang, Y. Zhang, Y. Wang, Y. Cheng, and S. Cui, "Modeling and Analysis of Periodic Energy Control for Series-Series Wireless Power Transfer System," in *IEEE Transactions on Power Electronics*, vol. 39, no. 4, pp. 4837-4849, April 2024.

Characteristics of PEC -- Mathematical Model

- Voltage gain of the SS-compensated by the EDF model and experiments with different coupling coefficients.

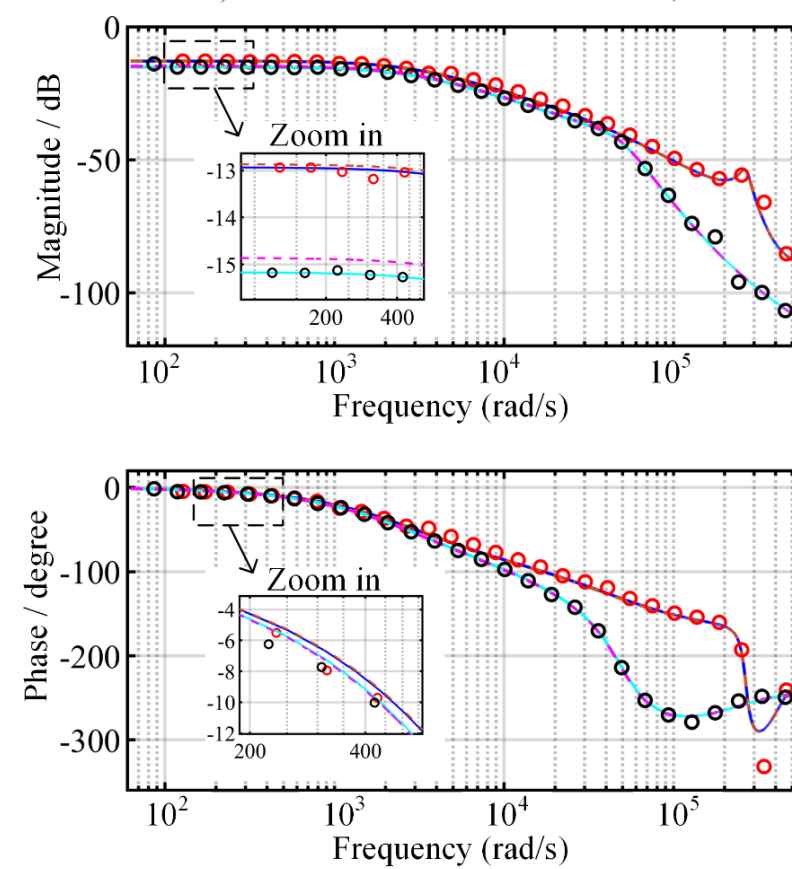
— Model with ESR, $k = 0.17$ — Model with ESR, $k = 0.35$
 - - - Model w/o ESR, $k = 0.17$ - - - Model w/o ESR, $k = 0.35$
 ○ Exp., $k = 0.17$ ○ Exp., $k = 0.35$



The EDF model of PEC is accurate considering the ESR of coils

- Frequency response of PEC by EDF model and MATLAB/ Simulink.

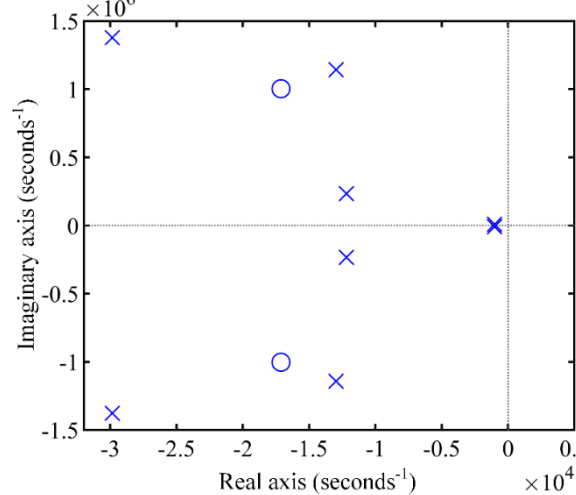
— Model with ESR, $k = 0.40$ — Model with ESR, $k = 0.10$
 - - - Model w/o ESR, $k = 0.40$ - - - Model w/o ESR, $k = 0.10$
 ○ Simulation, $k = 0.40$ ○ Simulation, $k = 0.10$



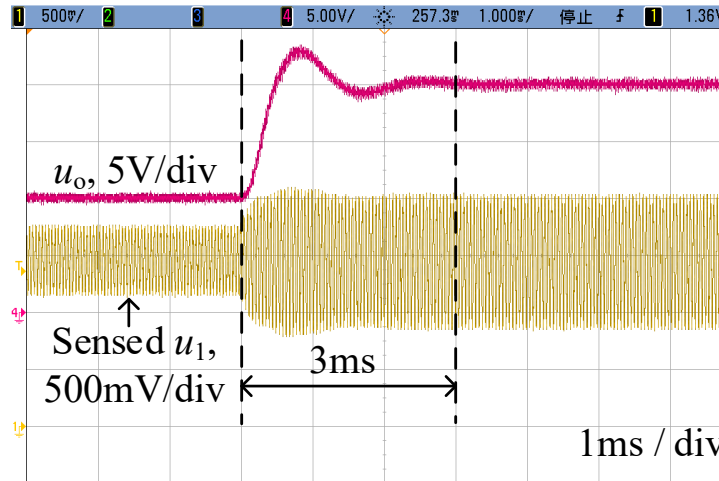
Characteristics of PEC -- Fast Dynamic Response

Variable frequency control (VFC)

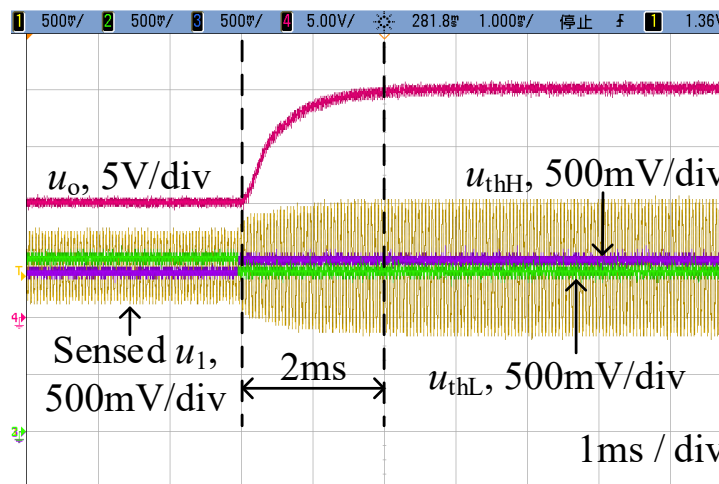
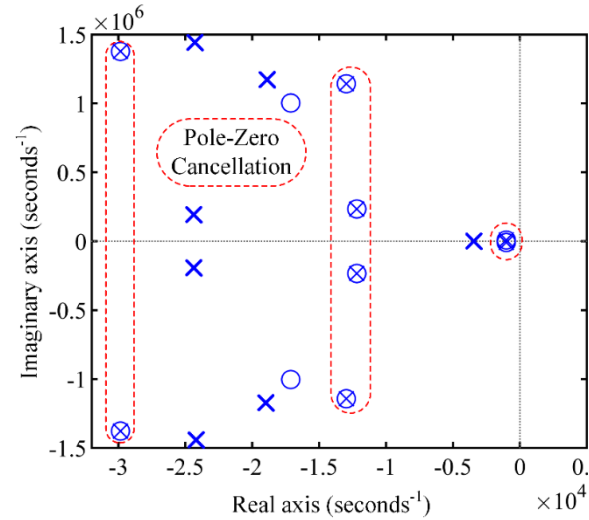
Pole-zero maps by the EDF model
(Frequency domain)



Dynamic response by experiments
(Time domain)



PEC

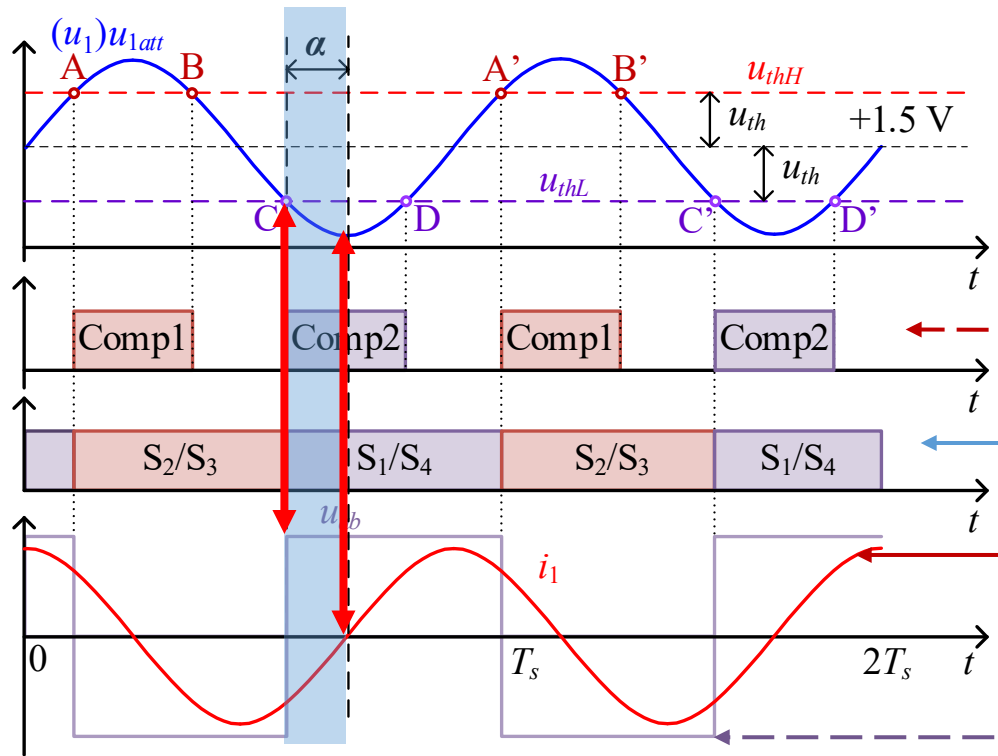


❑ Pole-zero cancellation occurs in PEC (The area circled in red). As a result, the dominant poles are farther from the imaginary axis, which is beneficial to improving the system's dynamic response.

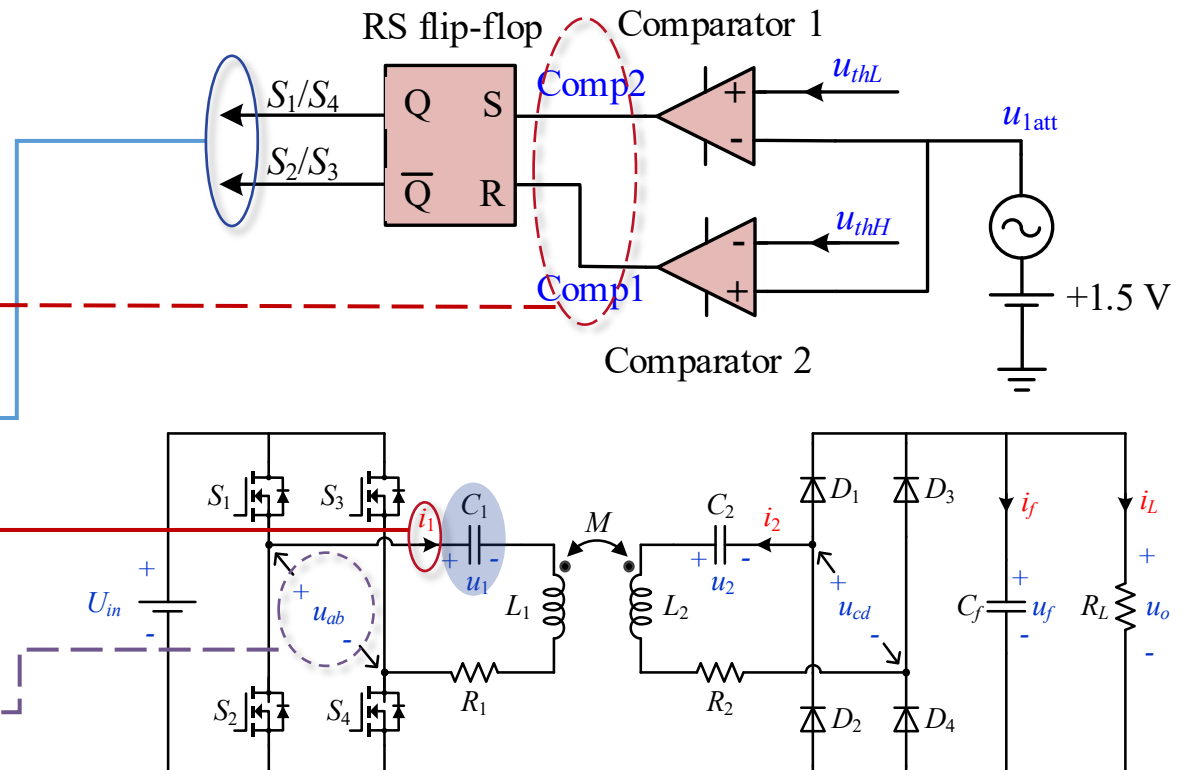
❑ The experiments illustrate PEC has a fast dynamic response without overvoltage.

Characteristics of PEC -- ZVS Operation

- Main signals of the WPT system using PEC



- Main driving circuit of the WPT system using PEC



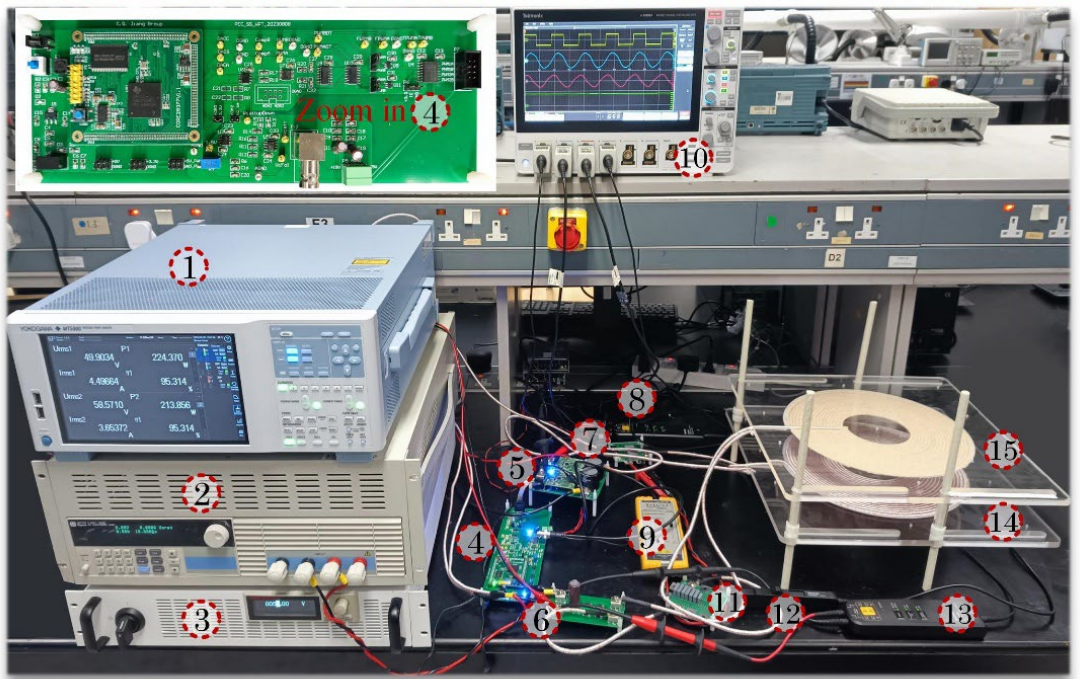
- The phase of current i_1 lags the phase of u_{ab} , and the driving circuit determines that PEC meets the ZVS conditions.

ZVS operation is met always!

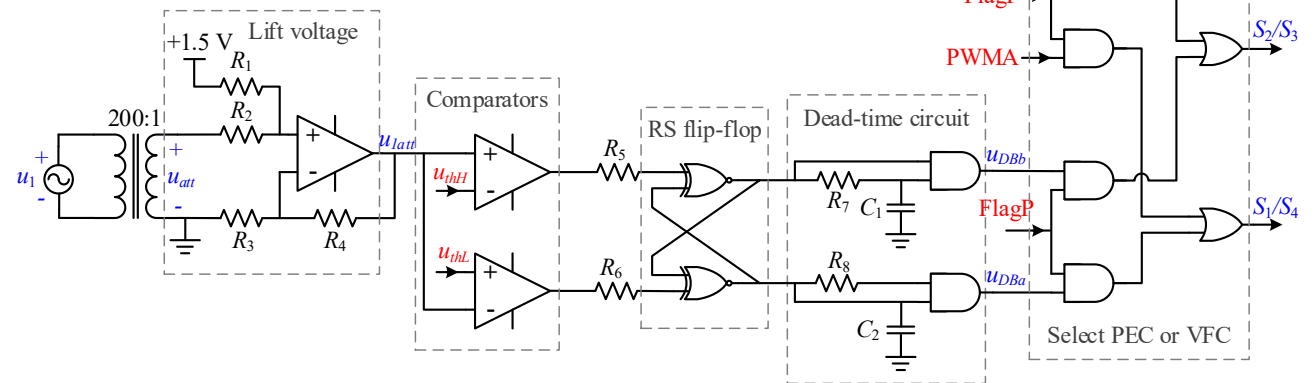
Characteristics of PEC -- Experiment Verification

Experimental setup of PEC

- | | | |
|-------------------------|--------------------|-----------------------|
| 1. Power analyzer | 6. Rectifier | 11. Capacitor C_2 |
| 2. Electronic load | 7. Capacitor C_1 | 12. Current probe |
| 3. DC power supply | 8. Voltage probe | 13. Voltage probe |
| 4. Driving circuit | 9. Voltage probe | 14. Transmitting coil |
| 5. Full-bridge inverter | 10. Oscilloscope | 15. Receiving coil |



Driving circuit



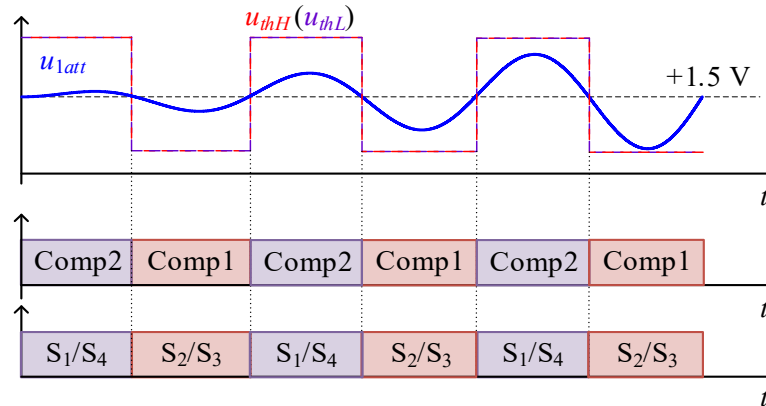
Driving circuit board of periodic energy control.



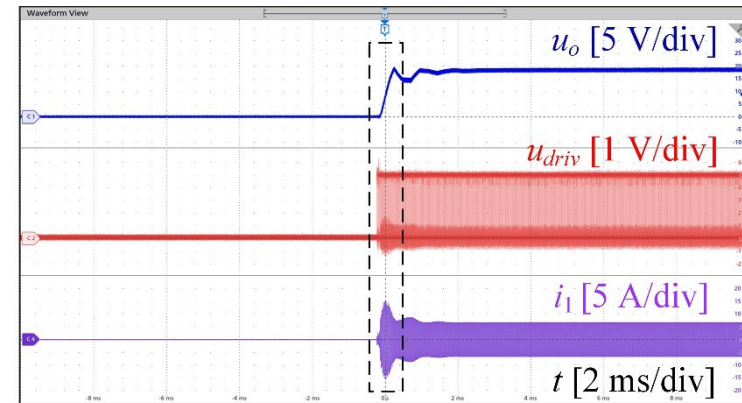
- | |
|--------------------------|
| 1. Digital isolation |
| 2. PWM channel selection |
| 3. Driving circuit |
| 4. Voltage interface |
| 5. Voltage boost circuit |
| 6. TMS320F28377D |
| 7. Power isolation |

Characteristics of PEC -- Experiment Verification

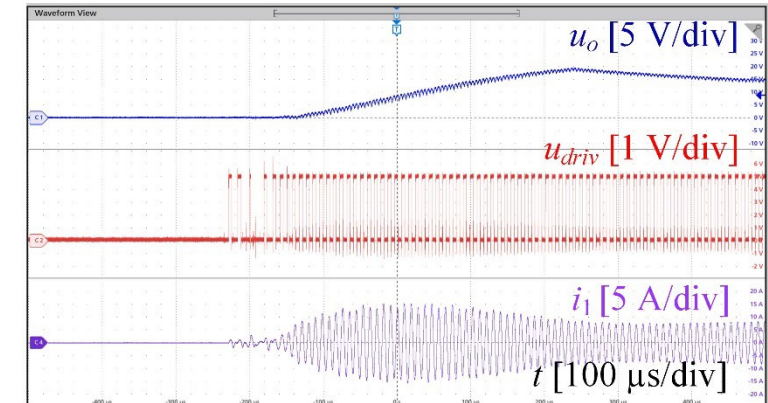
➤ PEC startup operation



Main waveforms of PEC startup process

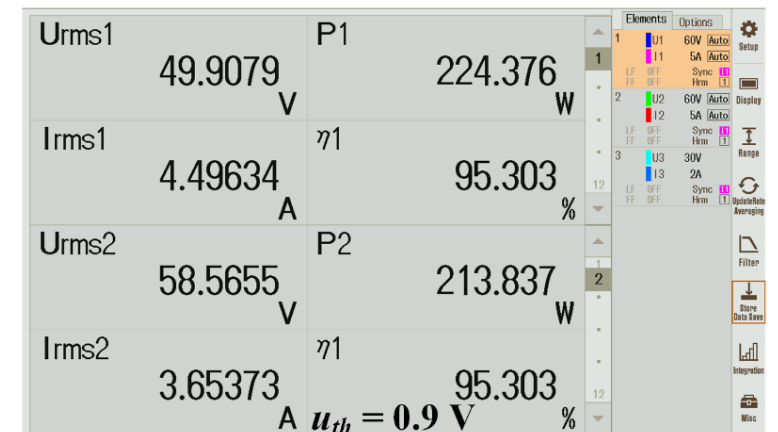
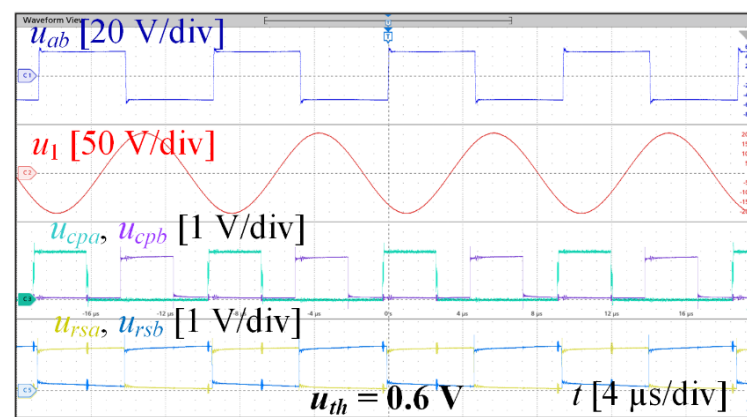
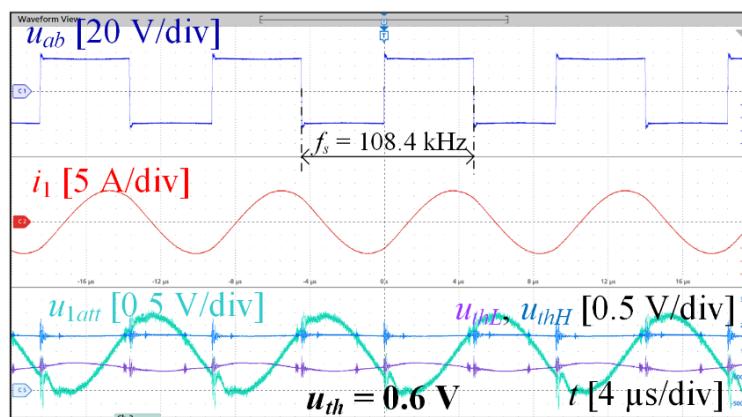


Overall waveforms during startup



Zoomed waveforms during startup

➤ Steady-state waveforms



01

Background and Motivation

02

Modeling and Control for Stationary WPT

03

Modeling and Control for Dynamic WPT

04

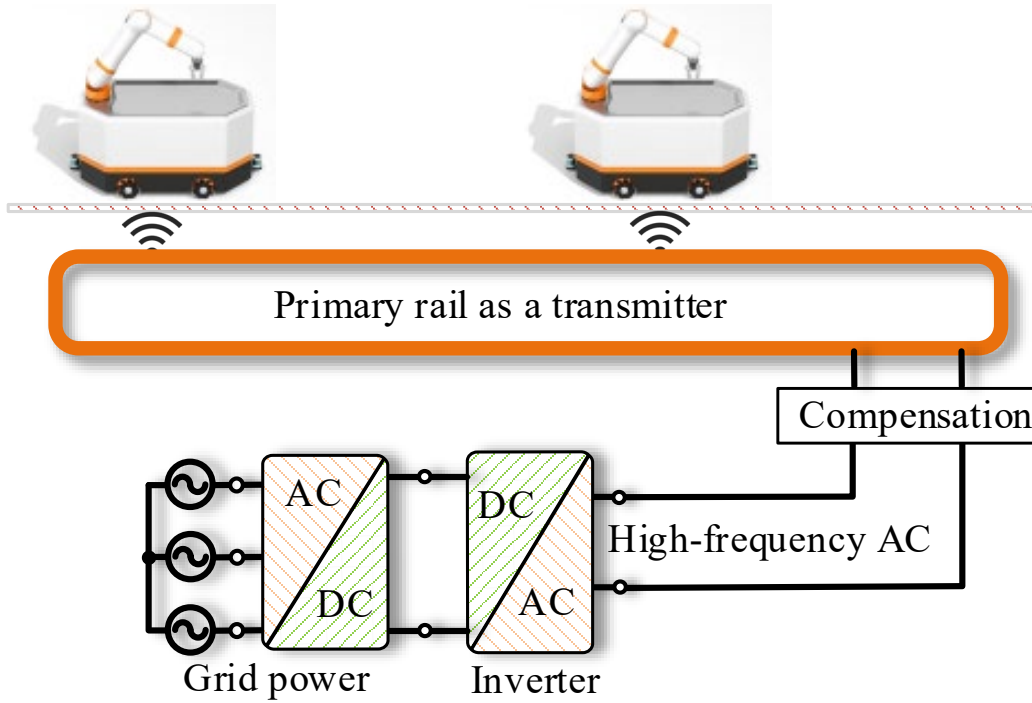
MHz WPT in Biomedical Application

05

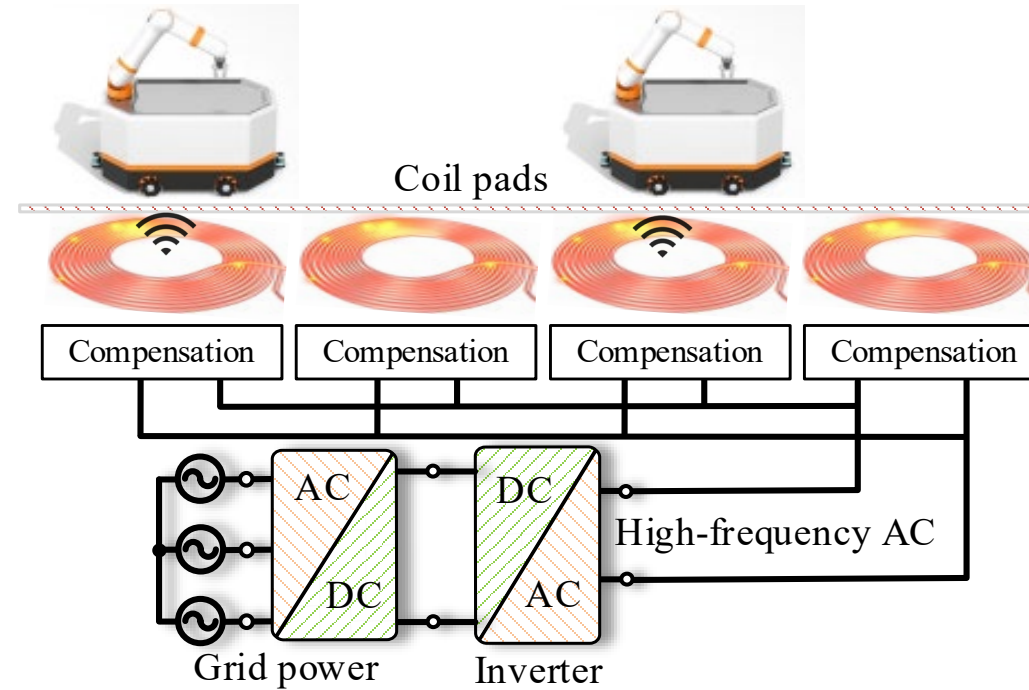
Conclusion and Future Outlook

Classification of DWPT Systems

Long-track DWPT System



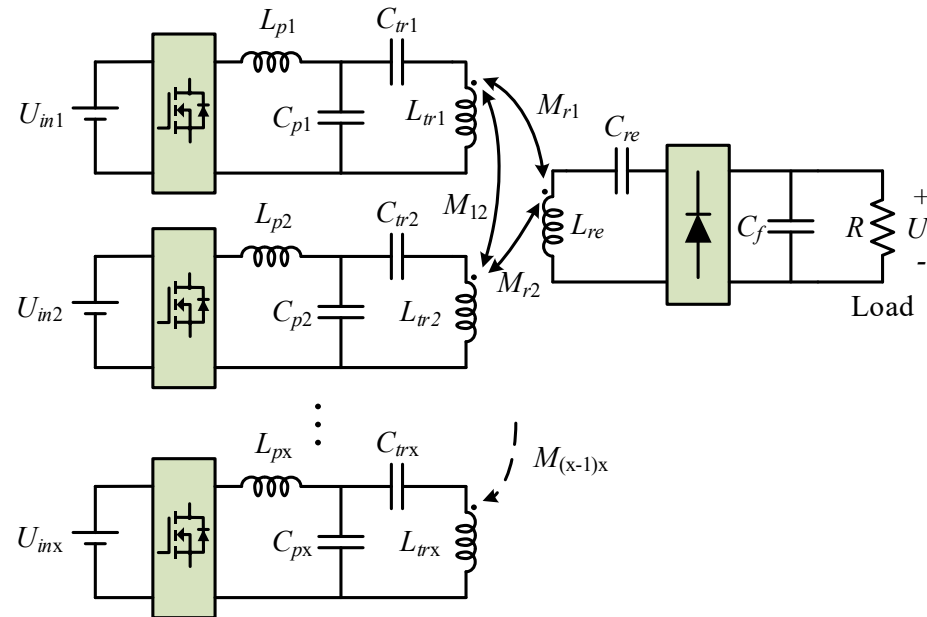
Segmented DWPT System



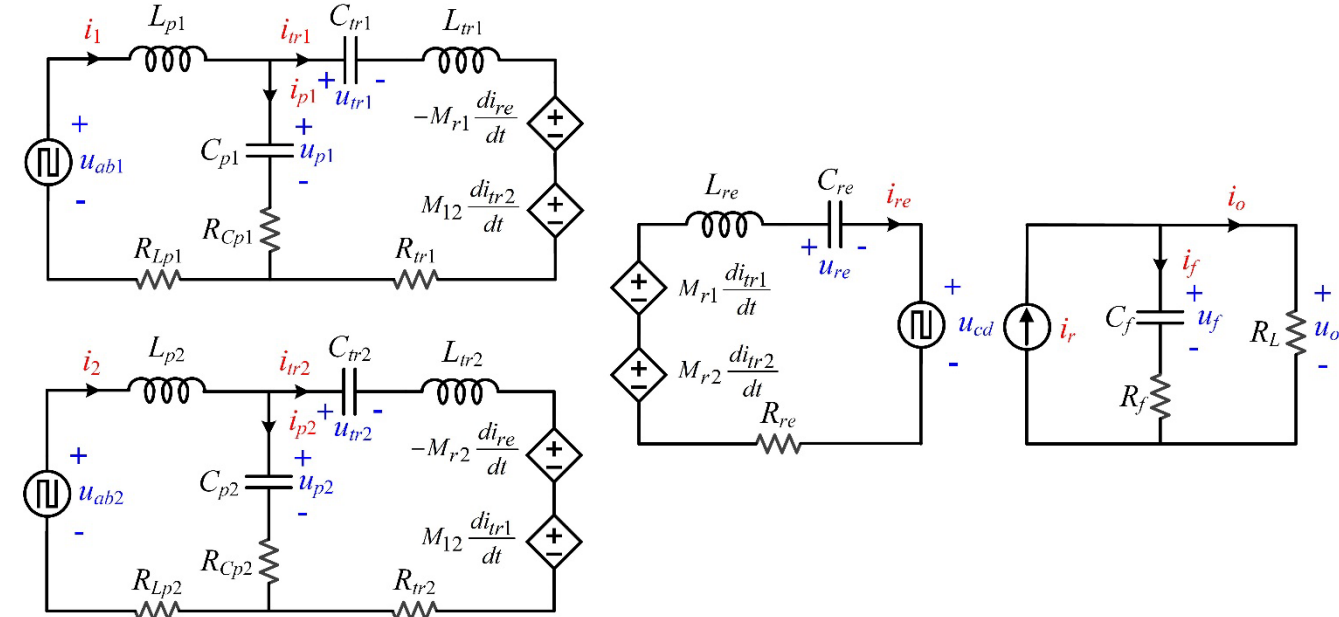
- Long-track DWPT system: the primary coil is much longer than the receiver coil, which **lowers the coupling coefficient and transmission efficiency**. In addition, it also faces the problem of electromagnetic interference.
- Segmented DWPT system: There are many transmitting coils, whose sizes are similar to the receiving coil. The transmission efficiency of the segmented type is higher than that of the former. Meanwhile, multiple transmitters correspond to high cost and complex control.

Generalized State-space Averaging (GSSA) Model of DWPT

➤ State Space Description



Equivalent circuit of the DWPT system with two transmitters and one receiver.



□ The state equations of the DWPT system can be derived based on KCL and KVL, i.e.,

$$u_{ab1} = L_{p1} \frac{di_1}{dt} + u_{p1} + i_{p1}R_{Cp1} + i_1R_{Lp1} \quad u_{p1} = u_{tr1} + L_{tr1} \frac{di_{tr1}}{dt} - M_{r1} \frac{di_{re}}{dt} + M_{12} \frac{di_{tr2}}{dt} + i_{tr1}R_{tr1} - i_{p1}R_{Cp1} \quad u_{ab2} = L_{p2} \frac{di_2}{dt} + u_{p2} + i_{p2}R_{Cp2} + i_2R_{Lp2}$$

$$u_{p2} = u_{tr2} + L_{tr2} \frac{di_{tr2}}{dt} - M_{r2} \frac{di_{re}}{dt} + M_{12} \frac{di_{tr1}}{dt} + i_{tr2}R_{tr2} - i_{p2}R_{Cp2} \quad M_{r1} \frac{di_{tr1}}{dt} + M_{r2} \frac{di_{tr2}}{dt} = L_{re} \frac{di_{re}}{dt} + u_{re} + u_{cd} + i_{re}R_{re}$$

GSSA Model of DWPT Systems

□ Equations can be organized as follows:

$$\begin{aligned}\frac{di_1}{dt} &= \frac{1}{L_{p1}}u_{ab1} - \frac{1}{L_{p1}}u_{p1} - \frac{R_{Cp1}}{L_{p1}}i_{p1} - \frac{R_{Lp1}}{L_{p1}}i_1 & \frac{di_2}{dt} &= \frac{1}{L_{p2}}u_{ab2} - \frac{1}{L_{p2}}u_{p2} - \frac{R_{Cp2}}{L_{p2}}i_{p2} - \frac{R_{Lp2}}{L_{p2}}i_2 \\ \frac{di_{tr1}}{dt} &= \frac{1}{L_{eq1,tr1}}u_{tr1} + \frac{1}{L_{eq1,tr2}}u_{tr2} + \frac{1}{L_{eq1,p1}}u_{p1} + \frac{1}{L_{eq1,p2}}u_{p2} + \frac{1}{L_{eq1,s}}u_{re} + \frac{1}{L_{eq1,tr1}}u_{cd} + \frac{R_{tr1}}{L_{eq1,tr1}}i_{tr1} + \frac{R_{tr2}}{L_{eq1,tr2}}i_{tr2} + \frac{R_{Cp1}}{L_{eq1,p1}}i_{p1} + \frac{R_{Cp2}}{L_{eq1,p2}}i_{p2} + \frac{R_{re}}{L_{eq1,s}}i_{re} \\ \frac{di_{tr2}}{dt} &= \frac{1}{L_{eq2,tr1}}u_{tr1} + \frac{1}{L_{eq2,tr2}}u_{tr2} + \frac{1}{L_{eq2,p1}}u_{p1} + \frac{1}{L_{eq2,p2}}u_{p2} + \frac{1}{L_{eq2,s}}u_{re} + \frac{1}{L_{eq2,tr1}}u_{cd} + \frac{R_{tr1}}{L_{eq2,tr1}}i_{tr1} + \frac{R_{tr2}}{L_{eq2,tr2}}i_{tr2} + \frac{R_{Cp1}}{L_{eq2,p1}}i_{p1} + \frac{R_{Cp2}}{L_{eq2,p2}}i_{p2} + \frac{R_{re}}{L_{eq2,s}}i_{re} \\ \frac{di_{re}}{dt} &= \frac{1}{L_{eqr,tr1}}u_{tr1} + \frac{1}{L_{eqr,tr2}}u_{tr2} + \frac{1}{L_{eqr,p1}}u_{p1} + \frac{1}{L_{eqr,p2}}u_{p2} + \frac{1}{L_{eqr,s}}u_{re} + \frac{1}{L_{eqr,tr1}}u_{cd} + \frac{R_{tr1}}{L_{eqr,tr1}}i_{tr1} + \frac{R_{tr2}}{L_{eqr,tr2}}i_{tr2} + \frac{R_{Cp1}}{L_{eqr,p1}}i_{p1} + \frac{R_{Cp2}}{L_{eqr,p2}}i_{p2} + \frac{R_{re}}{L_{eqr,s}}i_{re}\end{aligned}$$

where

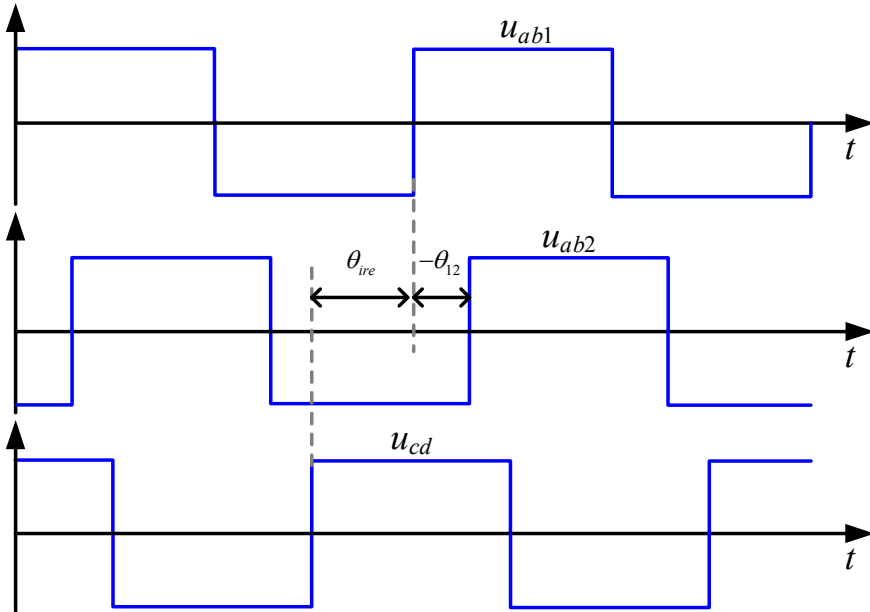
$$\begin{cases} L_{eq1,tr1} = \frac{\Delta}{M_{r2}^2 - L_{re}L_{tr2}}, L_{eq1,tr2} = \frac{\Delta}{L_{re}M_{12} - M_{r1}M_{r2}}, L_{eq1,p1} = \frac{\Delta}{L_{re}L_{tr2} - M_{r2}^2}, L_{eq1,p2} = \frac{\Delta}{M_{r1}M_{r2} - L_{re}M_{12}}, L_{eq1,s} = \frac{\Delta}{M_{12}M_{r2} - L_{tr2}M_{r1}} \\ L_{eq2,tr1} = \frac{\Delta}{L_{re}M_{12} - M_{r1}M_{r2}}, L_{eq2,tr2} = \frac{\Delta}{M_{r1}^2 - L_{re}L_{tr1}}, L_{eq2,p1} = \frac{\Delta}{M_{r1}M_{r2} - L_{re}M_{12}}, L_{eq2,p2} = \frac{\Delta}{L_{re}L_{tr1} - M_{r1}^2}, L_{eq2,s} = \frac{\Delta}{M_{12}M_{r1} - L_{tr1}M_{r2}} \\ L_{eqr,tr1} = \frac{\Delta}{M_{12}M_{r2} - L_{tr2}M_{r1}}, L_{eqr,tr2} = \frac{\Delta}{M_{12}M_{r1} - L_{tr1}M_{r2}}, L_{eqr,p1} = \frac{\Delta}{M_{12}M_{r2} - L_{tr2}M_{r1}}, L_{eqr,p2} = \frac{\Delta}{L_{tr1}M_{r2} - M_{12}M_{r1}}, L_{eqr,s} = \frac{\Delta}{M_{12}^2 - L_{tr1}L_{tr2}} \end{cases}$$

$$\Delta = L_{re}L_{tr1}L_{tr2} - L_{re}M_{12}^2 - L_{tr1}M_{r2}^2 - L_{tr2}M_{r1}^2 + 2M_{12}M_{r1}M_{r2}$$

□ The capacitor current and voltage are as follows:

$$i_{tr1} = C_{tr1} \frac{du_{tr1}}{dt}, i_{tr2} = C_{tr2} \frac{du_{tr2}}{dt}, i_{p1} = C_{p1} \frac{du_{p1}}{dt}, i_{p2} = C_{p2} \frac{du_{p2}}{dt}, i_{re} = C_s \frac{du_s}{dt}, i_f = C_f \frac{du_f}{dt}$$

➤ Extended Describing Function



Phase reference u_{ab1} : $u_{ab1}(t) = \frac{4}{\pi} U_{in1} \sin(\omega_s t)$ (Phase reference)

$$u_{ab2}(t) = \frac{4}{\pi} U_{in2} \sin(\omega_s t + \theta_{12}) = \frac{4}{\pi} U_{in2} \cos(\theta_{12}) \sin(\omega_s t) + \frac{4}{\pi} U_{in2} \sin(\theta_{12}) \cos(\omega_s t)$$

$$u_{cd}(t) = \frac{4}{\pi} u_o \sin(\omega_s t + \theta_{ire}) = \frac{4}{\pi} u_o \cos(\theta_{ire}) \sin(\omega_s t) + \frac{4}{\pi} u_o \sin(\theta_{ire}) \cos(\omega_s t)$$

The receiver current:

$$\begin{aligned} i_{re}(t) &= i_{repk} \sin(\omega_s t + \theta_{ire}) \\ &= i_{repk} \cos(\theta_{ire}) \sin(\omega_s t) + i_{repk} \sin(\theta_{ire}) \cos(\omega_s t) \\ &= i_{res} \sin(\omega_s t) + i_{rec} \cos(\omega_s t) \end{aligned}$$

where $i_{repk}^2 = i_{res}^2 + i_{rec}^2$, $\cos \theta_{ire} = \frac{i_{res}}{i_{repk}}$, $\sin \theta_{ire} = \frac{i_{rec}}{i_{repk}}$

Input voltage of the rectifier can be organized as:

$$\begin{aligned} u_{cd}(t) &= \frac{4}{\pi} u_o \sin(\omega_s t + \theta_{ire}) \\ &= \frac{4}{\pi} u_o \cos(\theta_{ire}) \sin(\omega_s t) + \frac{4}{\pi} u_o \sin(\theta_{ire}) \cos(\omega_s t) \\ &= \frac{4i_{res}}{\pi i_{repk}} u_o \sin(\omega_s t) + \frac{4i_{rec}}{\pi i_{repk}} u_o \cos(\omega_s t) \end{aligned}$$

➤ Harmonic Balance

$$\frac{di_1}{dt} = \frac{1}{L_{p1}} u_{ab1} - \frac{1}{L_{p1}} u_{p1} - \frac{R_{Cp1}}{L_{p1}} i_{p1} - \frac{R_{Lp1}}{L_{p1}} i_1$$

Sine item Cosine item

$$\frac{di_{1s}}{dt} = \frac{1}{L_{p1}} \cdot \frac{4}{\pi} U_{in1} - \frac{1}{L_{p1}} u_{p1s} - \frac{R_{Cp1}}{L_{p1}} (i_{1s} - i_{tr1s}) - \frac{R_{Lp1}}{L_{p1}} i_{1s} + \omega_s i_{1c}$$

$$\frac{di_{1c}}{dt} = -\frac{1}{L_{p1}} u_{p1c} - \frac{R_{Cp1}}{L_{p1}} (i_{1c} - i_{tr1c}) - \frac{R_{Lp1}}{L_{p1}} i_{1c} - \omega_s i_{1s}$$

➤ GSSA Model

$$\frac{dx}{dt} = Ax + Bu$$

System matrix A is 20 by 20, input matrix B is 20 by 1, and the state vector x is 20 by 1.

$$x = [i_{1s} \quad i_{2s} \quad i_{tr1s} \quad i_{tr2s} \quad i_{res} \quad u_{p1s} \quad u_{p2s} \quad u_{tr1s} \quad u_{tr2s} \quad u_{res} \quad i_{1c} \quad i_{2c} \quad i_{tr1c} \quad i_{tr2c} \quad i_{rec} \quad u_{p1c} \quad u_{p2c} \quad u_{tr1c} \quad u_{tr2c} \quad u_{rec}]^T$$

The state variables can be solved by setting the time derivative of the state variable to 0, and any state variable can be obtained, i.e.,

$$x(t) = x_s \sin(\Omega_s t) + x_c \cos(\Omega_s t) = x_{pk} \sin(\Omega_s t + \theta_x)$$

$$x_{pk} = \sqrt{x_s^2 + x_c^2}, \theta_x = \arcsin\left(\frac{x_c}{\sqrt{x_s^2 + x_c^2}}\right)$$

➤ Adjacent Coil Phase Optimization

- System efficiency: $\eta = \frac{P_{out}}{P_{in}} \times 100\%$

- Output power: $P_{out} = \frac{U_o^2}{R_L} = \frac{4}{\pi^2} I_{2pk}^2 R_L$

- Input power:

$$P_{in} = P_{in1} + P_{in2} = U_{ab1_rms} I_{1_rms} \cos(\delta_1) + U_{ab2_rms} I_{2_rms} \cos(\delta_2)$$

- RMS of voltage and current:

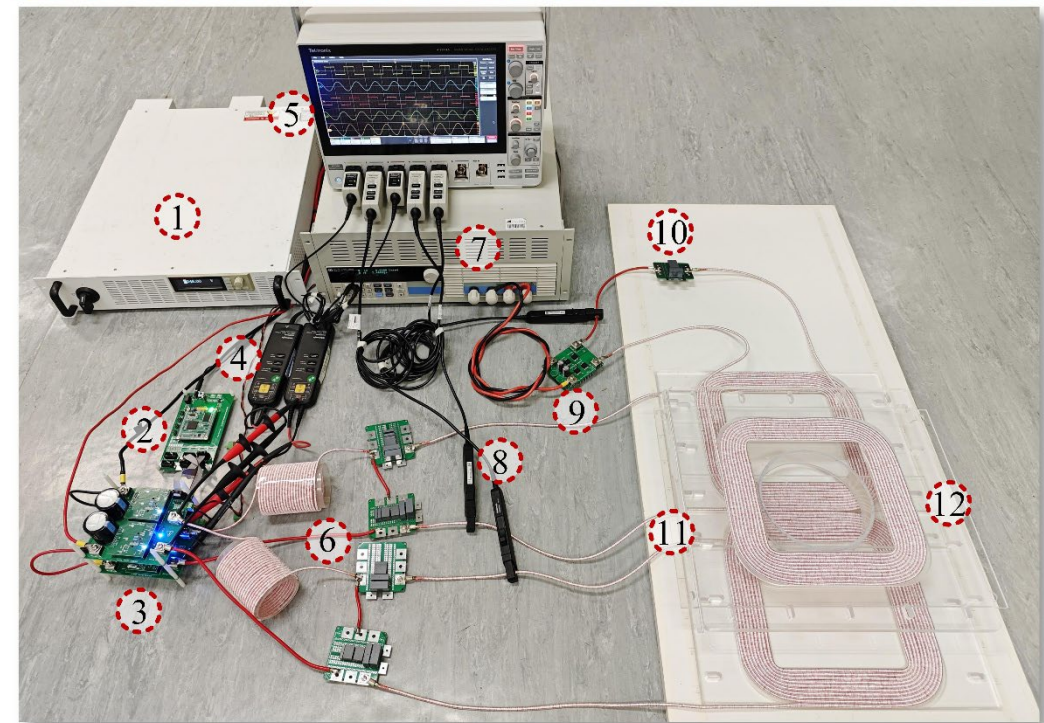
$$U_{ab1_rms} = \frac{4}{\pi\sqrt{2}} U_{in1}, I_{1_rms} = \frac{\sqrt{I_{1s}^2 + I_{1c}^2}}{\sqrt{2}}, U_{ab2_rms} = \frac{4}{\pi\sqrt{2}} U_{in2}, I_{2_rms} = \frac{\sqrt{I_{2s}^2 + I_{2c}^2}}{\sqrt{2}}$$

- Phase between voltage and current:

$$\delta_1 = \angle U_{ab1} - \angle I_1 = 0 - \arcsin\left(\frac{I_{1c}}{\sqrt{I_{1s}^2 + I_{1c}^2}}\right), \delta_2 = \angle U_{ab2} - \angle I_2 = \theta_{12} - \arcsin\left(\frac{I_{2c}}{\sqrt{I_{2s}^2 + I_{2c}^2}}\right)$$

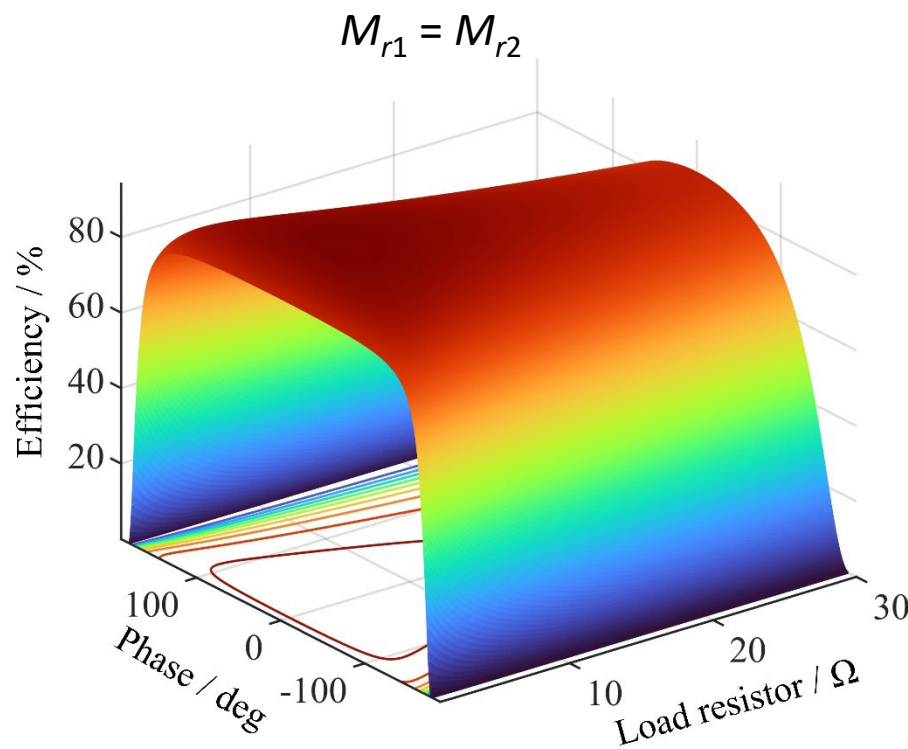
□ DWPT experimental setup

- | | | |
|-----------------------|--------------------|-------------------------|
| 1. DC power supply | 5. Oscilloscope | 9. Passive rectifier |
| 2. DSP controller | 6. LCC networks | 10. Capacitors C_{re} |
| 3. H-bridge inverters | 7. Electronic load | 11. Tx coils |
| 4. Voltage probes | 8. Current probes | 12. Rx coil |

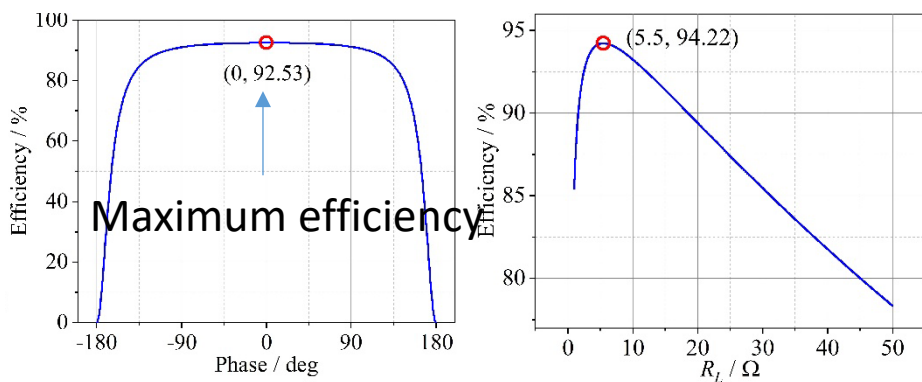


GSSA Model of DWPT Systems

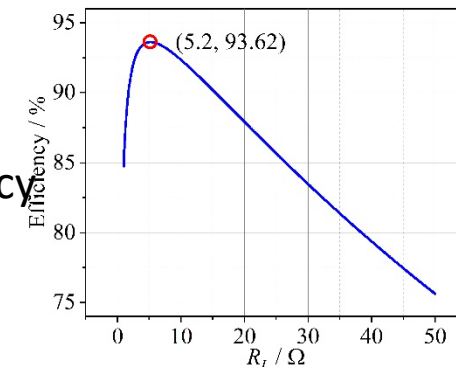
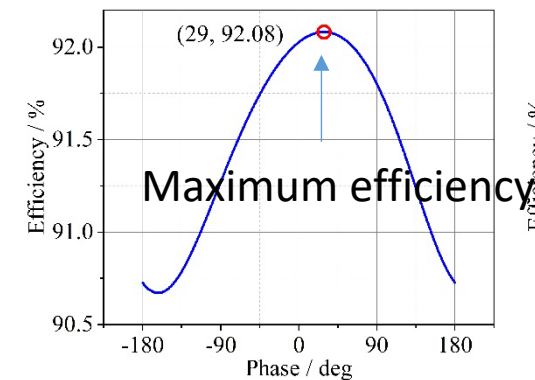
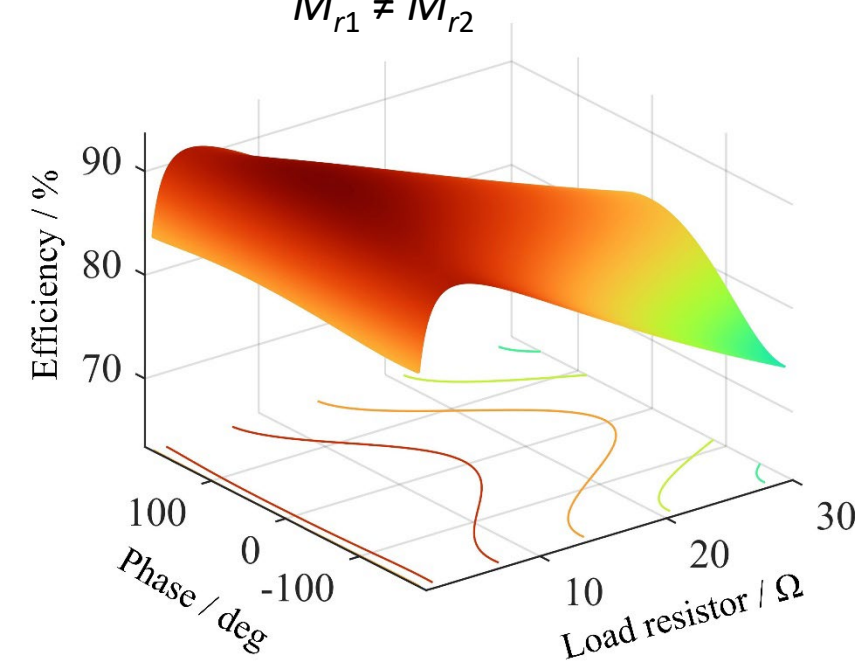
3D
Diagram



2D
Diagram

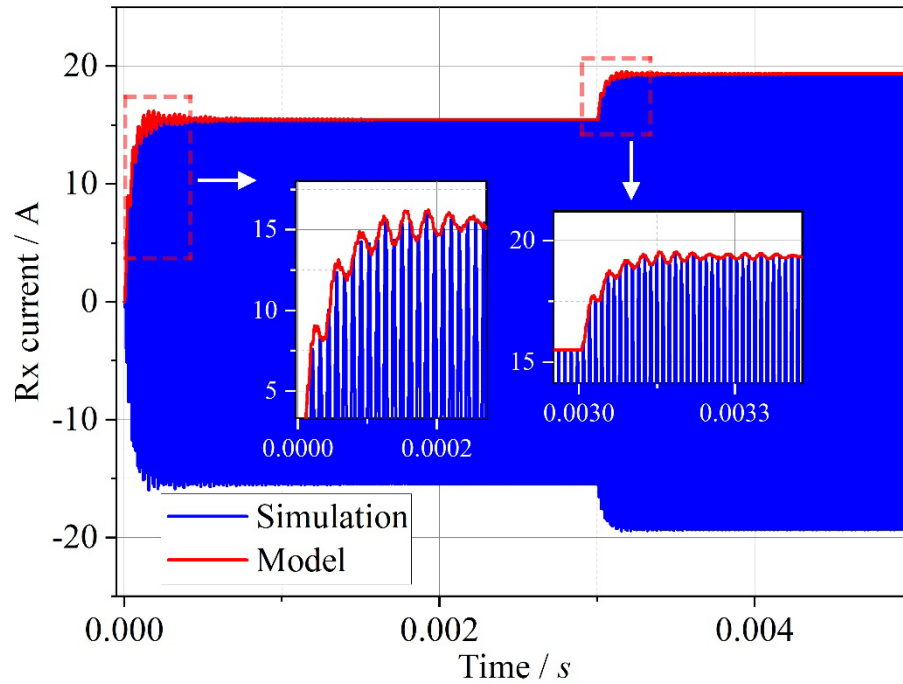


$M_{r1} \neq M_{r2}$



➤ Model Validation in Simulations and Experiments

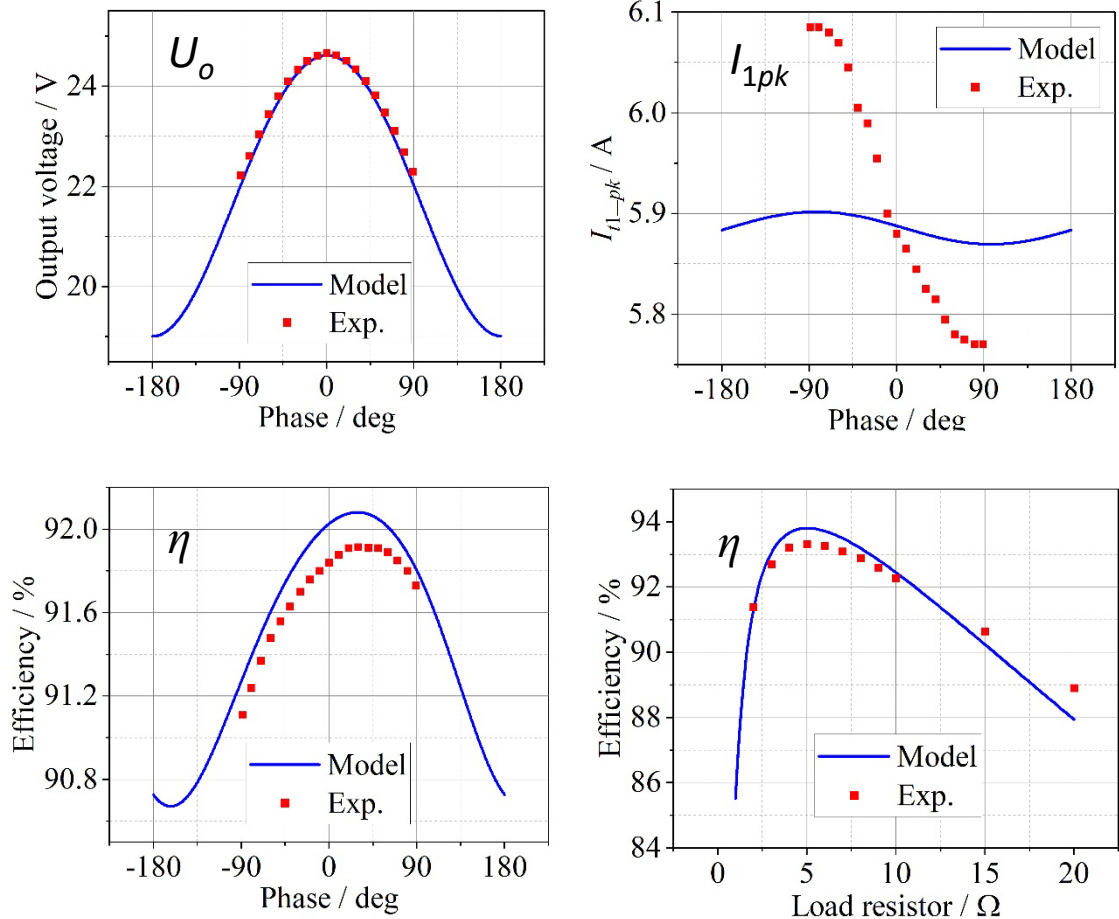
Currents of the Rx coil obtained by simulation and GSSA model when U_{in1} and U_{in2} step from 48 to 60 V.



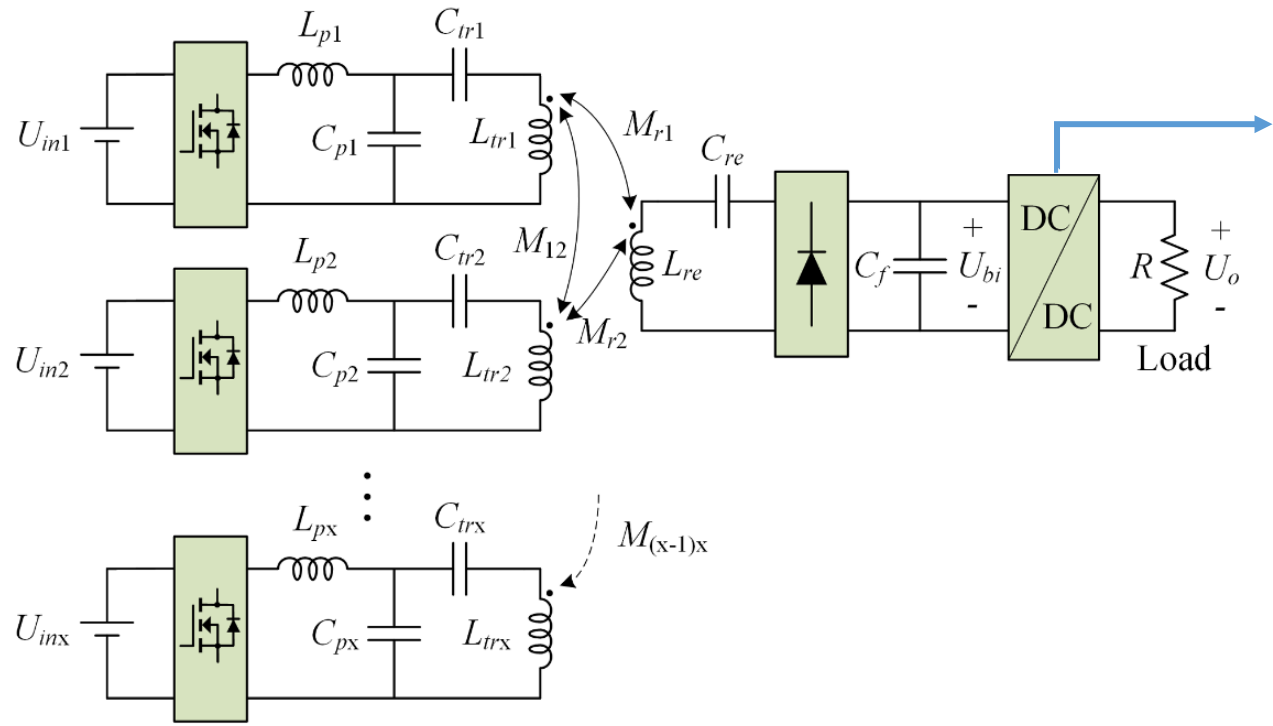
[4] T. Ma, Z. Zhu, C. Jiang, S. Ren, W. Guo, and T. Long, "Modeling and Efficiency Optimization for Dynamic Wireless Power Transfer Systems" in *IEEE Transactions on Industrial Electronics*, Under review.

Comparisons between experiments and the GSSA model

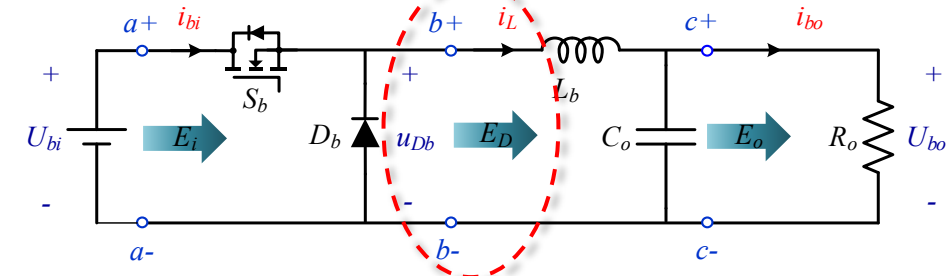
$$M_{r1} = 1.24 \mu\text{H} \text{ and } M_{r2} = 9.50 \mu\text{H}$$



Periodic Energy Control for DWPT Systems



Equivalent circuit of a typical Buck converter



There are three ports for the Buck converter. The port energy can be expressed as:

$$\text{Port } a: E_i = \int_0^{T_s} U_{bi}(t) i_{bi}(t) dt$$

$$\text{Port } b: E_o = \int_0^{T_s} U_{bo}(t) i_{bo}(t) dt$$

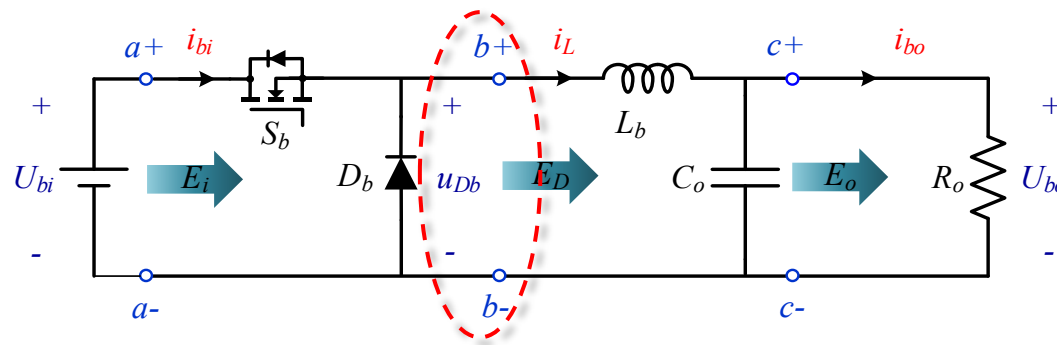
$$\text{Port } c: E_D = \int_0^{T_s} u_{Db}(t) i_L(t) dt$$

- The key point of PEC is to choose the optimal port to control its port energy. Two rules should be followed: (1) **The port should be closed to the system output** to allow the port energy to approach the energy consumed on the load. (2) **The port voltage or current should have significant variation with the state switching of active power switches**, like MOSFETs or IGBTs, which can keep the fast dynamic response of the control method.

[5] T. Ma, C. Jiang, X. Wang, J. Xiang, L. Mo, and K. T. Chau, "A Novel Periodic Energy Control for Nonisolated DC-DC Converters With Overshoot Suppression," in *IEEE Transactions on Power Electronics*, vol. 38, no. 10, pp. 12325-12330, Oct. 2023

Periodic Energy Control for DWPT Systems

□ Equivalent circuit of a typical Buck converter



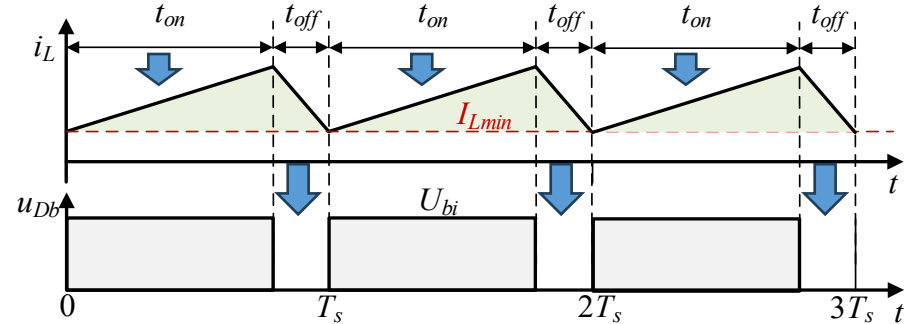
$$E_D = \int_0^{T_s} u_{Db}(t) i_L(t) dt = \int_0^{t_{on}} u_{Db}(t) i_L(t) dt = U_{bi} \int_0^{t_{on}} i_L(t) dt$$

KVL: $U_{bi} = L_b \frac{di_L}{dt} + U_{bo}$ $\rightarrow k_L = \frac{di_L}{dt} = \frac{U_{bi} - U_{bo}}{L_b}$

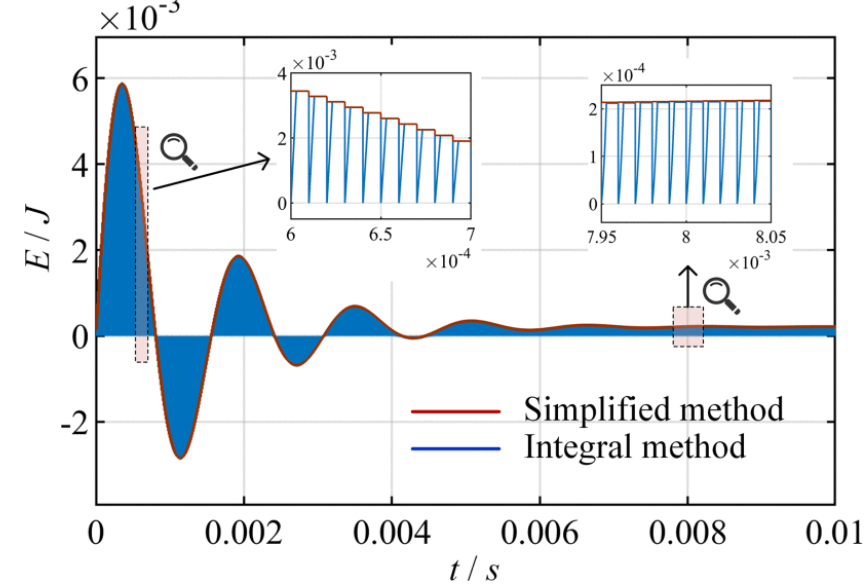
$$\begin{aligned} E_D &= U_{bi} \int_0^{t_{on}} i_L(t) dt = U_{bi} \int_0^{t_{on}} (k_L t + I_{L\min}) dt \\ &= U_{bi} \left(\frac{1}{2} k_L t^2 + I_{L\min} t + C \right) \Big|_0^{t_{on}} \\ &= U_{bi} \left(\frac{U_{bi} - U_{bo}}{2L_b} t_{on}^2 + I_{L\min} t_{on} \right) \end{aligned}$$

$$\rightarrow t_{on} = \frac{-I_{L\min} + \sqrt{I_{L\min}^2 + 2k_L \frac{E_{tar}}{U_{bi}}}}{k_L}$$

□ Main waveforms of the Buck converter



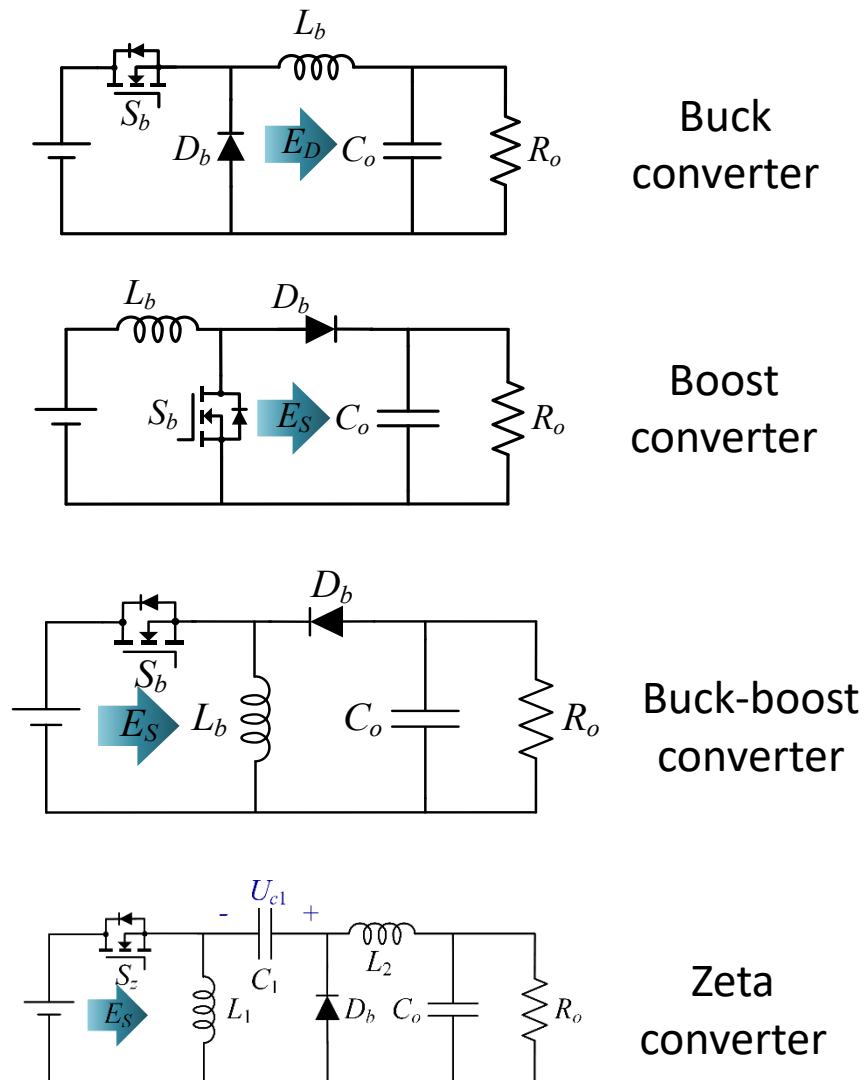
□ Comparison of port energy between the integral method and simplified method



Periodic Energy Control for DWPT Systems

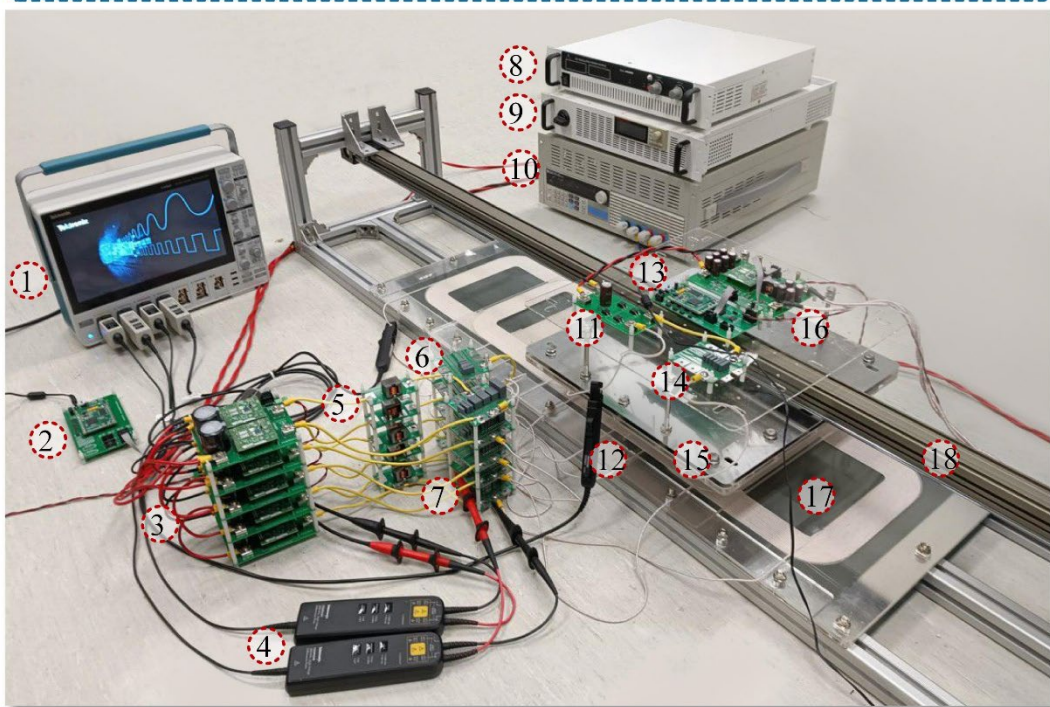
- Simplified energy calculation formulas and conduction time of four non-isolated DC-DC converters.

| Topology | Voltage gain | Simplified energy calculation | Conduction time |
|----------------------|------------------------------------|--|---|
| Buck converter | $\frac{U_o}{U_i} = D$ | $E_D = U_i \left(\frac{1}{2} k_L t_{on}^2 + I_{L\min} t_{on} \right)$ $k_L = (U_i - U_o)/L_b$ | $t_{on} = \frac{-I_{L\min} + \sqrt{I_{L\min}^2 + 2k_L \frac{E_{tar}}{U_i}}}{k_L}$ |
| Boost converter | $\frac{U_o}{U_i} = \frac{1}{1-D}$ | $E_S = U_o \left(-\frac{1}{2} k_L t_{off}^2 + I_{L\min} t_{off} \right)$ $k_L = (U_i - U_o)/L_b$ | $t_{off} = \frac{-I_{L\min} + \sqrt{I_{L\min}^2 - 2k_L \frac{E_{tar}}{U_o}}}{-k_L}$ $t_{on} = T_s - t_{off}$ |
| Buck-boost converter | $\frac{U_o}{U_i} = \frac{-D}{1-D}$ | $E_S = U_i \left(\frac{1}{2} k_L t_{on}^2 + I_{L\min} t_{on} \right)$ $k_L = U_i/L_b$ | $t_{on} = \frac{-I_{L\min} + \sqrt{I_{L\min}^2 + 2k_L \frac{E_{tar}}{U_i}}}{k_L}$ |
| Zeta converter | $\frac{U_o}{U_i} = \frac{D}{1-D}$ | $E_s = U_i \left(\frac{1}{2} k_s t_{on}^2 + I_{s\min} t_{on} \right)$ $k_s = \frac{U_i}{L_1} + \frac{U_i - U_o + U_{cl}}{L_2}$ | $t_{on} = \frac{-I_{s\min} + \sqrt{I_{s\min}^2 + 2k_s \frac{E_{tar}}{U_i}}}{k_s}$ |



➤ Experimental Verification

- | | | |
|-------------------------|------------------------|-------------------------|
| 1. Oscilloscope | 7. Capacitors C_{px} | 13. DSP controller |
| 2. DSP controller | 8. DC power supply 1 | 14. Capacitors C_{re} |
| 3. H-bridge inverters | 9. DC power supply 2 | 15. Receiver pad |
| 4. Voltage probes | 10. Electronic load | 16. Sync buck converter |
| 5. Inductors L_{px} | 11. Passive rectifier | 17. Transmitter pads |
| 6. Capacitors C_{trx} | 12. Current probes | 18. Guide rail |



Parameters of the DWPT experimental setup.

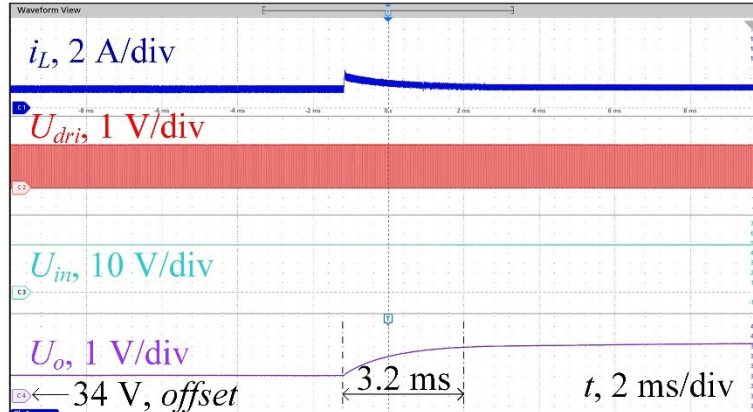
| System parameters | Value |
|---|---|
| Transmitters' self-inductance $L_{tr1}-L_{tr5}$, μH | 223.80, 227.97, 230.34, 228.98, 223.16 |
| Compensation inductors $L_{p1}-L_{p5}$, μH | 19.65, 19.57, 19.82, 19.57, 19.87 |
| Compensation capacitors $C_{p1}-C_{p5}$, nF | 178.15, 179.08, 176.72, 178.96, 176.45 |
| Compensation capacitors $C_{tr1}-C_{tr5}$, nF | 17.59, 16.95, 17.55, 16.55, 17.65 |
| Receiving coil self-inductance L_{re} , μH | 182.82 |
| Compensation capacitor C_{re} , nF | 18.47 |
| Filter capacitor C_f , μF | 1320 |
| Filter capacitor C_o , μF | 880 |
| Inductor of Buck converter L_b , μH | 220 |
| Nominal resonant frequency f_0 , kHz | 85 |
| Switching frequency f_s , kHz | 20 |

Periodic Energy Control for DWPT Systems

➤ Comparisons between the duty cycle control and PEC with PI controllers (Closed-loop)

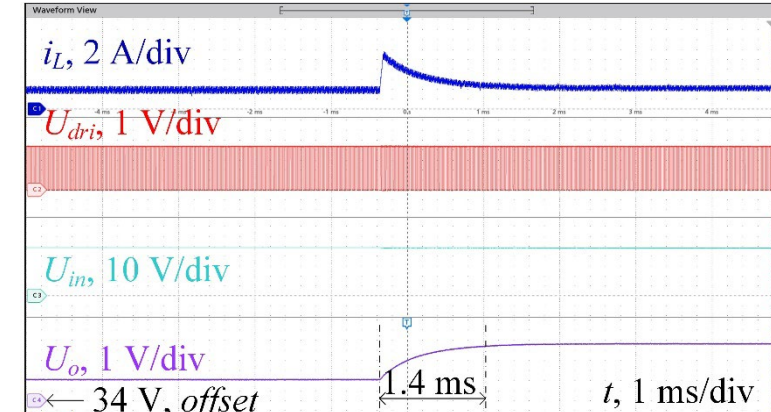
PEC with PI controller

$$K_p = 10, K_i = 400.$$



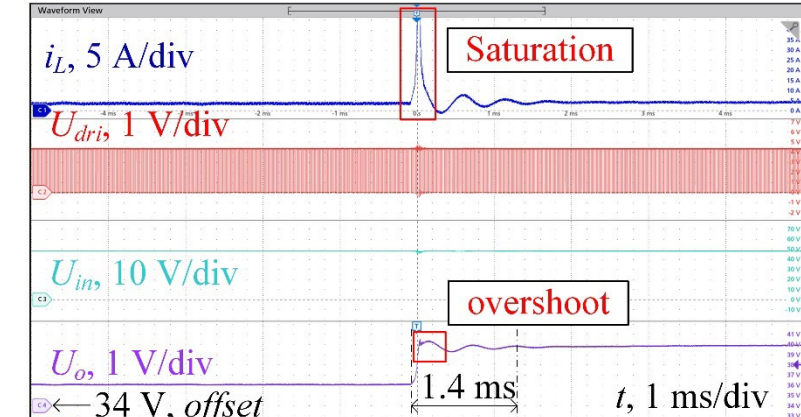
PEC with PI controller

$$K_p = 30, K_i = 400.$$

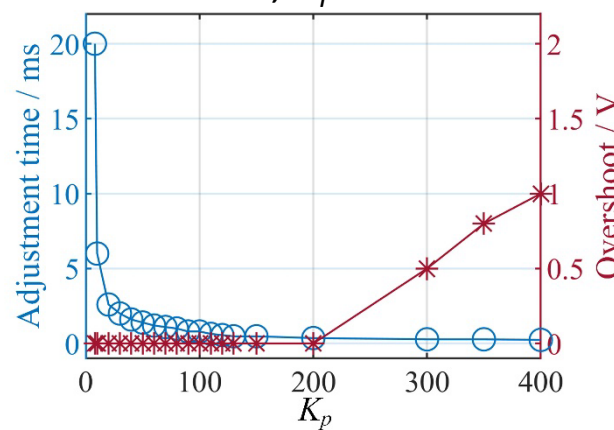


PI control by regulating the duty cycle

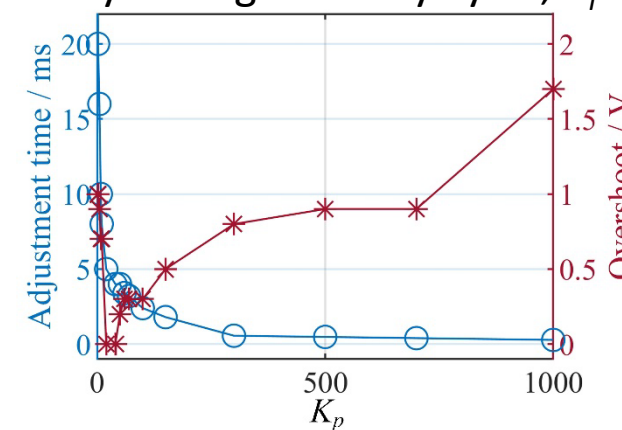
$$K_p = 150, K_i = 40000.$$



PEC, $K_i = 400$.

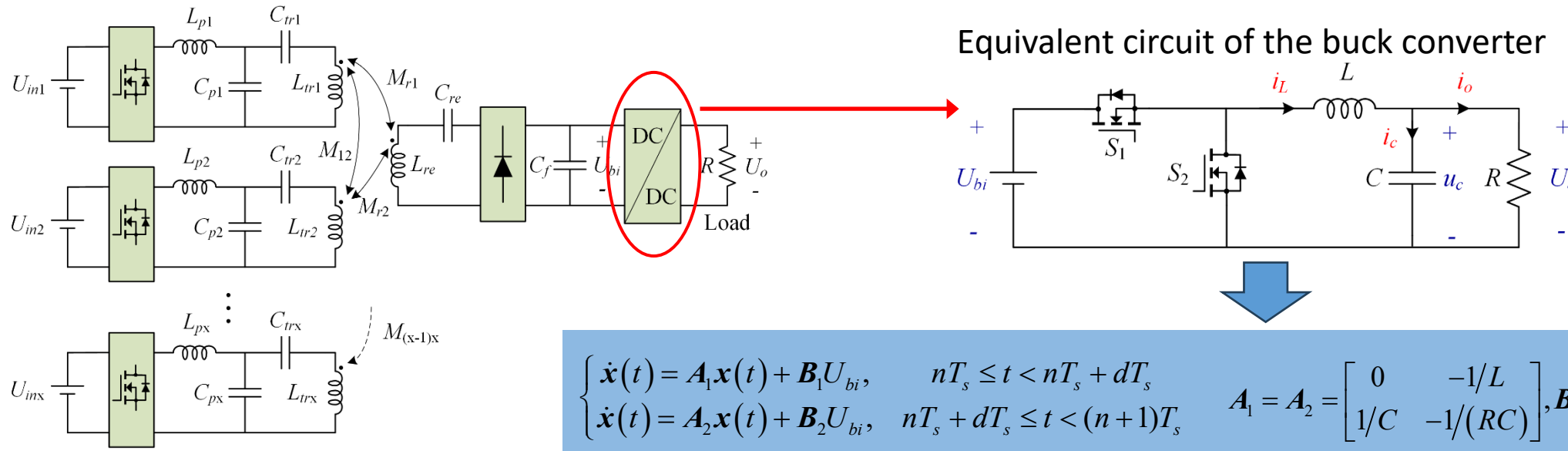


PI control by tuning the duty cycle, $K_i = 40000$.



- By comparison, the overshoot voltage of PEC is smaller when the adjustment time of the two control methods is the same.
- **To sum up, PEC can effectively suppress the system overshoot.**

A Low Computational Burden MPC for Dynamic WPT



Equivalent circuit of the buck converter

$$\begin{cases} \dot{x}(t) = A_1 x(t) + B_1 U_{bi}, & nT_s \leq t < nT_s + dT_s \\ \dot{x}(t) = A_2 x(t) + B_2 U_{bi}, & nT_s + dT_s \leq t < (n+1)T_s \end{cases}$$

$$A_1 = A_2 = \begin{bmatrix} 0 & -1/L \\ 1/C & -1/(RC) \end{bmatrix}, B_1 = \begin{bmatrix} 1/L \\ 0 \end{bmatrix}, B_2 = \begin{bmatrix} 0 \\ 0 \end{bmatrix}$$

□ Parsing solution of the sampled-data model by matrix exponential.

$$x_{n+1} = F(d)x_n + G(d)U_{bi}$$

$$\begin{cases} F(d) = e^{A_2 t_{n2}} e^{A_1 t_{n1}} = e^{A_1 T_s} = e^{A_2 T_s} \\ G(d) = e^{A_2 t_{n2}} \psi_1 + \psi_2 \\ \quad = e^{A_2 t_{n2}} A_1^{-1} (e^{A_1 t_{n1}} - I) B_1 \end{cases}$$

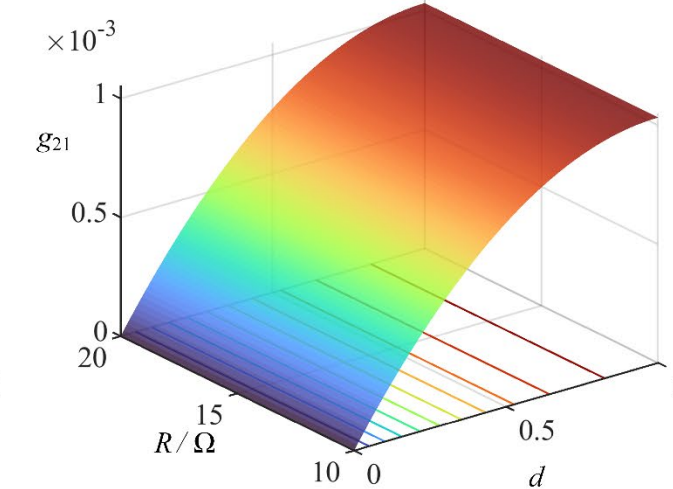
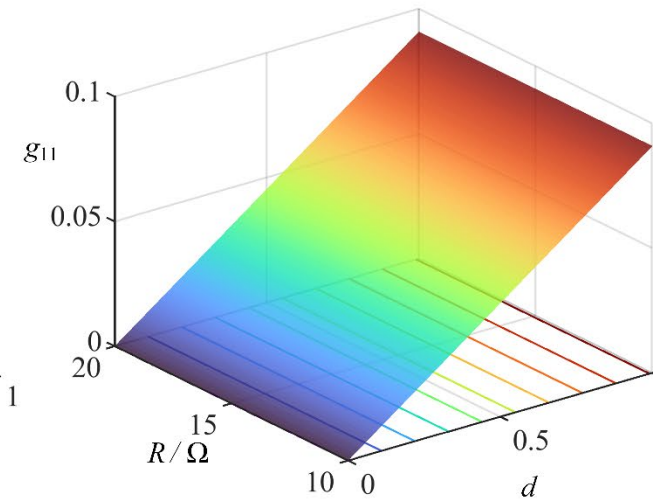
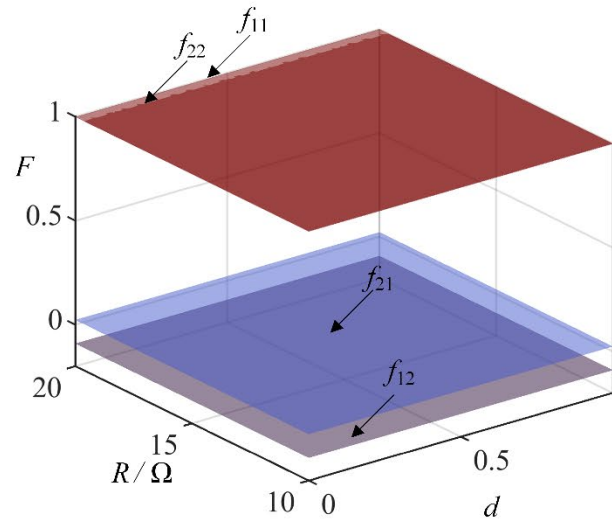
$$F = \begin{pmatrix} \frac{\lambda_1 e^{T_s \lambda_2} - \lambda_2 e^{T_s \lambda_1}}{\lambda_1 - \lambda_2} & -\frac{e^{T_s \lambda_1} - e^{T_s \lambda_2}}{L(\lambda_1 - \lambda_2)} \\ \frac{L\lambda_1 \lambda_2 (e^{T_s \lambda_1} - e^{T_s \lambda_2})}{\lambda_1 - \lambda_2} & \frac{\lambda_1 e^{T_s \lambda_1} - \lambda_2 e^{T_s \lambda_2}}{\lambda_1 - \lambda_2} \end{pmatrix}$$

$$\sigma_1 = \frac{L\lambda_1 \lambda_2 (e^{T_s \lambda_1 d} - e^{T_s \lambda_2 d})}{\lambda_1 - \lambda_2}, \sigma_2 = \frac{\lambda_2 e^{T_s \lambda_1 d} - \lambda_1 e^{T_s \lambda_2 d}}{\lambda_1 - \lambda_2} + 1, \sigma_3 = L(\lambda_1 - \lambda_2), \sigma_4 = \frac{L\lambda_1 \lambda_2 (\sigma_7 - \sigma_6)}{\lambda_1 - \lambda_2}, \sigma_5 = \frac{\lambda_1 \sigma_6 - \lambda_2 \sigma_7}{\lambda_1 - \lambda_2}, \sigma_6 = e^{T_s \lambda_2 (1-d)}, \sigma_7 = e^{T_s \lambda_1 (1-d)}$$

$$G(d) = \begin{bmatrix} \left(\frac{\sigma_6 - \sigma_7}{\sigma_3} + \frac{\sigma_5}{R} \right) \sigma_2 + \frac{C}{L} \sigma_5 \sigma_1 \\ \left(\frac{L(\lambda_1 \sigma_7 - \lambda_2 \sigma_6)}{\sigma_3} + \frac{\sigma_4}{R} \right) \sigma_2 + \frac{C}{L} \sigma_4 \sigma_1 \end{bmatrix}$$

A Low Computational Burden MPC for Dynamic WPT

- Elements of the system matrix and input matrix versus load resistor and duty cycle.



$$\mathbf{F} = \begin{bmatrix} f_{11} & f_{12} \\ f_{21} & f_{22} \end{bmatrix}$$

$$\mathbf{G}(d) = \begin{bmatrix} g_{11}(d) \\ g_{21}(d) \end{bmatrix}$$

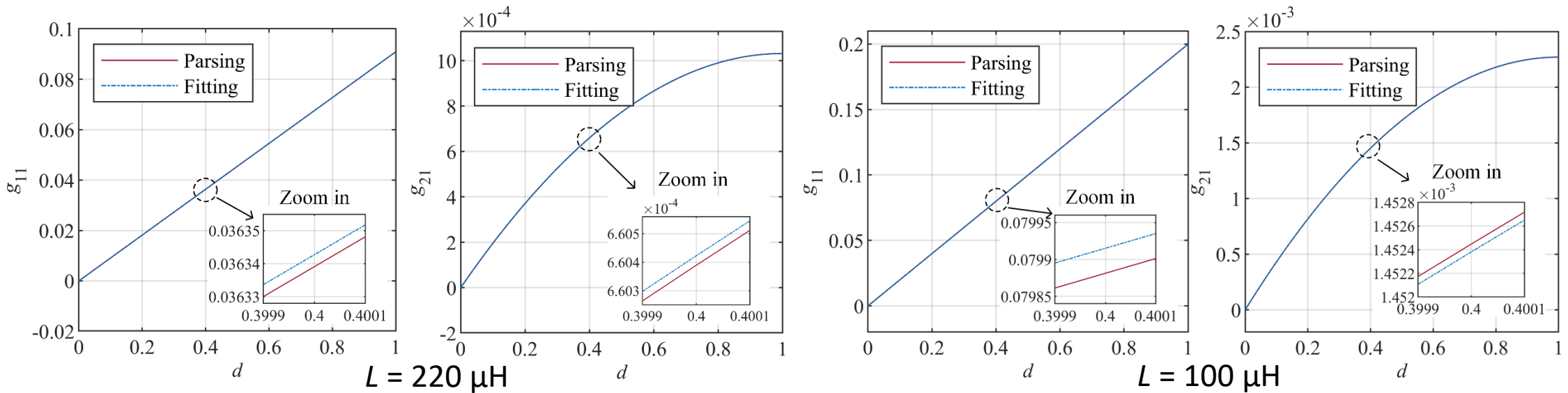
TABLE I. Sensitivity of each element of matrix \mathbf{F} and \mathbf{G} to system parameters ($L = 220 \mu\text{H}$, $C = 880 \mu\text{F}$, and $R = 10 \Omega$)

| Parameter X | $S_X^{f_{11}}$ | $S_X^{f_{12}}$ | $S_X^{f_{21}}$ | $S_X^{f_{22}}$ | $S_X^{g_{11}(d)}$ | $S_X^{g_{21}(d)}$ |
|---------------|-----------------------|-----------------------|-----------------------|-----------------------|---|---|
| L | 1.03×10^{-3} | 0.9997 | 3.45×10^{-4} | 1.03×10^{-3} | 0.9990 - 0.9997 | 0.9997 - 0.9998 |
| C | 1.03×10^{-3} | 1.48×10^{-3} | 0.9986 | 3.31×10^{-3} | $3.44 \times 10^{-4} - 1.02 \times 10^{-3}$ | 0.9985 - 0.9991 |
| R | 7.82×10^{-7} | 1.14×10^{-3} | 1.14×10^{-3} | 2.27×10^{-3} | $1.96 \times 10^{-7} - 7.71 \times 10^{-7}$ | $7.57 \times 10^{-4} - 1.13 \times 10^{-3}$ |

- Since matrix \mathbf{F} is constant, the sensitivity of \mathbf{F} to system parameters should also be constant. Whereas the sensitivity of \mathbf{G} to system parameters is related to the duty cycle. **Elements of matrix \mathbf{F} and \mathbf{G} all have small sensitivity to the load resistor.**

A Low Computational Burden MPC for Dynamic WPT

- Polynomial fitting based on parsing solution $\mathbf{G}(d) = \begin{bmatrix} g_{11}(d) \\ g_{21}(d) \end{bmatrix} \xrightarrow{\text{fitting}} \begin{cases} \hat{g}_{11}(d) = q_1 d + q_2 \\ \hat{g}_{21}(d) = p_1 d^2 + p_2 d + p_3 \end{cases}$ $\Rightarrow \begin{cases} \hat{g}_{11}(d) = \chi_1 d \\ \hat{g}_{21}(d) = -\chi_2 d^2 + 2\chi_2 d \end{cases}$
- The elements of the input matrix are fitted by **linear and quadratic functions**. The coefficients of the fitting function are only related to the system parameters. The goodness of fitting results can be evaluated by the sum of squared error (SSE), which is quite low.



- To sum up, the system trajectory can be solved by simple polynomials instead of the complex matrix exponential. And the computational burden will be reduced dramatically for MPC.

A Low Computational Burden MPC for Dynamic WPT

- Let the predicted output voltage equal to U_{ref} , and the optimal duty cycle can be solved by

$$U_{o(n+2)}^{pre} = u_{c(n+2)}^{pre} = f_{21}i_{L(n+1)}^{pre} + f_{22}u_{c(n+1)}^{pre} + g_{21}(d_{n+1})U_{bi} \quad \longrightarrow \quad g_{21}(d_{opt(n+1)}) = C = \frac{U_{ref} - f_{21}i_{L(n+1)}^{pre} - f_{22}u_{c(n+1)}^{pre}}{U_{bi}}$$

- The effective zone of the duty cycle is from 0 to 1.0, and the maximum and minimum values of g_{21} in this range are g_{max} and g_{min} . The three cases are analyzed as follows.

- $C > g_{max}$. The optimal duty cycle will be 1.0.
- $g_{min} \leq C \leq g_{max}$. There will be two solutions, d_1 and d_2 ; the smaller d is the effective solution, i.e.,

$$d_1 = \left(p_2 - \sqrt{p_2^2 - 4p_1(p_3 - C)} \right) / (-2p_1)$$

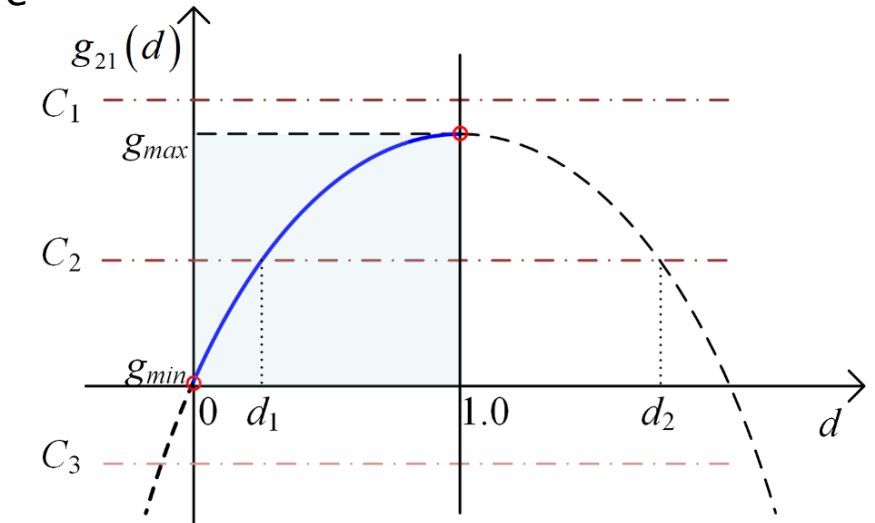
- $C < g_{min}$. The optimal duty cycle will be 0.

MPC with Current Limitation

Current prediction: $i_{L(n+2)}^{pre} = f_{11}i_{L(n+1)}^{pre} + f_{12}u_{c(n+1)}^{pre} + g_{11}(d_{n+1})U_{bi}$

Current limitation: $f_{11}i_{L(n+1)}^{pre} + f_{12}u_{c(n+1)}^{pre} + g_{11}(d_{n+1})U_{bi} \leq I_{lim}$

Duty cycle limitation: $d_{n+1} \leq \left[\left(I_{lim} - f_{11}i_{L(n+1)}^{pre} - f_{12}u_{c(n+1)}^{pre} \right) / U_{bi} - q_2 \right] / q_1$

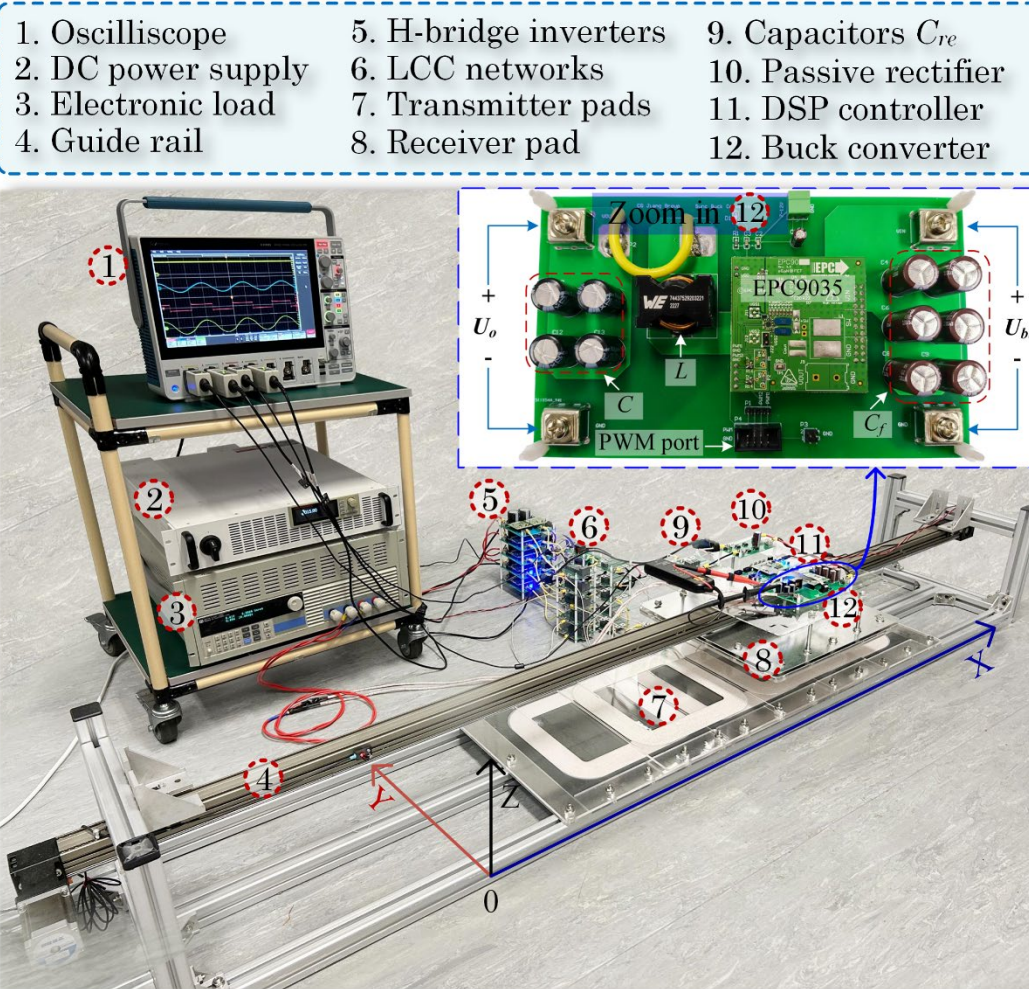


- The current limitation can limit the current amplitude, thus protecting the system. Meanwhile, it will affect the system's response.

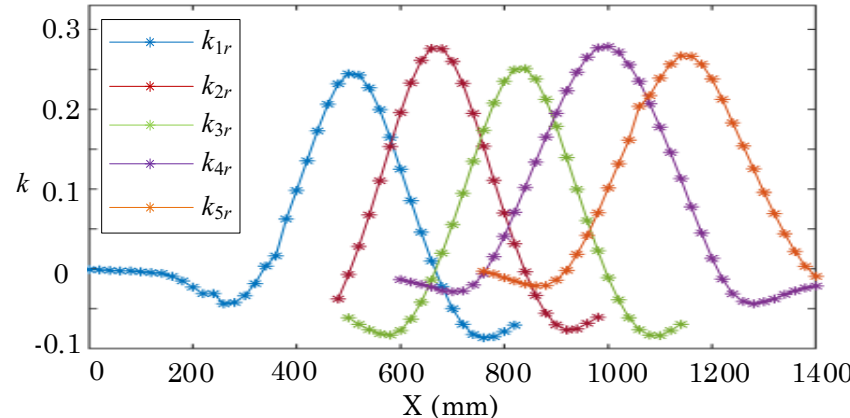
MPC for Dynamic WPT -- Experiment Verification

DWPT experimental setup

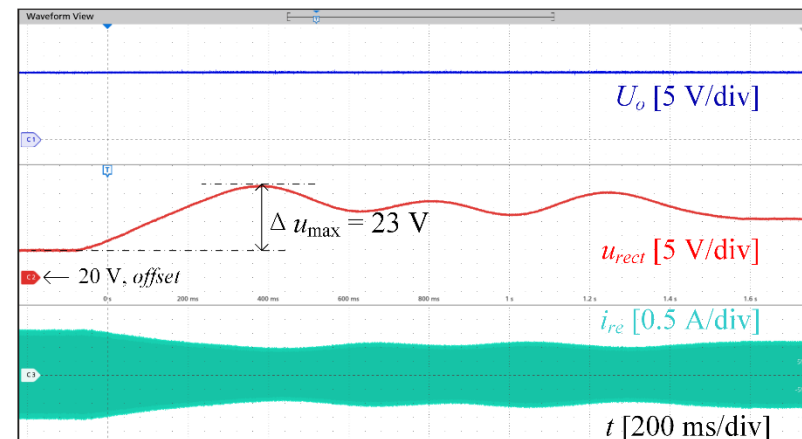
(2000 mm long and 400 mm wide)



Coupling coefficients between transmitters and receiver versus the position.

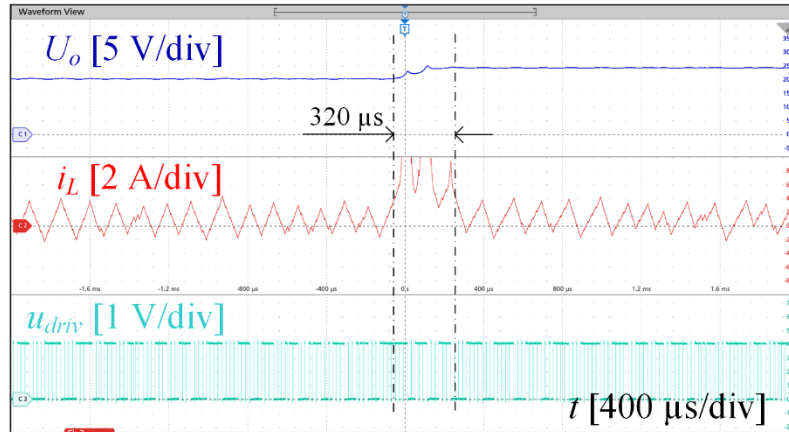


The output voltage is stable when the receiver is moving from $X=510$ mm to $X = 1100$ mm

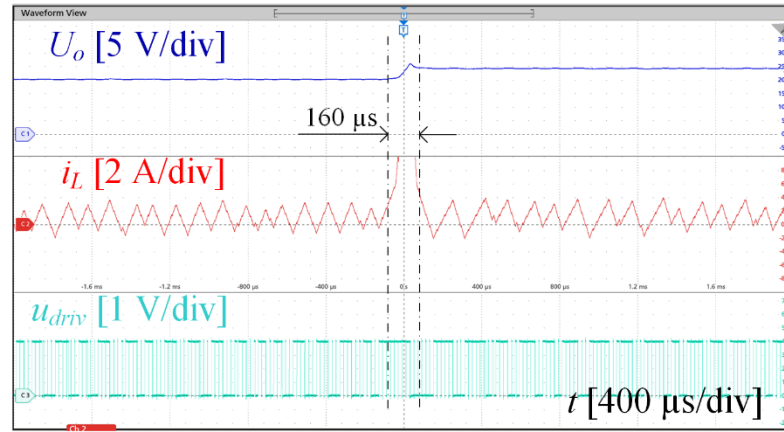


MPC for Dynamic WPT -- Experiment Verification

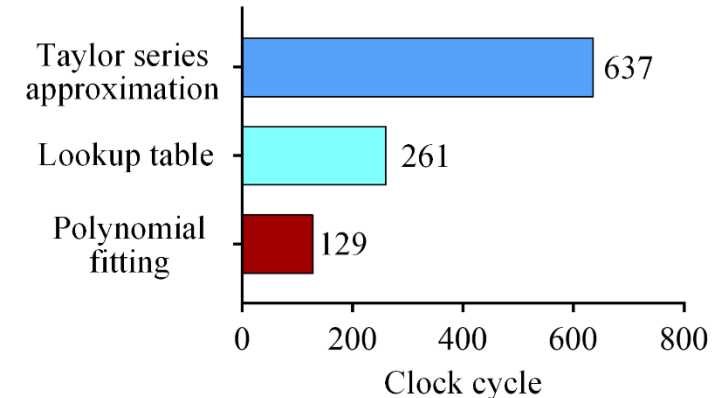
- Proposed MPC has a faster dynamic response and lower computational burden than MPC with the lookup table method.



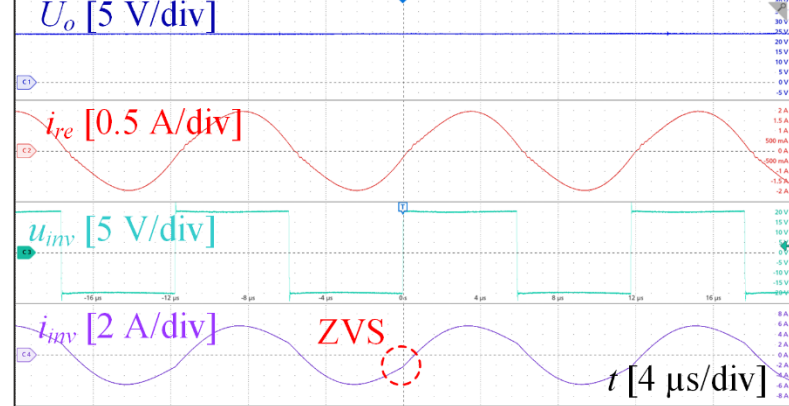
MPC with the lookup table method



MPC with the polynomial fitting



Computational overhead comparison



Steady-state waveform at X=990mm

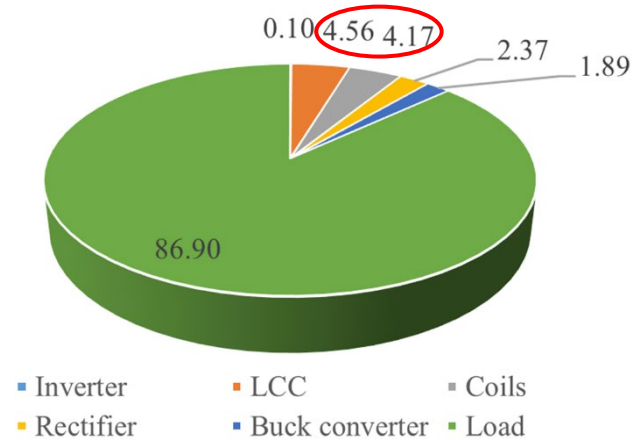
| | Element 1 | Element 2 | Element 3 | - |
|----------|------------|------------|------------|---|
| Urms [V] | 20.070 | 24.049 | 55.486 | |
| Irms [A] | 1.6585 | 1.2041 | 0.5336 | |
| P [W] | 0.03328 k | 0.02892 k | 0.02955 k | |
| S [VA] | 0.03329 k | 0.02896 k | 0.02961 k | |
| Q [var] | -0.00044 k | -0.00145 k | -0.00191 k | |
| λ [] | 0.99991 | 0.99875 | 0.99792 | |
| ϕ [°] | 0.763 | 0.2868 | 0.3692 | |
| fU [Hz] | 0.0000 | 0.0000 | 0.0000 | |
| η1 [%] | 86.897 | | | |

P1 0.03328 kW η1 86.897 %

η2 88.772 % η3 97.888 %

η_{total} 4.17 %

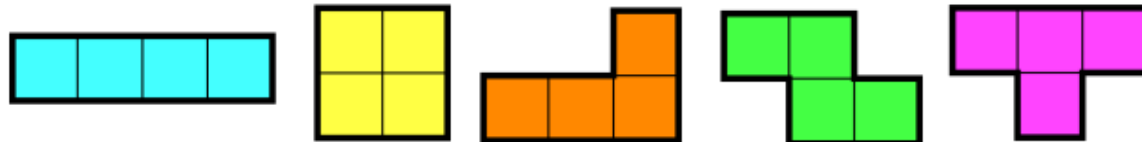
Efficiency measurement



Loss analysis

Tetris-Shaped Coils for DWPT

Tetris shapes: Rectangular coil, square coil, L-shaped coil, Z-shaped coil, and T-shaped coil.



Schematic diagram and dimension of T-shaped coil.

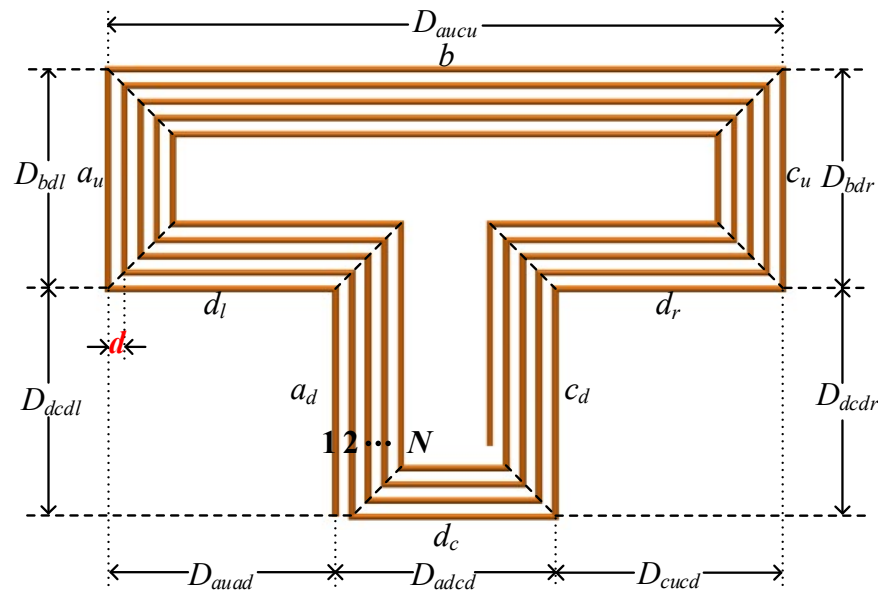
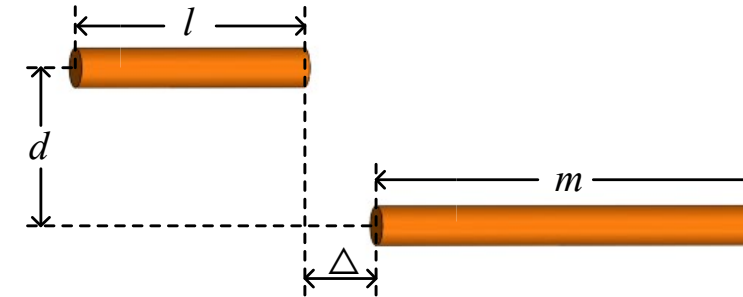


Diagram of two straight round wires.



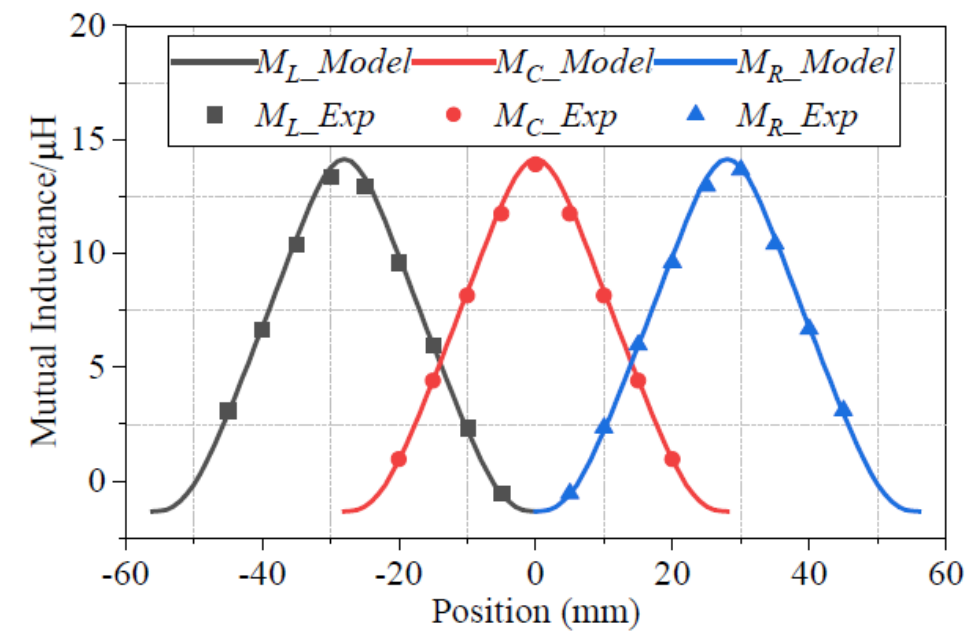
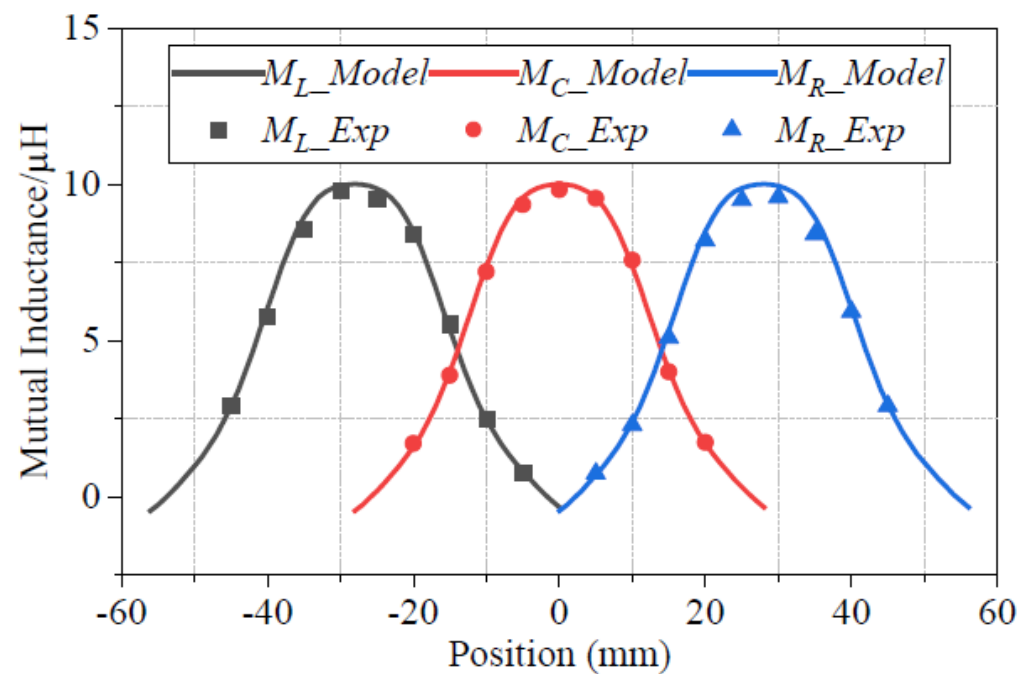
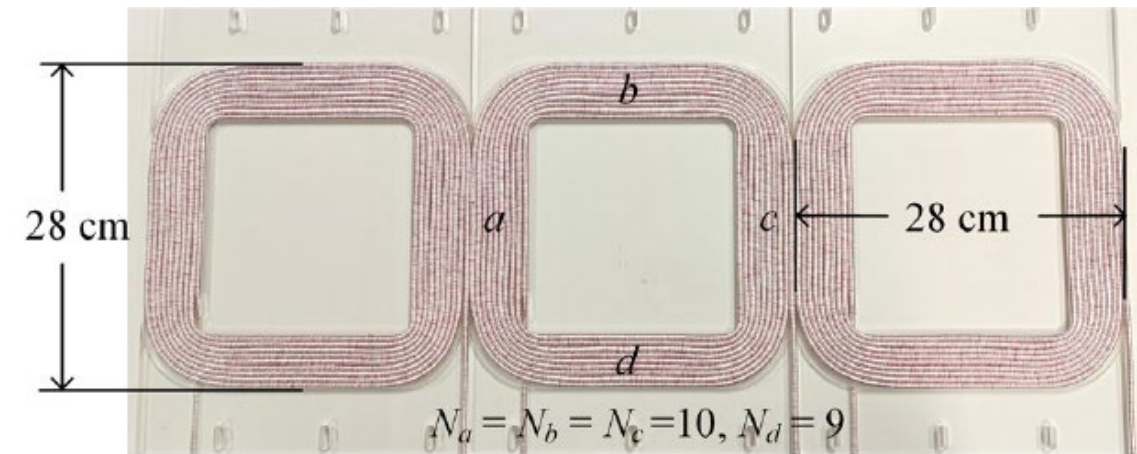
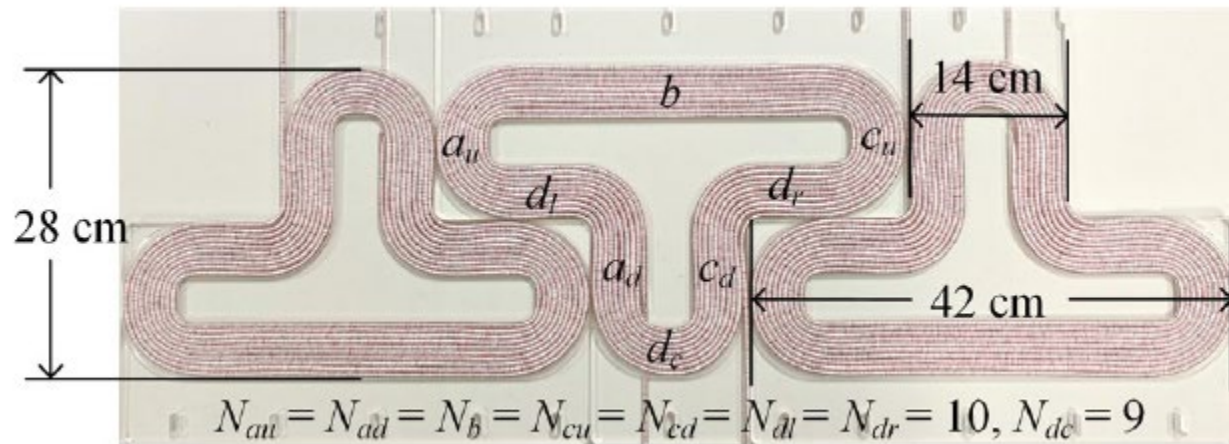
Basic Calculation Formulas of Self-inductance and Mutual Inductance

$$L(l, r) = \frac{\mu_0}{2\pi} \left[l \cdot \ln \left(\frac{l + \sqrt{l^2 + r^2}}{r} \right) - \sqrt{l^2 + r^2} + \frac{l}{4} + r \right]$$

$$M(l, m, d, \Delta) = \frac{\mu_0}{4\pi} \left[\alpha \sinh^{-1} \left(\frac{\alpha}{d} \right) - \beta \sinh^{-1} \left(\frac{\beta}{d} \right) - \gamma \sinh^{-1} \left(\frac{\gamma}{d} \right) + \Delta \sinh^{-1} \left(\frac{\Delta}{d} \right) - \sqrt{\alpha^2 + d^2} + \sqrt{\beta^2 + d^2} + \sqrt{\gamma^2 + d^2} - \sqrt{\Delta^2 + d^2} \right]$$

$$\alpha = l + m + \Delta \quad \beta = l + \Delta \quad \gamma = m + \Delta$$

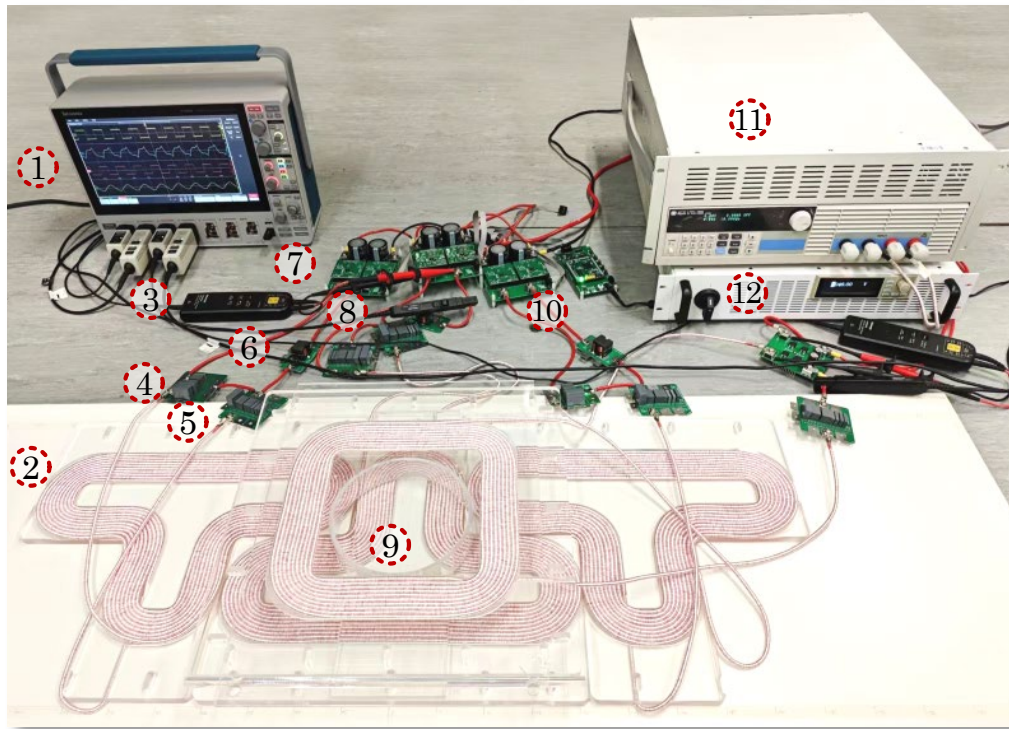
Tetris-Shaped Coils for DWPT



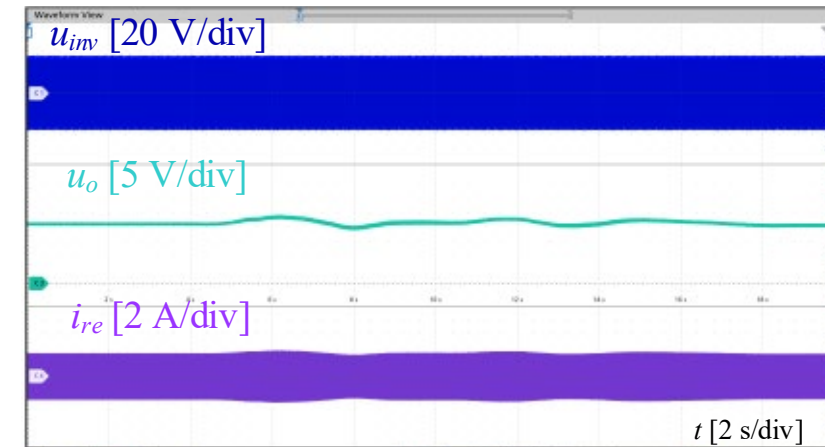
Tetris-Shaped Coils for DWPT

Experimental setup of the DWPT system with three T-shaped Tx coils and one square Rx coil.

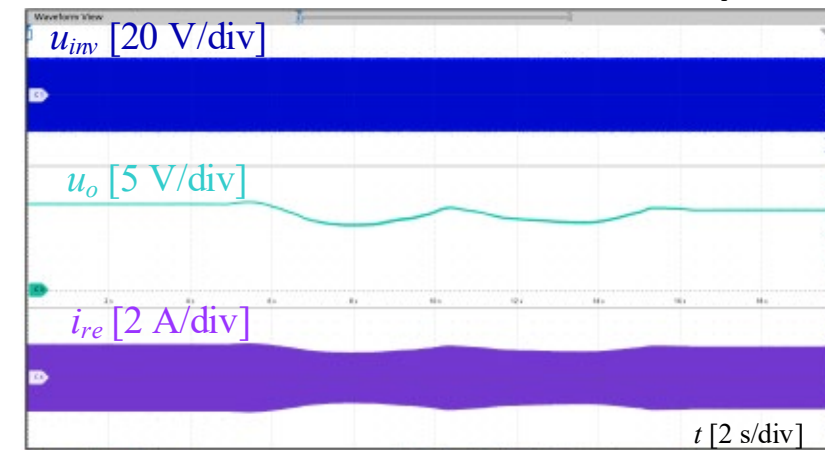
- | | | |
|--------------------|-----------------------|---------------------|
| 1. Oscilloscope | 5. Capacitor C_1 | 9. Receiver coil |
| 2. T-shaped coil | 6. Inductor L_1 | 10. DSP controller |
| 3. Voltage probe | 7. H-bridge inverters | 11. Electronic load |
| 4. Capacitor C_p | 8. Current probe | 12. DC source |



Rx moves from X = -30 to +30 cm with a **T-shaped** coil array.



Rx moves from X = -30 to +30 cm with a **square** coil array.



[7] T. Ma, C. Jiang, J. Zhou, C. Chen, Y. Wang, and Q. Zhu, "Modeling and Analysis of Tetris-Shaped Coils for Dynamic Wireless Power Transfer System" in *IEEE Transactions on Power Electronics*, Under review.

01

Background and Motivation

02

Modeling and Control for Stationary WPT

03

Modeling and Control for Dynamic WPT

04

MHz WPT in Biomedical Application

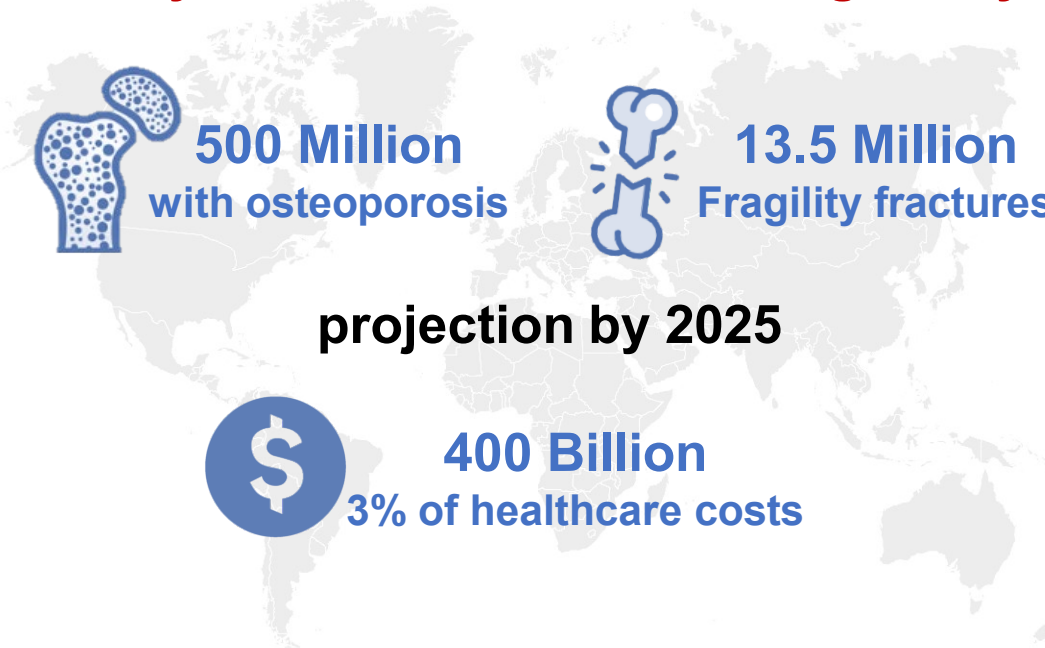
05

Conclusion and Future Outlook



Background

Heavy socio-economic burden globally



B. Wildemann et al., *Nat. Rev. Dis. Primers.* (2021);

Pharmacological treatment

- Bisphosphonates (alendronate)
- Hormone-related therapy (Estrogen)
- RANK-ligand inhibitor (denosumab)
- Growth factors (BMP2)

- ✗ Unsatisfied with efficacy and efficiency;
- ✗ Difficult to customize therapy in individual patients;
- ✗ All can contribute to life-threatening complications;
- ✗ Financial burden due to high cost for long-term usage.

Surgical treatment

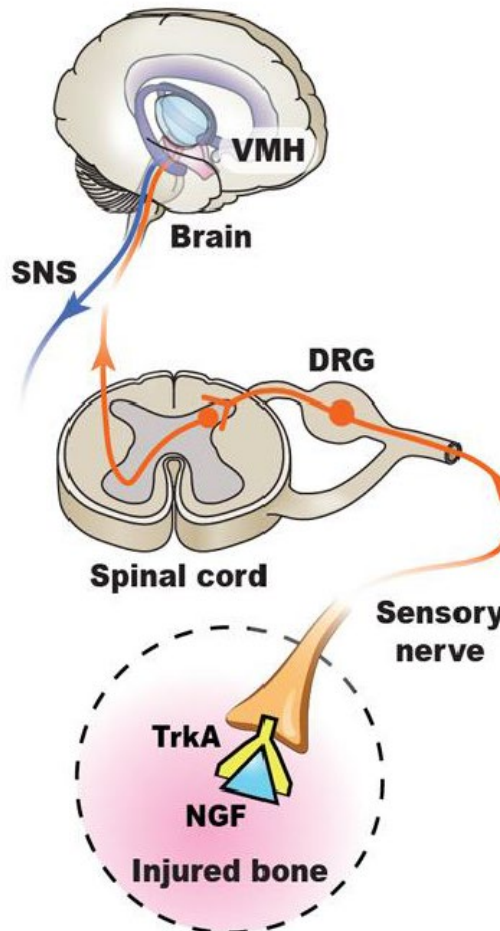
- Open reduction with internal fixation
- External fixation

- ✗ Slow healing process with immobilization;
- ✗ Risk of infection, prolonged inflammation, and non-union;
- ✗ Compromised long-term function outcome.



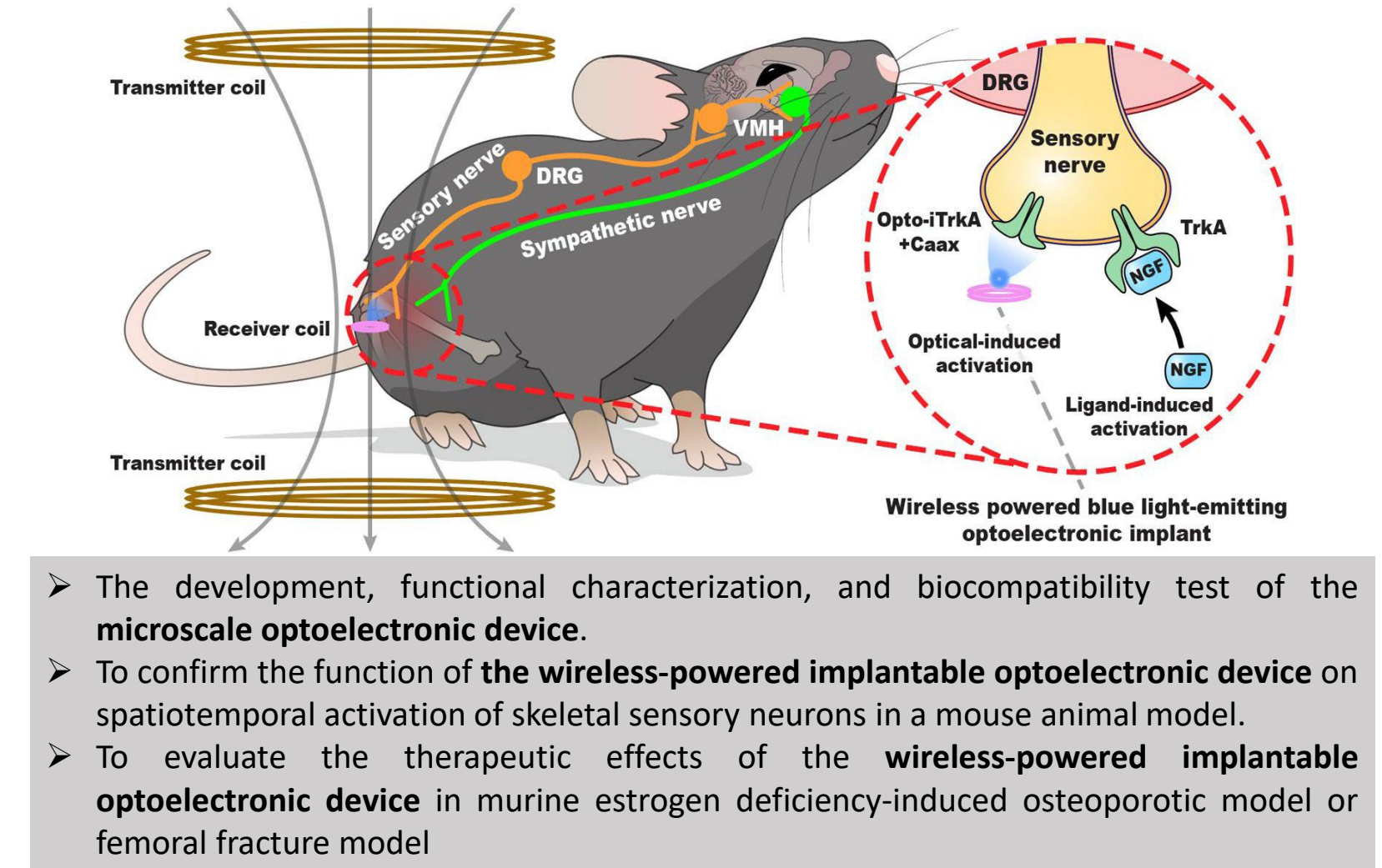
Background

TrkA signaling in bone



W. QIAO et al, Nature comm (2022)

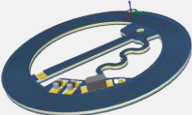
Research objectives





Research Plan and Methodology

For Objective 1



Design and fabrication of the implantable optogenetic device
(photolithographic technique)



Biocompatibility evaluation
(Temp. change when powered by WPT)
(ISO 10993-1 tests using murine fibroblast cell line (L929) and dorsal subcutaneous implantation in mouse model)



Optical activation of TrkA signaling *in vitro*
(Sensory neuron isolated from mouse DRG)
Live cell imaging Immunocytochemistry staining Western blots RT-qPCR

For Objective 2



Functional expression of the optogenetic system in mice
(Cre recombinase-activated AAV)



Surgical placement of the optogenetic device
(Lower limb via minimal invasive surgery)



Optical activation of TrkA signaling *in vivo*
(Daily optogenetic stimulation for 1 week)
Immunocytochemistry staining Western blots ELISA

For Objective 3



Osteoporosis model
(ovariectomy)



Fracture model
(internal fixation)



Surgical placement of the optogenetic device and stimulation
(monitored by live-animal µCT scan)



Histological study (At week 4 the endpoint)
Fluorochrome labeling
Immunohistochemistry staining H&E staining



Transcriptome sequencing
(L4-5 DRGs specimens)
RNA sequencing and RT-qPCR



Compact Receiver Design

PCB Design

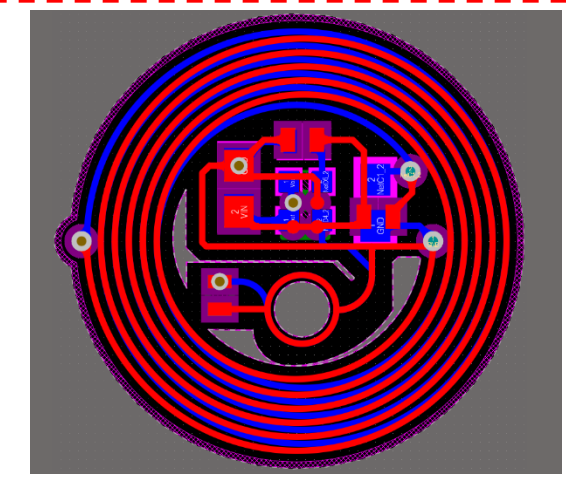
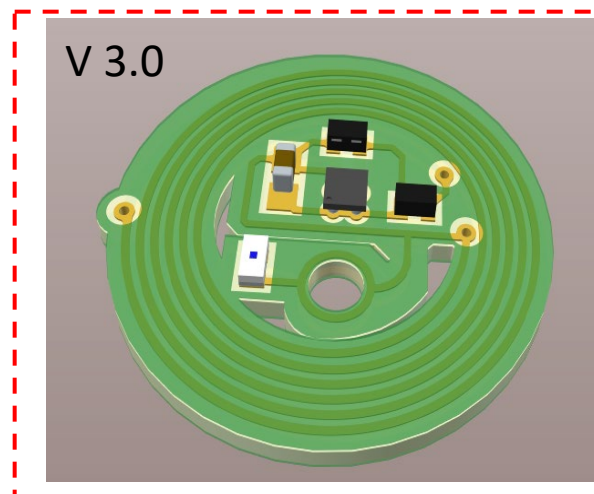
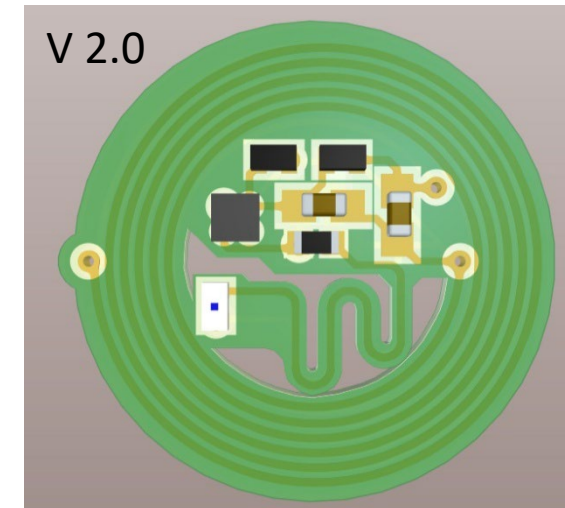
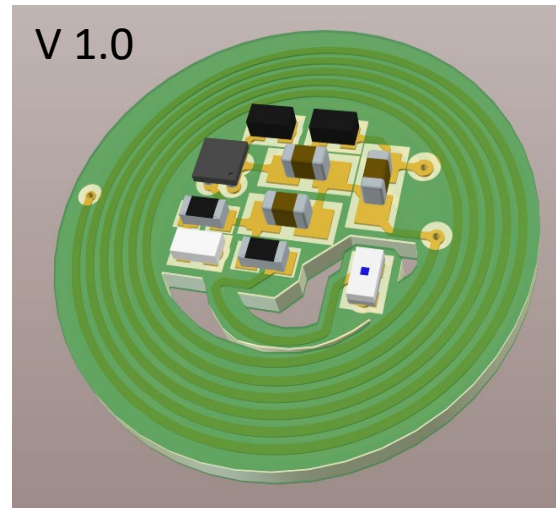
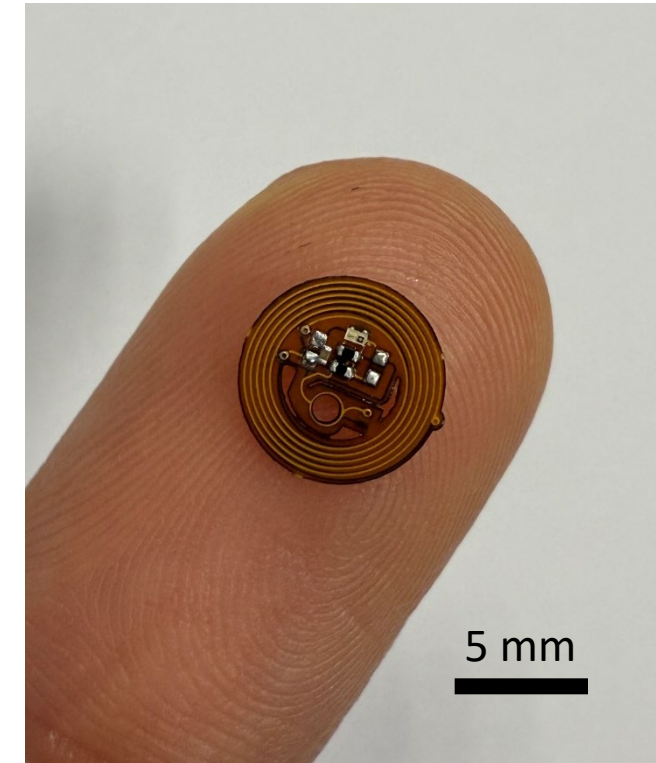


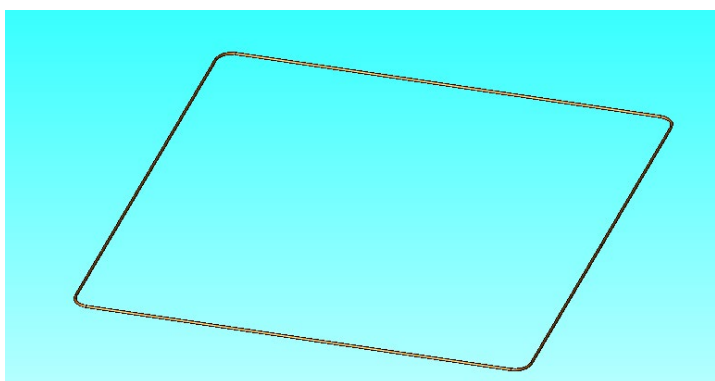
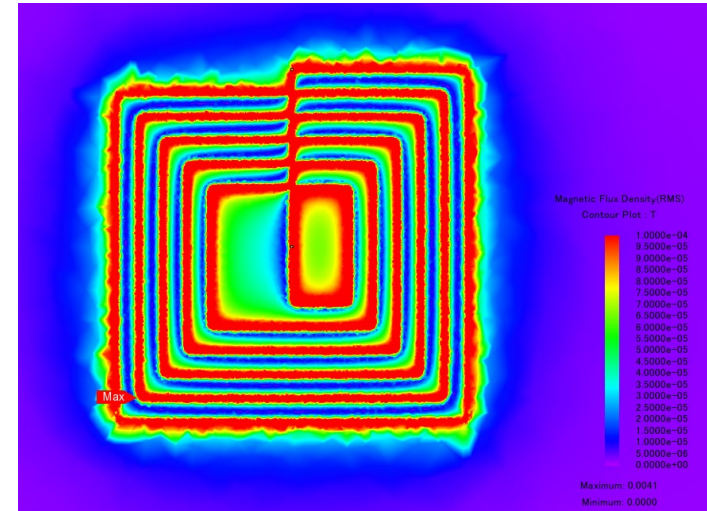
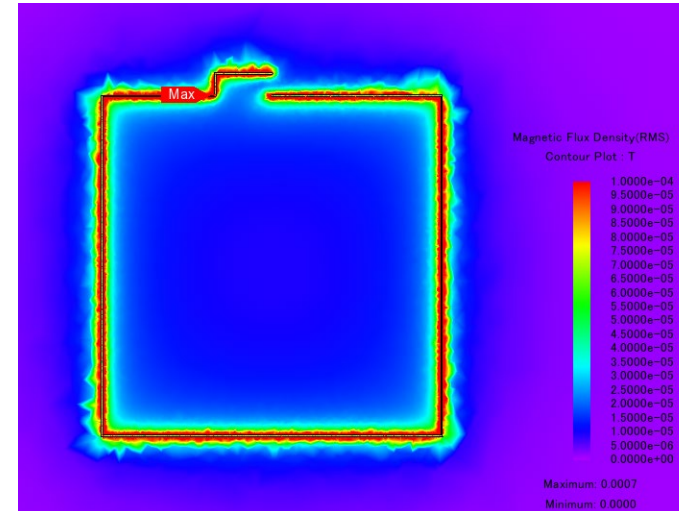
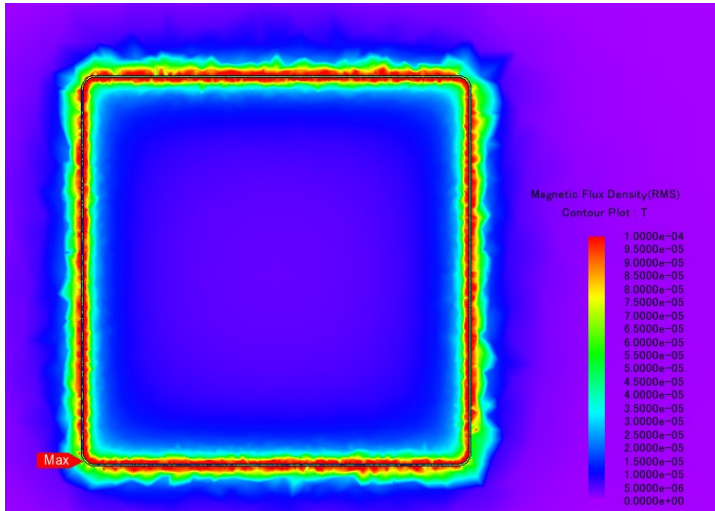
Photo of the physical object



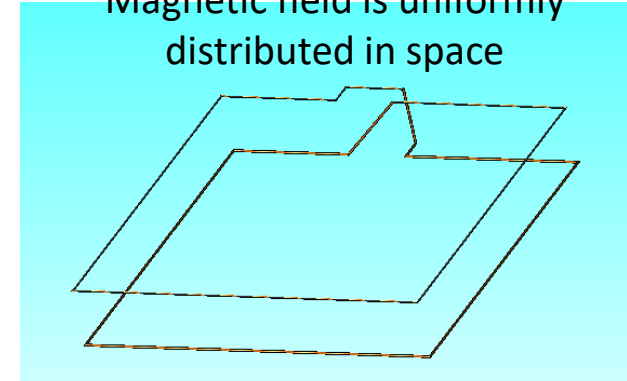


Transmitter Design

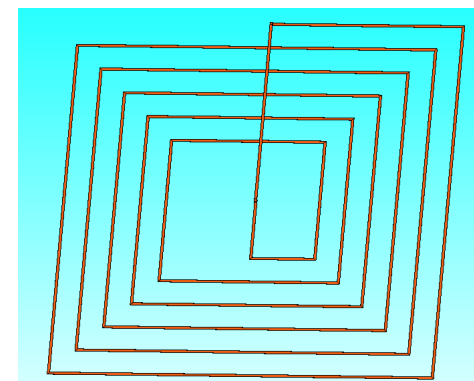
- Magnetic flux density of three types of transmitters (Transmitter current = 2 A, size: 30*30 cm)



Single turn



Helix with two turns



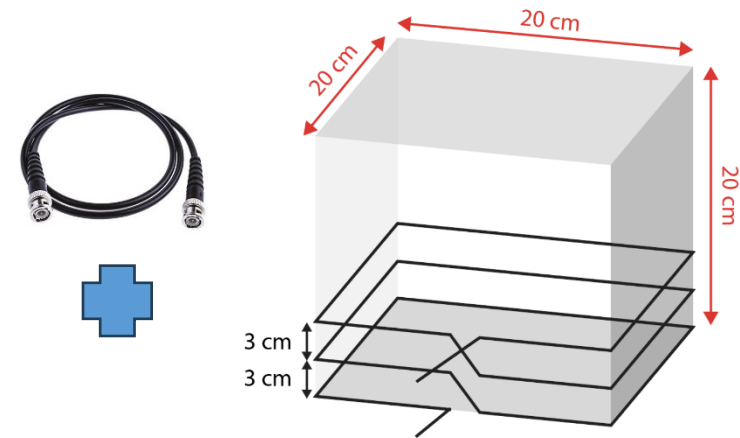
Spiral coil

Experimental Testing

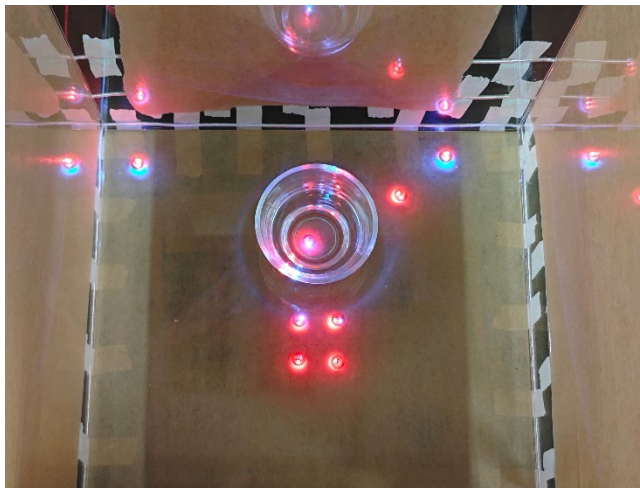
Signal Generator



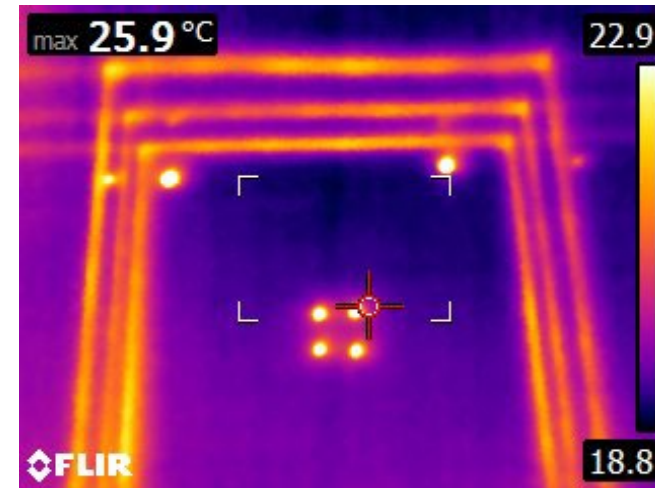
RF Amplifier



Waterproof Test



Thermal Test



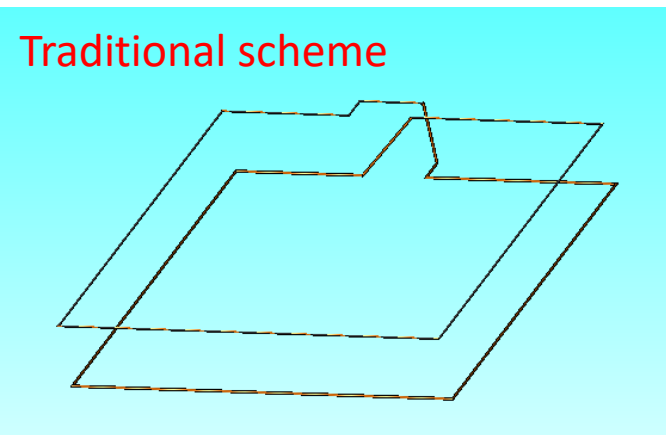
Animal Test



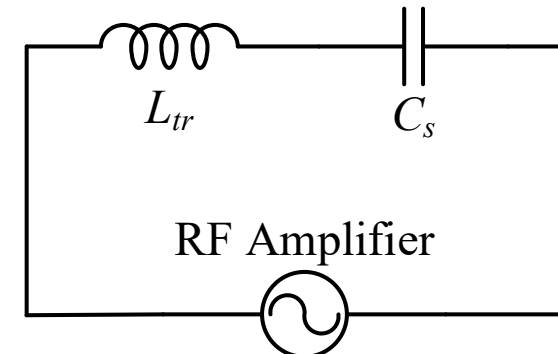


Innovation in Transmitter Design

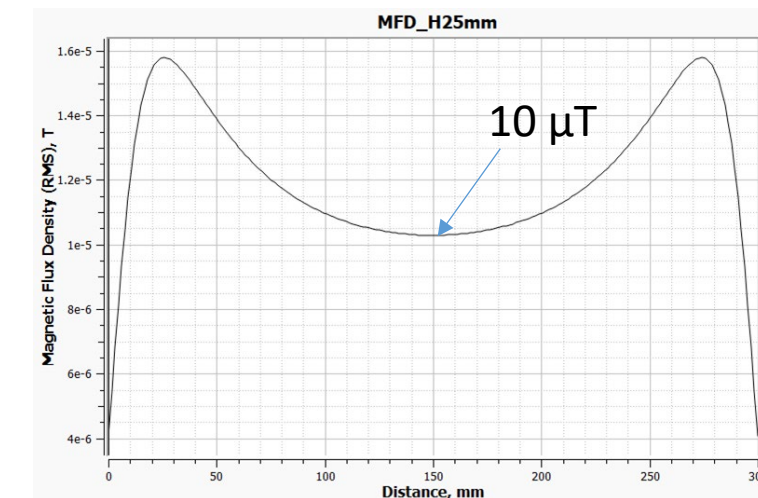
3D Structure



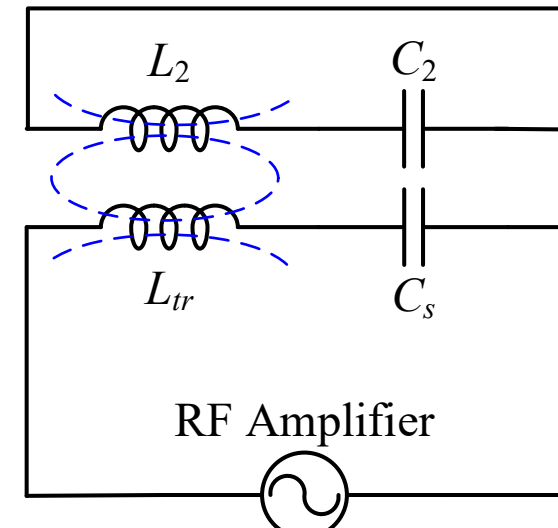
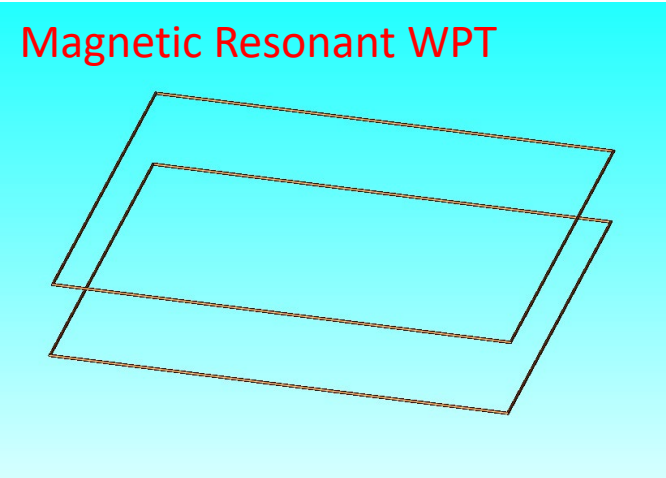
Equivalent Circuit



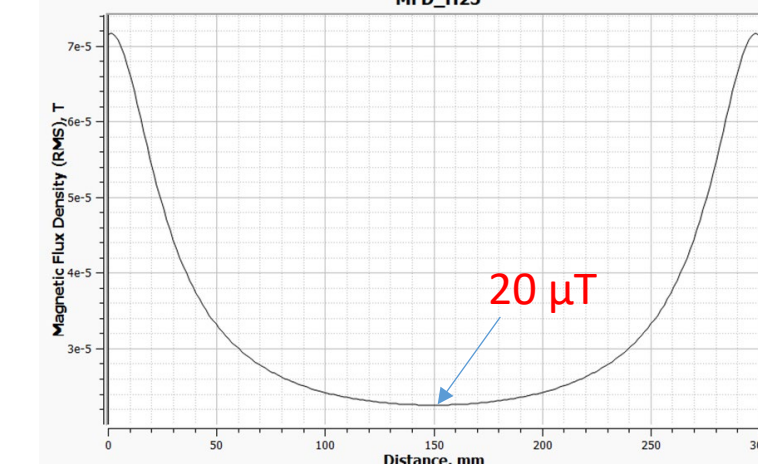
Magnetic Flux Density



Magnetic Resonant WPT



MFD_H25



- 01 Background and Motivation**
- 02 Modeling and Control for Stationary WPT**
- 03 Modeling and Control for Dynamic WPT**
- 04 MHz WPT in Biomedical Application**
- 05 Conclusion and Future Outlook**

Conclusion

Modeling for SWPT and DWPT Systems

- Two modeling methods are elaborated for SWPT systems. One is the GSSA model, representing of frequency-domain model, and the other is the UFDT model, on behalf of the time-domain model.
 - **GSSA model:** Only fundamental harmonic is considered, and the GSSA approach is used to model the periodic energy control.
 - **UFDT model:** Analyze the full-load range characteristics, especially for **discontinuous conduction of the rectifier at the light load.**
- The GSSA model of the DWPT system with two transmitters and one receiver is first established, and **the efficiency is improved by optimizing the phase between the adjacent transmitting coils.**

Control Strategies for SWPT and DWPT Systems

- Periodic energy control (PEC) is first proposed and its characteristics, such as **ZVS operation and fast dynamic response**, are analyzed by the GSSA model.
- PEC is applied to the DC-DC converters on the secondary side of the DWPT systems, which is proven to have **good performance in overshoot suppression.**
- A **low computational burden** model predictive control is also proposed for the DWPT systems by using polynomials to fit the system matrix and input matrix of the sampled-data model of the DC-DC converter.

Dynamic Wireless Power Transfer

- Efficiency optimization strategies
- Reduced-order model for the DWPT system
- High-power DWPT system (Thermal issues, EMI, coupler design, etc.)

MHz WPT in Biomedical Application

- High-efficiency WPT system in biomedical application.
- Specific applications: flexible electronic devices, wearable devices, etc.

AI Technology in WPT

- AI technology for coupler design
- AI technology for modeling and control

List of Publications

Journal
papers

18

Conference
papers

7

Book
chapter

1

Patents

4

Awards

10

Published 14 Top Tier Journal Papers (5 of them as First author).

[1] T. Ma, Y. Wang, X. Hu, D. Zhao, Y. Jiang, and C. Jiang, "Periodic Energy Control for Wireless Power Transfer System," in *IEEE Transactions on Power Electronics*, vol. 37, no. 4, pp. 3775-3780, April 2022.

[2] T. Ma, C. Jiang, X. Wang, J. Xiang, L. Mo, and K. T. Chau, "A Novel Periodic Energy Control for Nonisolated DC-DC Converters With Overshoot Suppression," in *IEEE Transactions on Power Electronics*, vol. 38, no. 10, pp. 12325-12330, Oct. 2023

[3] T. Ma, C. Jiang, Y. Zhang, Y. Wang, Y. Cheng, and S. Cui, "Modeling and Analysis of Periodic Energy Control for Series-Series Wireless Power Transfer System," in *IEEE Transactions on Power Electronics*, doi: 10.1109/TPEL.2023.3346460, early access.

[4] T. Ma, C. Jiang, J. Xiang, X. Wang, K. T. Chau, and T. Long, "Modeling and Analysis of Wireless Power Transfer System Via Unified Full-Load Discrete-Time Model," in *IEEE Transactions on Industrial Electronics*, vol. 70, no. 6, pp. 5626-5636, June 2023.

[5] T. Ma, C. Jiang, C. Chen, Y. Wang, J. Geng, and C. K. Tse, "A Low Computational Burden Model Predictive Control for Dynamic Wireless Charging," in *IEEE Transactions on Industrial Electronics*, doi: 10.1109/TIE.2023.3344844, early access.

List of Publications

Published Conference Papers (First author)

- [1] T. Ma, J. Huang, J. Yang, Z. Zhu, C. Chen, and C. Jiang, "T-shaped Transmitting Coil Array for Dynamic Wireless Charging" 2024 International Conference of Wireless Power Transfer (ICWPT2024), Xuzhou, China, 2024, pp. 1-7.
- [2] T. Ma, C. Jiang, S. Zhang, C. Chen, J. Zhou, and J. Xiang, "Discrete-Time Modeling for IPT Systems with Constant Voltage Load," 2024 IEEE Wireless Power Technology Conference and Expo (WPTCE), Kyoto, Japan, 2024, pp. 830-833.
- [3] T. Ma et al., "Secondary Periodic Energy Control for LCC-S Compensated Wireless Power Transfer Systems," 2023 11th International Conference on Power Electronics and **ECCE Asia** (ICPE 2023 - ECCE Asia), 2023, pp. 823-828.

Published and Accepted Patents

- [1] T. Ma, C. Jiang, A periodic energy control method, device, and system for DC-DC converter. CN202310983575.9, 2023.
- [2] T. Ma, C. Jiang, A control method and device applied to the buck converter. CN202311058125.5, 2023.
- [3] Y. Wang, T. Ma, X. Hu, Z. Lin, A periodic energy control method for wireless power transmission system. CN202110744716.2, 2021.
- [4] L. MO, C. Jiang, T. Ma, X. Wang, Y. Wang, A topology deduction method for single-inductor multi-port converter based on graph analysis. CN202410744857.8, 2024.
- [5] L. MO, C. Jiang, T. Ma, Y. Wang, Method and equipment for identifying redundant openings in a type of changer. CN202311753848.7, 2023.

List of Publications

Published Book Chapter

- [1] C. Jiang, C. C. Chan, T. Ma, J. Xiang, X. Wang, C. Chen, H. Sun, and G. Y. Zhou, "Strategy of Integrated Humanity for Specific Applications," in book Integration of Energy, Information, Transportation and Humanity, *Elsevier*, 2023.

Awards and Honors

- [1] Outstanding Academic Performance Award for Research Degree Students, Aug. 2024
- [2] IET Young Professionals Exhibition and Competition 2024, Jul. 2024 **1st Runner Up**
- [3] 49th International Exhibition of Inventions of Geneva, Apr. 2024 **Gold Medal**
- [4] IEEE PELS Student Symposium on Power Electronics in Asia, Jan. 2024 **First Prize & Best Presentation Award**
- [5] 3rd Asia Exhibition of Innovations and Inventions in Hong Kong, Dec. 2023 **Gold Medal**
- [6] IET Young Professionals Exhibition and Competition 2023, Oct. 2023 **Best Innovation Award & 1st Runner-Up**
- [7] China (Shenzhen) Innovation & Entrepreneurship Competition 2024, Nov. 2024 **Third Prize**
- [8] Research Tuition Scholarship, Sept. 2023
- [9] Research Tuition Scholarship, Sept. 2024
- [10] HKSAR Government Scholarship Fund (Non-academic Awards) - Talent Development Scholarship, Aug. 2024

Thank You For Your Attention

• Tianlu Ma •

Email: tianlu.ma@my.cityu.edu.hk

14 March 2025